INFORMATION TO USERS

This manuscript has been reproduced from the microfilm master. UMI films the text directly from the original or copy submitted. Thus, some thesis and dissertation copies are in typewriter face, while others may be from any type of computer printer.

The quality of this reproduction is dependent upon the quality of the copy submitted. Broken or indistinct print, colored or poor quality illustrations and photographs, print bleedthrough, substandard margins, and improper alignment can adversely affect reproduction.

In the unlikely event that the author did not send UMI a complete manuscript and there are missing pages, these will be noted. Also, if unauthorized copyright material had to be removed, a note will indicate the deletion.

Oversize materials (e.g., maps, drawings, charts) are reproduced by sectioning the original, beginning at the upper left-hand corner and continuing from left to right in equal sections with small overlaps.

ProQuest Information and Learning
300 North Zeeb Road, Ann Arbor, MI 48106-1346 USA
800-521-0600

University of Alberta

Design and Realization of Maximally-Decimated Filterbanks with High Computational Efficiency

by

Nan Li 

A thesis submitted to the Faculty of Graduate Studies and Research in partial fulfillment of the requirements for the degree of **Master of Science**.

Department of Electrical and Computer Engineering

Edmonton, Alberta
Spring 2005

I dedicate this thesis to my family. All my successes are based on their endless encouragement and support.

Abstract

Discrete Fourier transform (DFT) filterbanks are suitable for the realization of subchannels with linear-phase characteristics, and provide a high degree of computational efficiency in their corresponding hardware implementations. However, in situations when the DFT filterbank subchannels have very narrow transition bandwidths or when the number of subchannels is very large, the length of the constituent prototype filter becomes prohibitively large, curtailing the computational efficiency of the filterbank. This thesis is concerned with the investigation of the conventional DFT and modified-DFT (MDFT) filterbanks, and the development of a pair of novel maximally-decimated filterbanks exhibiting high computational efficiency. One of the proposed filterbanks is based on a multistage tree-structure. The other is based on the frequency-response masking technique. Compared to the corresponding conventional DFT and MDFT filterbanks, the resulting filterbanks possess much less number of filtering coefficients in their hardware implementations. Detailed application examples reveal that the proposed filterbanks satisfy the desirable perfect reconstruction property to an acceptable degree of approximation.

Acknowledgements

I would like to thank Dr. Nowrouzian, my supervisor, who gave me countless advice, guidance, and encouragement during the past three years.

Also, I would like to thank Wang Luqing. We used to work in the same research group. He gave me lots of help in both research and LaTeXwriting.

Last, I would like to thank NSERC, Micronet, and Nortel Networks for their financial and in-kind support.

Contents

List of Figures

List of Tables

Acronyms

AC Alias Component

CMFB Cosine-Modulated Filter Bank

DFT Discrete Fourier Transform

DCT Discrete Cosine Transform

FDM Frequency Division Multiplexing

FFT Fast Fourier Transform

FIR Finite Impulse Response

FRM Frequency-Response Masking

IDFT Inverse Discrete Fourier Transform

LPTV Linear Periodically Time-Varing

LTI Linear Time-Invariant

MDFT Modified DFT

PR Perfect Reconstruction

QMF Quadrature Mirror Filter

SBC Subband Coding

Notations

- $x(n)$: Lowercase letter represents the time-domain signal or symbol,
- $X(z)$, $X(e^{j\omega})$: Uppercase letter represents the transform-domain (z-domain or Fourier transform domain) signal or symbol,
- $\boldsymbol{X}(n)$: Uppercase bold letter represents a matrix or a vector,
- $\boldsymbol{X}_{r\times c}$: A matrix $\boldsymbol{X}$ with r rows and c columns,
- $x^{(k)}(n)$ or $X^{(k)}(z)$: The k-th polyphase component of $x(n)$ or $X(z)$,
- $x_R(n)$ or $x_I(n)$: The real part or imaginary part of $x(n)$,
- $X^{(R)}(z)$ or $X^{(I)}(z)$: The z-domain transforms of the real part or imaginary part of $x(n)$,
- $x(n) * y(n)$: Linear convolution of $x(n)$ and $y(n)$,
- $x(n) \otimes y(n)$: Circular convolution of $x(n)$ and $y(n)$,
- $(\cdot)_{\downarrow M}$: Decimating $(\cdot)$ by a factor of M,
- $(\cdot)_{\uparrow M}$: Expanding $(\cdot)$ by a factor of M,
- $\text{row}_i\{\mathcal{F}_N\}$: The i-th row of the DFT matrix $\mathcal{F}_N$,
- $(\cdot)^*$: Complex conjugate operation,
- W_M: The Mth root of unity, defined as $W_M = e^{-j2\pi/M}$,
- $(\cdot)^T$: Matrix transpose operation,
- $(\cdot)^\dagger$: Conjugate transpose operation,

- $(\cdot)^{-1}$: Matrix inverse operation,
- $\boldsymbol{I}$: The identity matrix,
- $\boldsymbol{J}$: The reverse identity matrix,
- $\boldsymbol{u}_i$: The i-th unit vector, where the i-th element of $\boldsymbol{u}_i$ is equal to 1 while other elements are 0, i.e. $\boldsymbol{u}_i = \begin{bmatrix} 0 & \cdots & 1 & \cdots & 0 \end{bmatrix}^T$.

Chapter 1

Introduction

Multirate digital signal processing (DSP) techniques have been under development and investigation for more than two decades. These techniques find a wide variety of applications, for example in speech and image compression, digital audio industry, statistical and adaptive signal processing, numerical solution of differential equations, and in many other fields. They are also relevant to certain special classes of time-frequency representations, for example short-term Fourier transform and wavelet transform, which are useful in analyzing the time-varying nature of digital signal spectra.

1.1 Background

A traditional single-rate DSP system can be considered as an interconnection of computational building blocks such as digital multipliers, adders and unit-delays, and digital modulators, as shown in Fig. 1.1. Well known examples of single-rate DSP systems are digital filters and Fourier transformers.

In a multirate DSP system, there are a pair of additional building blocks, namely the M-fold decimator and the L-fold interpolator as shown in Fig. 1.2[1], where $x(n)$ represents the input signal, $y_D(n)$ and $y_I(n)$ represent the decimator and interpolator output signals, respectively, and n represents the discrete-time sample index. The M-fold decimator is a device that is used to reduce the sampling rate by a integer factor M, whereas the L-fold interpolator is a device used to increase the sampling rate by a integer factor L. Such sampling rate changes can be introduced at the input

[1]Please see the next section for the details of these building blocks

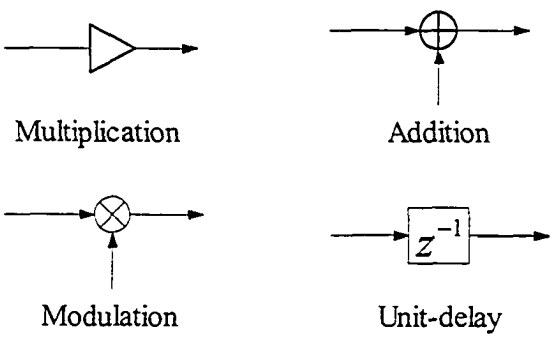

Figure 1.1: Building blocks in a single-rate DSP system

and/or output of a multirate DSP system or in its internal environment, depending on the particular application.

(a) M-folder decimator (b) L-fold interpolator

Figure 1.2: The decimator and interpolator building blocks

In its earliest applications, multirate DSP was predominantly focused on professional digital music [16]. Let us consider the case of sampling an analog signal for situations when most of the signal energy is concentrated in frequencies below f_M. In single-rate DSP, this can be achieved by bandlimiting the analog signal to the frequency f_M by employing an analog lowpass filter (to avoid aliasing effects), followed by sampling the resulting bandlimited signal. In this way, the required analog lowpass filter should have a very narrow transition band (between passband and stopband). In multirate DSP, on the other hand, it is possible to employ a bandlimiting analog lowpass filter with a wide transition band by using oversampling techniques[2]. Then, the resulting oversampled signal can be bandlimited in digital domain by using a linear-phase digital filter and then decimated to reduce the sampling rate to the desired rate. Clearly, multirate DSP can eliminate the need for sharp transition band analog filters, which not only are expensive, but also can introduce severe phase

[2]This will counteract the aliasing effects arising from the wide transition band analog lowpass filter.

distortions into the overall system.

Fractional sampling rate changes are also common in the digital audio industry [4]. For example, the sampling rate for studio signal processing is 48kHz, whereas that for compact disk (CD) production is 44.1kHz. The obvious way to perform this rate conversion would be to first convert the discrete-time signal into a continue-time signal and then sample it at the lower rate. This method is expensive and involves analog signal processing along with the associated inaccuracies. In the multirate DSP, such conversions can be performed directly by using fractional decimation and interpolation (by using appropriate combinations of decimators, interpolators and digital filters).

1.2 Fundamentals of Multirate Digital Signal Processing

1.2.1 Decimation and interpolation

The most basic operations in multirate DSP systems are decimation and interpolation; the corresponding building blocks are called the *decimator* (or *down-sampler*) and *interpolater* (or *up-sampler*) as shown in Fig. 1.2.

Decimators

A M-fold decimator down-samples a discrete-time input signal sequence $x(n)$, and produces the output signal

$$y_D(n) = x(Mn), \tag{1.1}$$

where M is an integer. Only those samples of $x(n)$ which occur at time instants equal to multiples of M are retained by the decimator. An example of decimation operation for $M = 2$ is shown in Fig. 1.3.

In the frequency-domain, the output signal $Y_D(e^{j\omega})$ can be expressed in terms of the corresponding input signal $X(e^{j\omega})$ as

$$Y_D(e^{j\omega}) = \frac{1}{M}\sum_{k=0}^{M-1} X(e^{j(\omega-2k\pi)/M}). \tag{1.2}$$

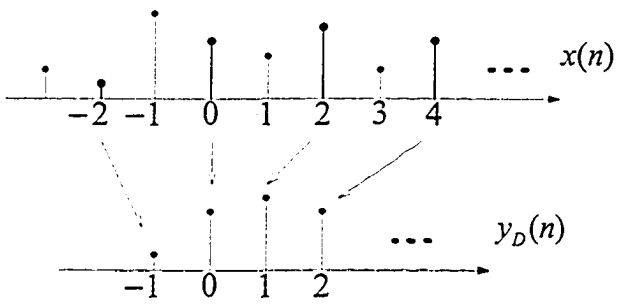

Figure 1.3: The decimation operation in time-domain (for $M = 2$)

where ω represents the discrete-time real frequency variable, or, in the z-transform domain, as

$$Y_D(z) = \frac{1}{M} \sum_{k=0}^{M-1} X(z^{1/M} W_M^k). \tag{1.3}$$

where W_M is the Mth root of unity defined as

$$W_M = e^{-j2\pi/M} \tag{1.4}$$

The operation of decimation can be graphically interpreted as follows: (a) stretch the spectrum of $X(e^{j\omega})$ by a factor M to obtain $X(e^{j\omega/M})$, (b) create $M-1$ copies of the stretched version by shifting it uniformly in succession by 2π shifts, and (c) add all the shifted and unshifted versions together, and scale their amplitudes by M. Fig. 1.4 demonstrates this process for $M = 2$.

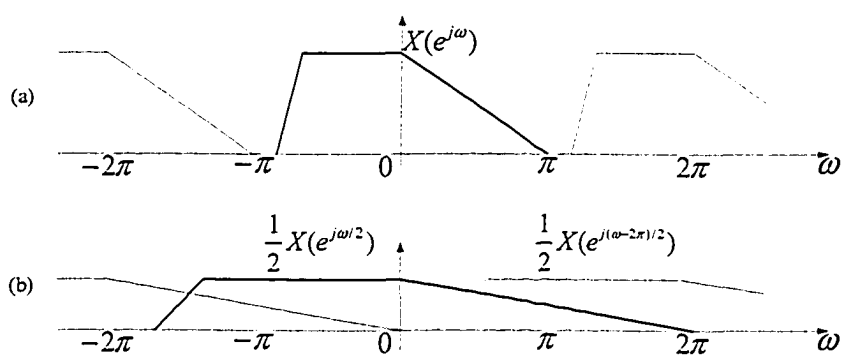

Figure 1.4: The decimation operation in frequency-domain (for $M = 2$)

Interpolators

A L-fold interpolator up-samples a discrete-time input signal sequence $x(n)$, and produces the output signal

$$y_I(n) = \begin{cases} x(n/L), & \text{if n is integer-multiple of } L \\ 0, & \text{otherwise.} \end{cases} \tag{1.5}$$

by inserting $L-1$ zeroes between successive samples of $x(n)$, where L is an integer. An example of interpolation operation for $L=2$ is shown in Fig. 1.5.

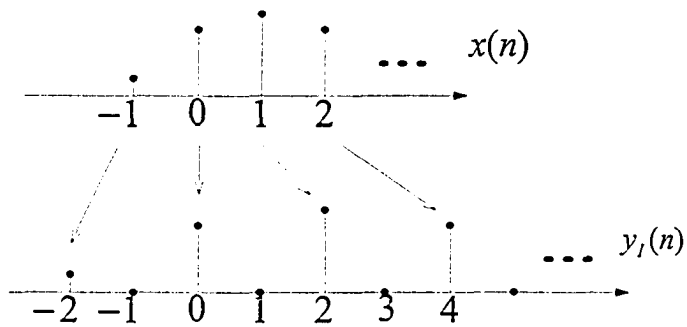

Figure 1.5: The interpolation operation in time-domain (for $L=2$)

In the frequency domain, the output signal $Y_I(e^{j\omega})$ can be expressed in term of the corresponding input signal $X(e^{j\omega})$ as

$$Y_I(e^{j\omega}) = X(e^{jL\omega}). \tag{1.6}$$

which is simply the squeezed version of the original signal by a factor L. The operation of interpolation in frequency-domain for $L=2$ is illustrated in Fig. 1.6.

The decimator and the interpolator are linear, but time-varying devices.

1.2.2 Noble identities

Fig. 1.7a shows a cascade connection of a digital filter of transfer function $G(z)$ preceded by a M-fold decimator. If the transfer function $G(z)$ is rational in z (i.e., if it is a ratio of two polynomials in z or z^{-1}), then Fig. 1.7a can be redrawn as shown in Fig. 1.7b.

From Fig. 1.7a, the signal $Y_1(z)$ can be obtained in accordance with

$$Y_1(z) = X(z)_{\downarrow M} G(z) = \frac{1}{M} \sum_{l=0}^{M-1} X(z^{1/M} W^l) G(z) \tag{1.7}$$

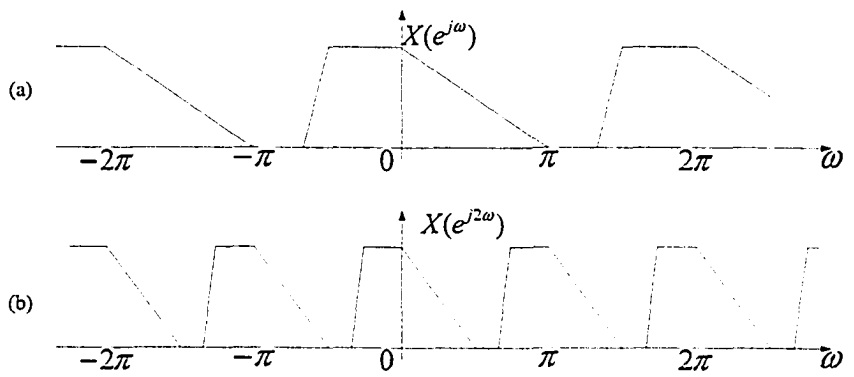

Figure 1.6: The interpolation operation in frequency-domain (for $L = 2$)

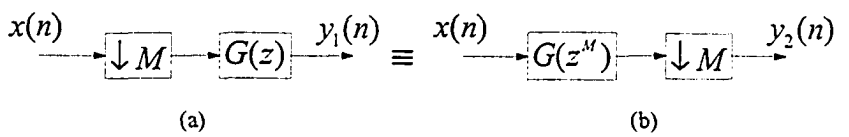

Figure 1.7: Identity involving decimators

and from Fig. 1.7b, the signal $Y_2(z)$ can be obtained in accordance with

$$\begin{aligned} Y_2(z) &= (X(z)G(z^M))_{\downarrow M} \\ &= \frac{1}{M}\sum_{l=0}^{M-1} X(z^{1/M}W^l)G((z^{1/M}W^l)^M) \\ &= \frac{1}{M}\sum_{l=0}^{M-1} X(z^{1/M}W^l)G(z) = Y_1(z) \end{aligned} \tag{1.8}$$

Similarly, Fig. 1.8a shows a cascade connection of a digital filter of transfer func-

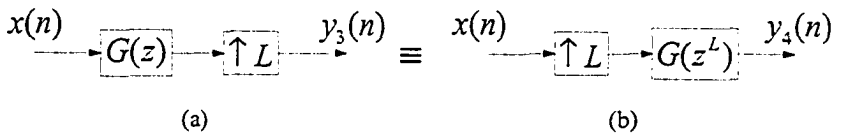

Figure 1.8: Identity involving interpolators

tion $G(z)$ followed by a L-fold interpolator. Once again, if the transfer function $G(z)$ is rational in z, Fig. 1.8a can be redrawn as in Fig. 1.8b, where the signal $Y_4(z)$ can be derived as

$$Y_4(z) = X(z)_{\uparrow L}G(z^L) = X(z^L)G(z^L) = (X(z)G(z))_{\uparrow L} = Y_3(z) \tag{1.9}$$

The equivalent representations in Figs. 1.7 and 1.8 are called *noble identities*. These identities are very useful, finding practical applications in the theory and implementation of multirate DSP systems.

It is important to point out that if the transfer function $G(z)$ is irrational in z, then noble identities may not hold true. For example, consider the DSP system in Fig. 1.9a with $G(z) = z^{-1/2}$. If the identities were holding true, then Fig. 1.9a could have been redrawn successively as in Fig. 1.9b and then Fig. 1.9c. But it can be shown that the DSP systems in Figs. 1.9a and 1.9c are not equivalent [33]. For

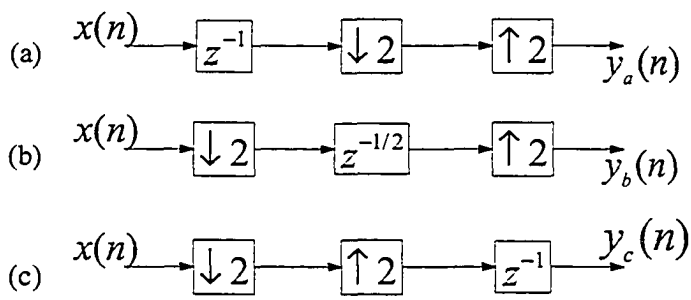

Figure 1.9: Investigation of noble identities

example, if the input signal $x(n)$ is such that $x(2n) = 0$ for all n, then the output signal $y_c(n)$ in Fig. 1.9c is zero for all n, whereas the output signal $y_a(n)$ in Fig. 1.9a is not necessarily zero for all n.

1.2.3 Polyphase decomposition

One of the main reasons behind practical usefulness of multirate DSP is the notion of polyphase decomposition [3] [35]. Polyphase decomposition often leads to dramatic enhancements in the computational efficiency of the underlying multirate DSP systems, achieved by realizing the constituent filtering operations at lower sampling rates.

Let us consider a digital filter having a transfer function $H(z) = \sum_{n=-\infty}^{\infty} h(n)z^{-n}$.

Then, the transfer function $H(z)$ can be decomposed in the form

$$\begin{aligned} H(z) = & \sum_{n=-\infty}^{\infty} h(nM)z^{-nM} + z^{-1} \sum_{n=-\infty}^{\infty} h(nM+1)z^{-nM} \\ & + \quad \cdots \quad + z^{-(M-1)} \sum_{n=-\infty}^{\infty} h(nM+M-1)z^{-nM} \end{aligned} \tag{1.10}$$

where M represents a positive integer. Compactly, Eqn. 1.10 can be rewritten as

$$H(z) = \sum_{l=0}^{M-1} z^{-l} E_l(z^M), \tag{1.11}$$

where

$$E_l(z) = \sum_{n=-\infty}^{\infty} e_l(n) z^{-n},$$

with

$$e_l(n) \triangleq h(Mn+l), \quad 0 \leq l \leq M-1.$$

Eqn. 1.11 is called the Type 1 polyphase representation of $H(z)$ (with respect to the factor M) and $E_l(z)$ are the corresponding polyphase components.

A variation of Eqn. 1.11 is given by

$$H(z) = \sum_{l=0}^{M-1} z^{-(M-1-l)} R_l(z^M), \tag{1.12}$$

where

$$R_l(z) = E_{M-1-l}(z)$$

Eqn. 1.12 is called the Type 2 polyphase representation of $H(z)$ and $R_l(z)$ are the corresponding polyphase components.

1.2.4 Perfect Reconstruction property

In multirate DSP, the reconstruction of the original input signal at the system output is subject to several artifacts (apart from the errors due to quantization) because the constituent digital filters are not ideal, and because the decimation and interpolation operations lead to aliasing effects. In this way, the z-transform of the reconstructed signal $\hat{x}(n)$ can be expressed in the form

$$\hat{X}(z) = T(z)X(z) + \text{terms due to alias} \tag{1.13}$$

where $T(z)$ represents the transfer function of the DSP system in the absence of aliasing effects. In certain situations, it may be possible to eliminate the aliasing effects completely (see, e.g., [8]). Then, if $T(z)$ can be forced to be a delay (i.e., if $T(z) = cz^{-n_0}$ for arbitrary n_0), then the alias-free DSP system is said to possess the Perfect Reconstruction (PR) property.

1.3 Applications of multirate DSP systems and filterbanks

1.3.1 Subband Coding

There are wide variety of applications involving multirate DSP, and some of these applications are based on the so-called subband decomposition. Subband decomposition is widely used for Subband Coding (SBC) in speech and music compression as well as in image compression (see, e.g., the classical papers in [11], [1], [37], [38]).

Let us consider a discrete-time signal $x(n)$ having an energy distribution concentrated in the low frequency region. Fig. 1.10 demonstrates the frequency spectrum of such a signal. It is possible to reduce the signal bit-rate by using SBC, where

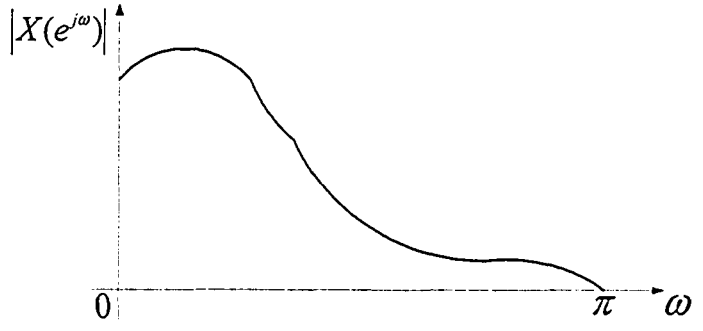

Figure 1.10: A signal with energy distribution concentrated in the low frequency region

the desired SBC can be realized, e.g., by using a QMF filterbank. The signal-flow diagram for a QMF filterbank is shown in Fig. 1.11. Here, the discrete-time signal $x(n)$ is passed through a pair of digital filters $H_k(z)$ called analysis filters having the magnitude-frequency responses shown in Fig. 1.12. The filtered (subband) signals $v_k(n)$ (for $k = 0, 1$) are bandlimited lowpass and highpass signals, respectively. These

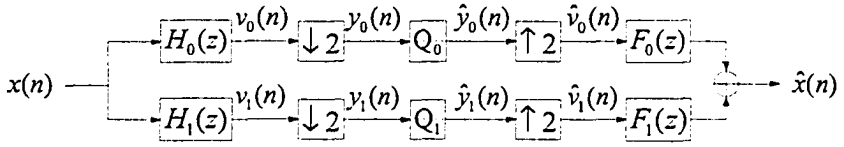

Figure 1.11: The structure of a basic QMF filterbank for SBC

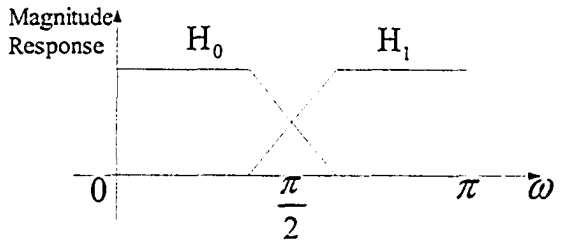

Figure 1.12: The magnitude frequency-response characteristics of analysis filters

signals are subsequently decimated by a factor of two to obtain the signals $y_k(n)$, so that the total sampling rate (in both subbands) is the same as that for the input signal $x(n)$. The decimated subband signals $y_k(n)$ are then quantized and transmitted to the receiver. At the receiver end, the subband signals $y_k(n)$ are recombined by using interpolators and synthesis filters $F_k(z)$, to generate an approximation version $\hat{x}(n)$ of the original signal $x(n)$.

In conventional DSP, the input signal $x(n)$ is quantized uniformly to, say, b bits per sample. In the SBC approach in Fig. 1.11, on the other hand, it is possible to quantize the lower sampling rate signals $y_0(n)$ and $y_1(n)$ to b_0 bits and b_1 bits per sample, respectively, so that the average bit rate is $b = 0.5(b_0 + b_1)$. If the input signal $x(n)$ has predominantly a lowpass characteristic as shown in Fig. 1.10, then one can make $b_0 > b$ and $b_1 < b$. Thus, depending on the frequency-domain energy distribution of the signal $x(n)$, one can allocate appropriate number of bits to subbands, thereby increasing the accuracy of representation of $x(n)$ for a fixed bit-rate b.

Digital music normally employs 16 bits per signal sample (at a sampling rate of 44.1 kHz). By using SBC, major bit-rate reductions can be obtained (compared to the traditional 16 bit representation), with little compromise in quality [37].

The M-channel filterbanks extends the above SBC schemes to more than two

subbands. Thus, a system with M subbands would have M analysis digital filters $H_k(z)$ as shown in Fig. 1.13a. A set of two typical frequency responses for digital filters $H_k(z)$ are sketched in the Fig. 1.13b and 1.13c. One of these, as shown in Fig. 1.13b, has uniform filter bandwidths and spacing, while the other, as shown in Fig. 1.13c, has nonuniform (octave) spacing. The latter is particularly useful in the analysis and coding of speech and music.

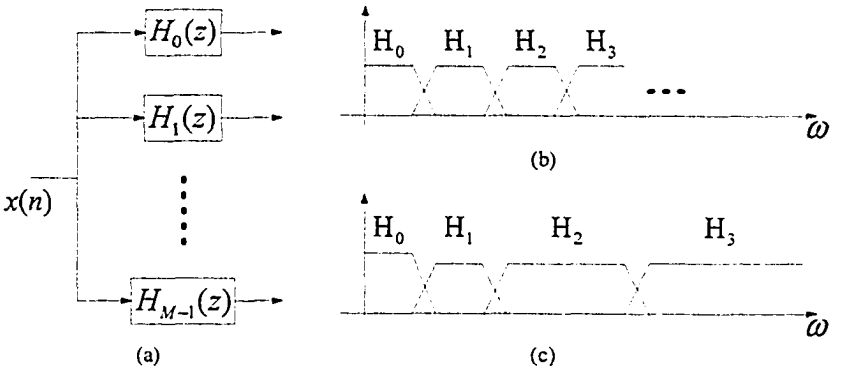

Figure 1.13: M-channel analysis filterbanks

1.3.2 Transmultiplexing

Another important application of multirate DSP is Frequency Division Multiplexing (FDM) in communication systems. Consider Fig. 1.14, where transforms of three signals $x_0(n)$, $x_1(n)$ and $x_2(n)$ are shown in (a), (b) and (c). 1.14d. The FDM signal $y(n)$ is a single composite signal, whose transform $Y(e^{j\omega})$ is obtained by adding the transforms of the individual signals next to each other. Each individual spectrum has to be compressed by a factor of 3, to make room for the three signals in the frequency range $0 \leq \omega < \pi$. The FDM operation can be performed by using the system shown in Fig. 1.14e. Each individual signal is first passed through a interpolator to obtain a 3-fold compression in the frequency domain. The interpolation filters $F_k(z)$ (assumed to be ideal for the sake of this discussion) retain one out of the three images which appear in the signals $X_k(e^{j\omega})$. By summing together the output signals of the three filters $F_k(z)$, one obtains the FDM signal $Y(e^{j\omega})$ as shown in Fig. 1.14d. Fig. 1.15 shows the signal-flow diagram of the complete transmultiplexer. The input signal components $x_k(n)$ can be recovered by separating the adjacent frequency bands of

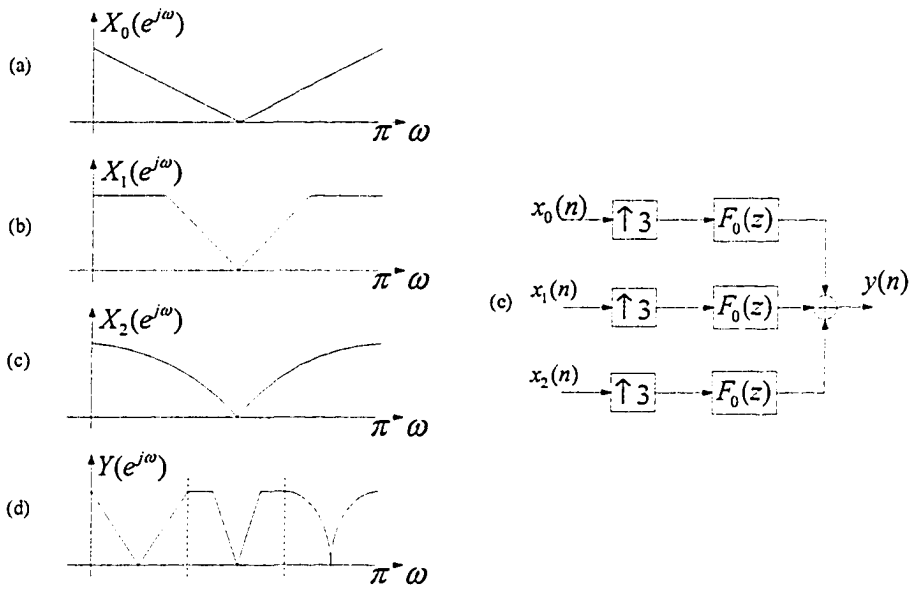

Figure 1.14: A 3-channel synthesis filterbank for transpultiplexing

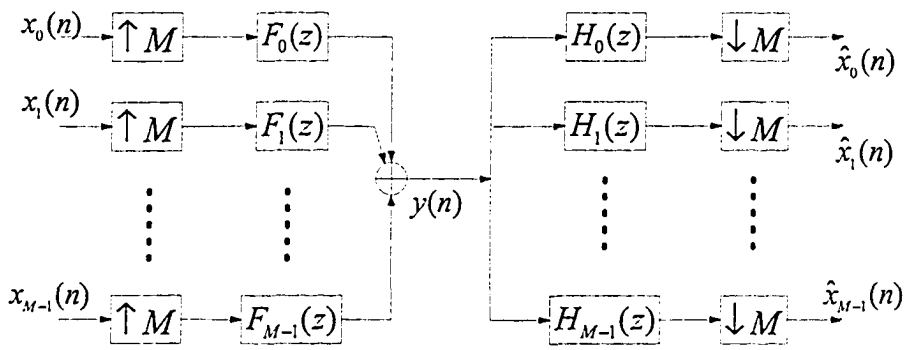

Figure 1.15: M-channel synthesis and analysis filterbanks for transmultiplexing

$Y(e^{j\omega})$ (which correspond to M message signals) with the help of an analysis filters $H_k(z)$ and by decimating the output signals produced by the filters $H_k(z)$.

If the synthesis filters $F_k(z)$ are not ideal, the adjacent frequency bands in 1.14d will tend to overlap. Similarly, if the analysis filters $H_k(z)$ are non-ideal, then the output signals of the filters $H_k(z)$ have contributions from $X_k(e^{j\omega})$ as well as $X_l(e^{j\omega})$, $l \neq k$. Therefore, in general, each of the reconstructed signal components $\hat{x}_k(n)$ has contributions from $x_k(n)$ as well as from the cross-talk terms $x_l(n)$, $l \neq k$. It can be shown that the cross-talk terms can be completely eliminated by careful judicious choice of relationships between the transfer functions of the analysis and synthesis

filters.

1.3.3 Some other applications

DFT filterbanks can be used for spectral analysis instead of traditional technique of Fast Fourier Transform (FFT). Comparing to the traditional FFT spectral analysis, DFT filterbanks can achieve much larger stopband attenuation (where FFT can only achieve a relative stopband attenuation of around 13dB[3]) and more "brick-wall-like" subchannel magnitude-frequency responses. Therefore, DFT filterbank can perform more accurate spectral analysis.

Cosine modulated filterbanks are also very popular filterbanks, mainly due to the fact that they lend themselves to PR reconstruction property. However, the main drawback of these filterbanks is their inherent nonlinear subchannel phase characteristics. This may be difficult or impossible to counteract in the overall filterbank to achieve linear phase characteristics. In contrast, DFT filterbanks preserve linear subchannel phase characteristics while permitting high computational efficiency [3].

Further applications in communications have been reported by others for high-speed analog-to-digital conversion and equalization [5] [36].

1.4 Problem Statement and Thesis Outline

In the conventional DFT filterbanks, the constituent analysis and synthesis filters are derived by shifting the frequency response of the same prototype filter along the frequency axis (so as to cover the entire frequency band). In DFT filterbanks incorporating a large number of subchannels or realizing subchannels with very narrow transition bandwidths, the length of the impulse response of the constituent prototype filter becomes prohibitively large, curtailing the computational efficiency of the filterbank[4]. This thesis is concerned with the development of a pair of novel maximally-decimated filterbanks resolving the aforementioned problems associated with a large number of subchannels or with subchannels with very narrow transition bandwidths, and exhibiting high computational efficiency. The remainder of the

[3]This is due to the fact that the corresponding prototype filter has a rectangular impulse response.

[4]Meanwhile, the design of filterbanks with a long prototype filter needs intense computational endeavor to obtain a filterbank which satisfies the PR reconstruction property.

thesis is organized as follows:

Chapter 2 is concerned with the investigations of various digital filterbanks. The basic QMF filterbanks are first discussed, which gives the conditions for PR reconstruction in QMF filterbanks. By extending the basic QMF filterbanks to M-channel QMF filterbanks and DFT filterbanks, the special case of M-channel QMF filterbanks is introduced. In order to eliminate aliasing effects, the synthesis filters in traditional DFT filterbank have to be much longer than the analysis filters. To circumvent this problem, MDFT filterbanks are introduced. Finally, several filterbank design methods are discussed to realize almost-PR reconstruction property.

Chapter 3 presents a tree-structured critically-decimated filterbank lending itself to a large number of subchannels without any recourse to the problems of the type mentioned above [22] [20]. The signal processing operations in the constituent tree-structured analysis filterbank consists of the decomposition of the input signal into the required number of subband signals, and the subsequent processing by analysis filters which are only required to satisfy mild conditions on their transition bandwidths. The signal processing operations in the constituent tree-structured synthesis filterbank, on the other hand, takes place in such a manner as to ensure PR reconstruction property while using synthesis filters which are the same as the corresponding analysis filters. Application examples are given to illustrate the proposed approach for the design of tree-structured filterbanks incorporating 2, 3 and 6 stages, together with computational complexity comparison with the conventional DFT and modified-DFT filterbanks.

Chapter 4 is concerned with the design and realization of an efficient modified-DFT filterbank employing the Frequency-Response Masking technique [23]. The FRM digital filter design technique is exploited and applied to the design of a novel cascaded DFT filterbank. The resulting DFT filterbanks lend themselves to the realization of selective subchannels with very narrow transition bandwidths. Two application examples are given to illustrate the design of the proposed DFT filterbanks. It is shown that resulting filterbanks entail substantially less computational complexity as compared to the corresponding conventional Modified-DFT filterbanks.

Chapter 5 presents the general conclusions of this thesis as well as suggestions for future work.

Chapter 2

QMF Filterbanks and their M-Channel Extensions

QMF filterbanks were originally introduced by Croisier et al. [8] as a 2-channel filterbank in the mid seventies. After Johnston presented his linear-phase QMF filterbank in [17], the M-channel extensions were developed [31] [6] for a wide variety of applications such as speech and image coding, biomedical signal processing, and transmultiplexer.

In this chapter, an overview of the conventional two-channel QMF filterbanks is first given in Section 2.1, followed by a discussion of their M-channel extensions in Section 2.2. In Section 2.3 and 2.4, the discrete Fourier transform (DFT) filterbanks and the modified-DFT (MDFT) filterbanks are introduced as special classes of QMF filterbanks. Finally, the design of the QMF filterbank to achieve almost-Perfect Reconstruction (PR) is discussed in Section 2.5.

2.1 QMF Filterbanks

This section is concerned with an overview of the basic two-channel QMF filterbanks. After introducing the structure of the QMF filterbanks, a mathematical investigation is undertaken to highlight various types of distortion in the 2-channel QMF filterbanks from its input signal to the corresponding reconstructed output signal. This is subsequently followed by a discussion of the conditions for PR reconstruction property. The interested reader is referred to [33] for further details.

2.1.1 Structure of QMF Filterbanks

The structure of the basic two-channel QMF filterbank is as shown in Fig. 2.1. In the

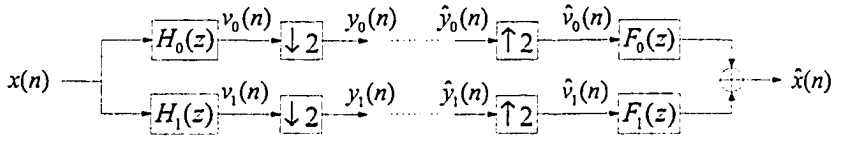

Figure 2.1: The structure of the basic QMF filterbank

QMF filterbank in Fig. 2.1, the input signal $x(n)$ is first filtered by a pair of filters $H_0(z)$ and $H_1(z)$, which are a low-pass and a high-pass filter, respectively. Each filtered (subband) signal $v_k(n)$ (for $k = 0, 1$) is therefore approximately bandlimited to a total width of π (in the frequency region $0 \leq \omega < 2\pi$) as shown in Fig. 1.12. The resulting subband signals are subsequently decimated by a factor of 2 to produce the output subchannel signals $x_k(n)$ for subchannel signal processing.

Since the filters $H_k(z)$ are used for splitting the input signal into subband signals, they are called analysis (or decomposition) filters, and the totality of the filters $H_k(z)$ is call the analysis filterbank.

After subchannel signal processing, each processed subchannel signal is sent to the receiver end for reconstructing the original input signal $x(n)$. First, the received signals $\hat{y}_k(n)$ pass through two-fold interpolators to produce the signals $\hat{v}_k(n)$. The interpolated signals subsequently pass through the filters $F_0(z)$ and $F_1(z)$, and are summed together to obtain the reconstructed signal $\hat{x}(n)$. Here, the filters $F_0(z)$ and $F_1(z)$ are called synthesis (or reconstruction) filters, and the totality of the filters $F_k(z)$ is called synthesis filterbank.

In order to satisfy the PR reconstruction property, the reconstructed signal $\hat{x}(n)$ should be a pure delayed version of the original input signal $x(n)$ in accordance with

$$\hat{x} = x(n - n_0), \quad i.e., \quad \hat{X} = z^{-n_0} X(z). \tag{2.1}$$

2.1.2 Distortions created in the QMF filterbanks

Aliasing and imaging

In practical situations, the analysis filters $H_k(z)$ have nonzero transition bandwidths and stopband gains. The signals $v_k(n)$ are, therefore, not bandlimited, and their

decimation results in aliasing effects. It is easy to find an expression for $\hat{X}(z)$. By inspection of Fig. 2.1, one has

$$V_k(z) = H_k(z)X(z), \quad k = 0, 1 \tag{2.2}$$

The z-transform of the decimated signals $y_k(n)$ are (c.f. Eqn. 1.3)

$$Y_k(z) = \frac{1}{2}[V_k(z^{1/2}) + V_k(-z^{1/2})], \quad k = 0, 1 \tag{2.3}$$

where the second term represents aliasing effects. The z-transform $V_k(z^2)$ of $\hat{v}_k(n)$ is obtained as

$$\begin{aligned} \hat{V}_k(z) = Y_k(z^2) &= \frac{1}{2}[V_k(z) + V_k(-z)] \\ &= \frac{1}{2}[H_k(z)X(z) + H_k(-z)X(-z)], \quad k = 0, 1 \end{aligned} \tag{2.4}$$

Consequently, the reconstructed output signal $\hat{X}(z)$ is given by

$$\begin{aligned} \hat{X}(z) &= F_0(z)\hat{V}_0(z) + F_1(z)\hat{V}_1(z) \\ &= \frac{1}{2}[H_0(z)F_0(z) + H_1(z)F_1(z)]X(z) \\ &+ \frac{1}{2}[H_0(-z)F_0(z) + H_1(-z)F_1(z)]X(-z). \end{aligned} \tag{2.5}$$

The second term containing $X(-z)$ in Eqn. 2.5 is generated due to decimation, representing the aliasing effects. In the following, this term is referred to as the alias component.

By inspection of Eqn. 2.5, it becomes evident that the alias component can be cancelled provided that the analysis filters $H_k(z)$ and the synthesis filters $F_k(z)$ satisfy the constraint [33]

$$H_0(-z)F_0(z) + H_1(-z)F_1(z) = 0 \tag{2.6}$$

This constraint can be satisfied in a straightforward manner by choosing

$$F_0(z) = H_1(-z), \quad F_1(z) = -H_0(-z) \tag{2.7}$$

In this way, for a given pair of analysis filters $H_0(z)$ and $H_1(z)$, it is possible to completely cancel the alias component through the choice of synthesis filters $F_0(z)$ and $F_1(z)$ in Eqn. 2.7, regardless of whether or not $H_0(z)$ and $H_1(z)$ have large transition bandwidths and large stopband gains.

Amplitude and phase distortions

Let us assume that the QMF filterbank is made free from aliasing effects (c.f. Eqn. 2.7). Consequently,

$$\hat{X}(z) = T(z)X(z) \tag{2.8}$$

Therefore, even in the absence of aliasing effects, the reconstructed signal $\hat{x}(n)$ suffers from a Linear Time-Invariant (LTI) distortion via the transfer function

$$T(z) = \frac{1}{2}[H_0(z)F_0(z) + H_1(z)F_1(z)] \tag{2.9}$$

which is called the distortion transfer function (or overall transfer function) of the alias-free filterbank. Let $T(e^{j\omega}) = |T(e^{j\omega})|e^{j\phi(\omega)}$, where $|T(e^{j\omega})|$ represents the magnitude and$\phi(\omega)$ represents the phase of $T(e^{j\omega})$. Then, one has

$$\hat{X}(e^{j\omega}) = |T(e^{j\omega})|e^{j\phi(\omega)}X(e^{j\omega}) \tag{2.10}$$

In this way, unless $T(z)$ is an allpass transfer function (i.e., unless $|T(e^{j\omega})| = d \neq 0$ for all ω), $\hat{X}(e^{j\omega})$ will suffer from amplitude distortion. Similarly, unless $T(z)$ is a linear-phase transfer function (i.e. unless $\phi(\omega) = a + b\omega$ for constant a, b), $\hat{X}(e^{j\omega})$ will suffer from phase distortion.

2.1.3 PR and QMF filterbanks

In the earliest known QMF filterbanks, the analysis filters $H_k(z)$ were interrelated in accordance with [33]

$$H_1(z) = H_0(-z) \tag{2.11}$$

For real $H_0(z)$ and $H_1(-z)$, this means $|H_1(e^{j\omega}) = |H_0(e^{j(\pi-\omega)})|$. In fact, $|H_1(e^{j\omega})$ is a mirror image of $|H_0(e^{j\omega})$ with respect to the quadrature frequency $\pi/2$, hence the name quadrature mirror filters.

If Eqn. 2.7 is used to cancel the alias components, then analysis filter $H_1(z)$ and the synthesis filters $F_0(z)$ and $F_1(z)$ can be completely determined in terms of a filter $H_0(z)$. Subsequently, the distortion function in Eqn. 2.9 can be rewritten as

$$T(z) = \frac{1}{2}(H_0^2(z) - H_0^2(-z)) \tag{2.12}$$

If $H_0(z)$ is realized as a Finite Impulse Response (FIR) filter, then it can be shown that, in order to satisfy the PR reconstruction property, $H_0(z)$ has to be of the simple form [33]

$$H_0(z) = \alpha z^{-2n_0} + \beta z^{-(2n_1+1)} \tag{2.13}$$

whether or not $H_0(z)$ has linear-phase, where n_0 and n_1 are positive integers. In this way, the analysis filters $H_k(z)$ will neither have narrow transition bandwidths nor have small stopband gains.

Due to the poor magnitude-frequency response characteristic of the analysis filter $H_0(z)$ in Eqn. 2.13, in practical situations, one may resort to the design of $H_0(z)$ to ensure that the filterbank has no phase and aliasing distortions. However, this can only be possible at the expense of a slight amplitude distortion [17] [7].

2.2 M-channel QMF filterbanks

The two-channel QMF filterbank structure in Fig. 2.1 can be extended to a more general class of filterbanks, namely M-channel maximally-decimated QMF filterbanks, as shown in Fig. 2.2.

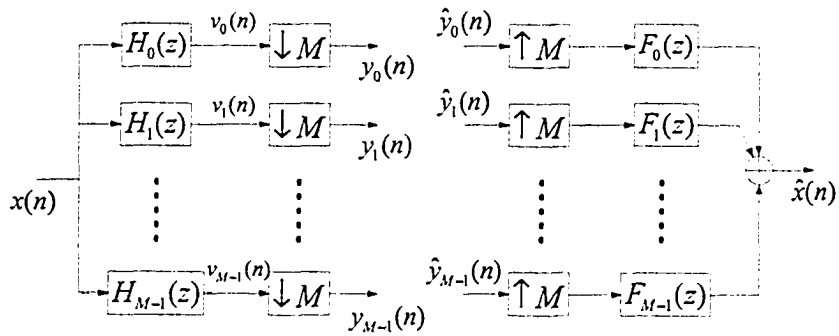

Figure 2.2: The M-channel maximally-decimated filterbank

In the M-channel filterbank in Fig. 2.2, the input signal $x(n)$ is split into M subband signals $v_k(n)$ (for $k = 1, 2, \cdots, M$) by M analysis filters $H_k(z)$. The subband signals $v_k(n)$ are then decimated by a factor M to obtain the signals $y_k(n)$. In the reconstruction stage, the received signals $\hat{y}_k(n)$ are eventually passed through M-fold interpolators, and are recombined via the synthesis filters $F_k(z)$ to produce the reconstructed signal $\hat{x}(n)$.

2.2.1 Derivation of the reconstructed signal

By using z-domain analysis, the subband signals $V_k(z)$ are given by

$$V_k(z) = H_k(z)X(z). \tag{2.14}$$

Consequently, the decimated subchannel output signals $x_k(n)$ have z-transforms

$$Y_k(z) = \frac{1}{M}\sum_{l=0}^{M-1} H_k(z^{1/M}W_M^l)X(z^{1/M}W_M^l), \tag{2.15}$$

where W_M has been defined in Eqn. 1.4. The interpolator output signals are therefore given by

$$U_k(z) = Y_k(z^M) = \frac{1}{M}\sum_{l=0}^{M-1} H_k(zW_M^l)X(zW_M^l), \tag{2.16}$$

giving rise to the reconstructed signal

$$\hat{X}(z) = \frac{1}{M}\sum_{l=0}^{M-1} X(zW_M^l)\sum_{k=0}^{M-1} H_k(zW_M^l)F_k(z). \tag{2.17}$$

More conveniently, this equation can be rewritten as

$$\hat{X}(z) = \sum_{l=0}^{M-1} A_l(z)X(zW_M^l), \tag{2.18}$$

where

$$A_l(z) = \frac{1}{M}\sum_{k=0}^{M-1} H_k(zW_M^l)F_k(z), \quad 0 \le l \le M-1. \tag{2.19}$$

By setting $z = e^{j\omega}$, $X(zW_M^l)$ in Eqn. 2.18 can be written as

$$X(e^{j\omega}W_M^l) = X(e^{j(\omega - \frac{2\pi}{M}l)}) \tag{2.20}$$

For $l \neq 0$, $X(e^{j\omega}W_M^l)$ represents a frequency-shifted version of the signal $X(e^{j\omega})$. Therefore, the reconstructed signal $\hat{X}(e^{j\omega})$ is a linear combination of $X(e^{j\omega})$ and its $M-1$ uniformly frequency-shifted versions.

2.2.2 Distortions created by M-channel QMF filterbank

The reconstructed signal $\hat{x}(n)$ differs from $x(n)$ due to several reasons such as aliasing, amplitude distortion, and phase distortion as explained next.

Aliasing effects

The presence of frequency-shifted versions $X(zW_M^l)$, $l > 0$ is due to the decimation and interpolation operations. $X(zW_M^l)$ is called the lth aliasing term, and $A_l(z)$ in Eqn. 2.18 is the gain for this aliasing term. It is clear that aliasing can be eliminated for every possible input $x(n)$, if, and only if

$$A_l(z) = 0, \quad 1 \leq l \leq M-1. \tag{2.21}$$

Amplitude and phase distortion

Unless the aliasing effects are cancelled, the M-channel QMF bank becomes a Linear Periodically Time-Varing (LPTV) system with a period of M. If the aliasing effects are cancelled (i.e. by forcing $A_l(z) = 0$ for $l > 0$), then

$$\hat{X}(z) = T(z)X(z). \tag{2.22}$$

Here $T(z)$ is the distortion function (or the transfer function) as given by

$$T(z) = A_0(z) = \frac{1}{M}\sum_{k=0}^{M-1} H_k(z)F_k(z). \tag{2.23}$$

Therefore, when aliasing effects are cancelled, the M-channel QMF filterbank is a LTI system with transfer function $T(z)$. If the magnitude-frequency response $|T(e^{j\omega})|$ is not a constant (independently of frequency), then the amplitude distortion exists through the filterbank. If the transfer function $T(z)$ has a nonlinear-phase, then phase distortion exists.

2.2.3 Distortions in matrix notations

Alias Component (AC) matrix

Let us introduce the following vectors in connection with the analysis filterbank, the synthesis filterbank, and the delay chain as

$$\mathbf{h}(z) = \begin{bmatrix} H_0(z) \\ H_1(z) \\ \vdots \\ H_{M-1}(z) \end{bmatrix}, \quad \mathbf{f}(z) = \begin{bmatrix} F_0(z) \\ F_1(z) \\ \vdots \\ F_{M-1}(z) \end{bmatrix}, \quad \mathbf{d}(z) = \begin{bmatrix} 1 \\ z^{-1} \\ \vdots \\ z^{-(M-1)} \end{bmatrix}, \tag{2.24}$$

respectively. Then, Eqn. 2.19 can be rewritten in a matrix-vector form as

$$\begin{bmatrix} A_0(z) \\ A_1(z) \\ \vdots \\ A_{M-1}(z) \end{bmatrix} = \frac{1}{M} \begin{bmatrix} H_0(z) & H_1(z) & \cdots & H_{M-1}(z) \\ H_0(zW_M) & H_1(zW_M) & \cdots & H_{M-1}(zW_M) \\ \vdots & \vdots & \ddots & \vdots \\ H_0(zW_M^{M-1}) & H_1(zW_M^{M-1}) & \cdots & H_{M-1}(zW_M^{M-1}) \end{bmatrix} \begin{bmatrix} F_0(z) \\ F_1(z) \\ \vdots \\ F_{M-1}(z) \end{bmatrix} \tag{2.25}$$

To cancel aliasing effects, all the entries in the left-hand vector (save for the first entry) must be zero, implying

$$\mathbf{H}(z)\mathbf{f}(z) = \mathbf{t}(z) \tag{2.26}$$

where

$$\mathbf{t}(z) = \begin{bmatrix} MA_0(z) \\ 0 \\ \vdots \\ 0 \end{bmatrix} = \begin{bmatrix} MT_0(z) \\ 0 \\ \vdots \\ 0 \end{bmatrix}. \tag{2.27}$$

Here, $M \times M$ matrix $\mathbf{H}(z)$ is called the Alias Component (AC) matrix.

By combining Eqn. 2.18 with Eqn. 2.25, the reconstructed signal $\hat{X}(z)$ can be rewritten as

$$\hat{X}(z) = \mathbf{A}^T(z)\mathbf{x}(z) = \frac{1}{M}\mathbf{f}^T(z)\mathbf{H}^T(z)\mathbf{x}(z), \tag{2.28}$$

where

$$\mathbf{x}(z) = \begin{bmatrix} X(z) \\ X(zW_M) \\ \vdots \\ X(zW_M^{M-1}) \end{bmatrix}. \tag{2.29}$$

It is clear that, given a set of analysis filters $H_k(z)$, it is in principle possible to cancel aliasing effects by solving for the synthesis filters $F_k(z)$ from Eqn. 2.26 in accordance with

$$\mathbf{f}(z) = \mathbf{H}^{-1}(z)t(z), \tag{2.30}$$

provided that the determinant $[\det\{\mathbf{H}(z)\}]$ is not identically zero. Moreover, in order to satisfy the PR reconstruction property, $\mathbf{t}(z)$ is required to be of the form

$$\mathbf{t}(z) = \begin{bmatrix} z^{-n_0} \\ 0 \\ \vdots \\ 0 \end{bmatrix}. \tag{2.31}$$

Polyphase representation of M-channel filterbank

An important advancement in multirate DSP is the notion of the polyphase representation [3] [2] [35]. This representation permits a great simplification of the theoretical results, leading to a computationally efficient implementations of decimation/interpolation filters and filterbanks.

For a given integer M (the fold number of decimation or interpolation), the analysis filters $H_k(z)$ can be decomposed in their Type 1 polyphase form in accordance with

$$H_k(z) = \sum_{l=0}^{M-1} z^{-l} E_{k,l}(z^M) \tag{2.32}$$

By using a vector-matrix notation, the analysis filters $H_k(z)$ can be expressed in the form

$$\begin{bmatrix} H_0(z) \\ H_1(z) \\ \vdots \\ H_{M-1}(z) \end{bmatrix} = \begin{bmatrix} E_{0,0}(z^M) & E_{0,1}(z^M) & \cdots & E_{0,M-1}(z^M) \\ E_{1,0}(z^M) & E_{1,1}(z^M) & \cdots & E_{1,M-1}(z^M) \\ \vdots & \vdots & \ddots & \vdots \\ E_{M-1,0}(z^M) & E_{M-1,1}(z^M) & \cdots & E_{M-1,M-1}(z^M) \end{bmatrix} \begin{bmatrix} 1 \\ z^{-1} \\ \vdots \\ z^{-(M-1)} \end{bmatrix} \tag{2.33}$$

or, more compactly, in the form

$$\mathbf{h}(z) = \mathbf{E}(z^M)\mathbf{d}(z) \tag{2.34}$$

where

$$\mathbf{E}(z) = \begin{bmatrix} E_{0,0}(z) & E_{0,1}(z) & \cdots & E_{0,M-1}(z) \\ E_{1,0}(z) & E_{1,1}(z) & \cdots & E_{1,M-1}(z) \\ \vdots & \vdots & \ddots & \vdots \\ E_{M-1,0}(z) & E_{M-1,1}(z) & \cdots & E_{M-1,M-1}(z) \end{bmatrix} \tag{2.35}$$

and where $\mathbf{h}(z)$ and $\mathbf{e}(z)$ have been defined in Eqn. 2.24. The matrix $\mathbf{E}(z)$ is the $M \times M$ Type 1 polyphase component matrix for the analysis filterbank. Then, the analysis filterbank can be depicted in an alterative way by employing the polyphase representation as shown in Fig. 2.3.

The synthesis filters $F_k(z)$ can be expressed in a similar manner by using Type 2 polyphase decomposition

$$F_k(z) = \sum_{l=0}^{M-1} z^{-(M-1-l} R_{k,l}(z^M) \tag{2.36}$$

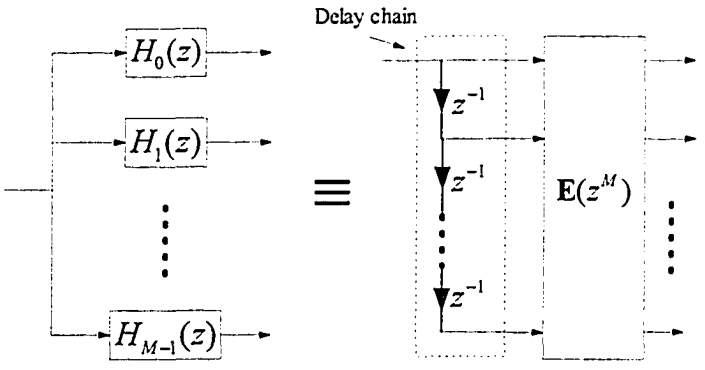

Figure 2.3: Type 1 polyphase representation of a M-channel analysis bank

By using matrix notations, one has

$$\begin{aligned}&[F_0(z) \quad \cdots \quad F_{M-1}(z)] = \\ &[z^{-(M-1)} \quad z^{-(M-1)} \quad \cdots \quad 1] \begin{bmatrix} R_{0,0}(z^M) & R_{0,1}(z^M) & \cdots & R_{0,M-1}(z^M) \\ R_{1,0}(z^M) & R_{1,1}(z^M) & \cdots & R_{1,M-1}(z^M) \\ \vdots & \vdots & \ddots & \vdots \\ R_{M-1,0}(z^M) & R_{M-1,1}(z^M) & \cdots & R_{M-1,M-1}(z^M) \end{bmatrix}\end{aligned} \tag{2.37}$$

In terms of $\mathbf{e}(z)$ and the synthesis filterbank vector $\mathbf{f}^T(z)$ becomes

$$\mathbf{f}^T(z) = z^{-(M-1)}\mathbf{d}^\dagger(z)\mathbf{R}(z^M) \tag{2.38}$$

where $\mathbf{d}^\dagger(z)$ represents the conjugate transposition of $\mathbf{d}(z)$, and where

$$\mathbf{R}(z) = \begin{bmatrix} R_{0,0}(z) & R_{0,1}(z) & \cdots & R_{0,M-1}(z) \\ R_{1,0}(z) & R_{1,1}(z) & \cdots & R_{1,M-1}(z) \\ \vdots & \vdots & \ddots & \vdots \\ R_{M-1,0}(z) & R_{M-1,1}(z) & \cdots & R_{M-1,M-1}(z) \end{bmatrix} \tag{2.39}$$

As a result, the synthesis filterbank can be depicted by using polyphase representation as shown in Fig. 2.4.

By using the above two representations for the filterbank in Fig. 2.2, one arrives at the equivalent representation shown in Fig. 2.5.

In the equivalent filterbank representation in Fig. 2.5, by using noble identities, the decimators can be moved and placed before the Type 1 polyphase matrix $\mathbf{e}(z)$, and the interpolators can be moved and placed after the Type 2 polyphase matrix $\mathbf{R}(z)$. This results in a simplified structure as shown in Fig. 2.6.

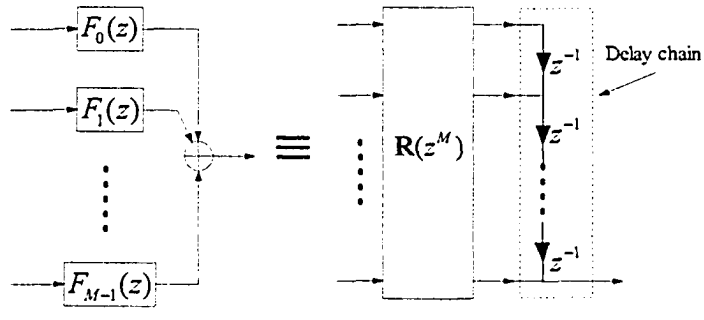

Figure 2.4: Type 2 polyphase representation of a M-channel synthesis bank

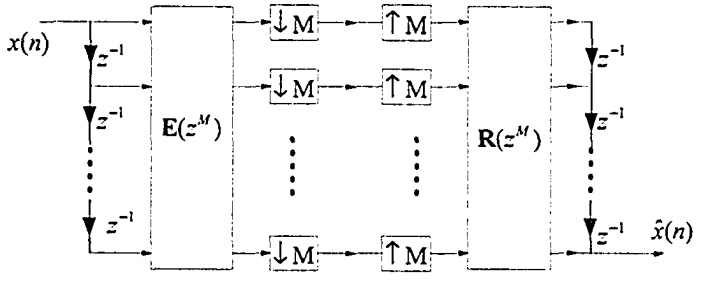

Figure 2.5: Equivalent polyphase representation of an M-channel maximally-decimated filterbank

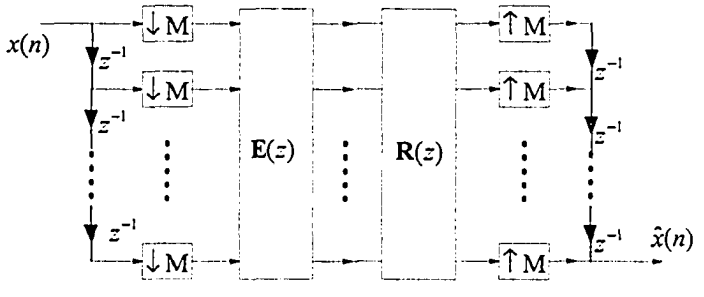

Figure 2.6: Simplified polyphase representation of an M-channel maximally-decimated filterbank

2.3 DFT Filterbanks

In QMF filterbank, the analysis filters $H_k(z)$ (the synthesis filters $F_k(z)$) can be derived by frequency-shifting of a prototype filter $H(z)$ ($F(z)$). This will make possible an efficient implementation of the filterbank. There are two types of popular filterbanks employing this technique: one of these is Cosine-Modulated Filter Bank (CMFB), which uses Discrete Cosine Transform (DCT) to produce the filterbank from the prototype filter; while the other is DFT filterbank, which uses the DFT

operation.

2.3.1 Structure of DFT filterbanks

In DFT filterbanks, the analysis filters $H_k(z)$ are all frequency-shifted versions of a common (baseband) prototype filter $H(z)$. Then,

$$\begin{aligned} H_k(e^{j(\omega-\frac{2\pi}{M})}) &= H(e^{j\omega}) \\ h_k(n) &= e^{j\frac{2\pi}{M}kn}h(n) \end{aligned} \tag{2.40}$$

where $H(e^{j\omega})$ represents the frequency response of the (low-pass) prototype filter, and where $h(n)$ represents its unit-impulse response. Having W_M defined in Eqn. 1.4, one has

$$\begin{aligned} H_k(z) &= H(zW_M^k) \\ h_k(n) &= W_M^{-kn}h(n) \end{aligned} \tag{2.41}$$

By using polyphase decomposition, the prototype filter $H(z)$ can be represented as

$$H(z) = \sum_{l=0}^{M-1} z^{-l}E_l(z^M) \tag{2.42}$$

where $E_l(z)$ are the Type 1 polyphase components of $H(z)$. Through the inspection of Eqn. 2.41, it becomes clear that

$$H_k(z) = \sum_{l=0}^{M-1} z^{-l}W_M^{-lk}E_l(z^M) \tag{2.43}$$

By using diagonal matrix

$$\mathbf{E}(z) = \begin{bmatrix} E_0(z) & 0 & \cdots & 0 \\ 0 & E_1(z) & \cdots & 0 \\ \vdots & \vdots & \ddots & \vdots \\ 0 & 0 & \cdots & E_{M-1}(z) \end{bmatrix} \tag{2.44}$$

to represent the polyphase components of the prototype filter $H(z)$ compactly, Eqn. 2.34 in Section 2.2 can be rewritten as

$$\mathbf{h}(z) = \mathbf{W}^\dagger\mathbf{E}(z^M)\mathbf{d}(z) \tag{2.45}$$

where $\mathbf{W}$ represents the M-point DFT matrix in accordance with

$$\mathbf{W} = \begin{bmatrix} 1 & 1 & \cdots & 1 \\ 1 & W_M & \cdots & W_M^{M-1} \\ \vdots & \vdots & \ddots & \vdots \\ 1 & W_M^{M-1} & \cdots & W_M^{(M-1)(M-1)} \end{bmatrix}, \tag{2.46}$$

and where $\mathbf{W}^\dagger$ represents the conjugate transpose of $\mathbf{W}$. Also,

$$\mathbf{W}^\dagger\mathbf{W} = \mathbf{W}\mathbf{W}^\dagger = M\mathbf{I} \tag{2.47}$$

implying that

$$\mathbf{W}^{-1} = \mathbf{W}^\dagger/M \tag{2.48}$$

For practical implementations, the computation of the matrix $\mathbf{W}$ ($\mathbf{W}^\dagger$) is achieved by using DFT (Inverse Discrete Fourier Transform (IDFT)). The efficiency of the DFT (IDFT) computation can be greatly increased through FFT or high speed convolution algorithms.

By using the above polyphase decomposition, the DFT analysis filterbank can be represented as shown in Fig. 2.7. Then, the analysis filterbank in Fig. 2.7 can be

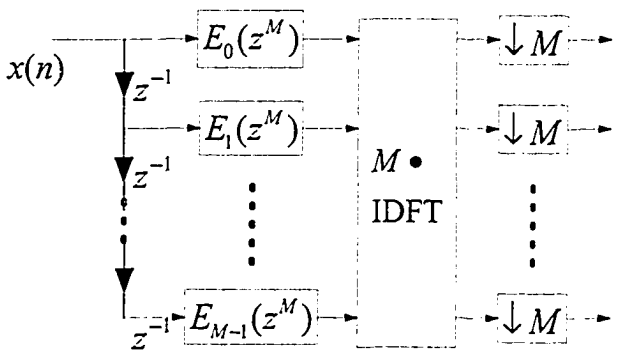

Figure 2.7: Polyphase representation of a maximally-decimated M-channel DFT analysis filterbank

simplified as shown in Fig. 2.8, simply by moving the decimators and placing them before the polyphase components.

The synthesis filters can be expressed in a similar manner as

$$F_k(z) = \sum_{l=0}^{M-1} R_l(z^M) z^{-(M-1-l)} W^{lk} \tag{2.49}$$

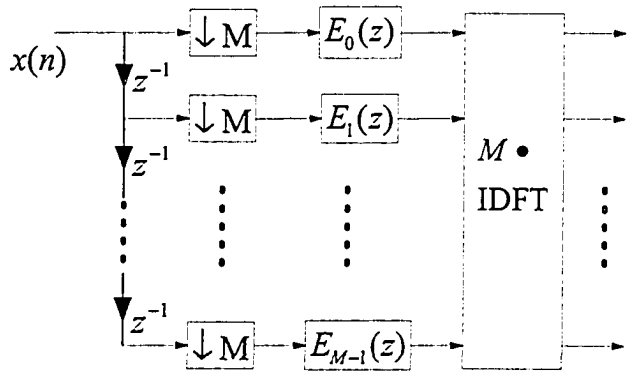

Figure 2.8: Simplified structure of a maximally-decimated M-channel DFT analysis filterbank

where $R_k(z)$ are Type 2 polyphase components of the synthesis prototype filter $F(z)$. More compactly, one has

$$\mathbf{f}^T(z) = z^{-(M-1)}\mathbf{d}^\dagger(z)\mathbf{R}(z^M)\mathbf{W} \tag{2.50}$$

where

$$\mathbf{R}(z) = \begin{bmatrix} R_0(z) & 0 & \cdots & 0 \\ 0 & R_1(z) & \cdots & 0 \\ \vdots & \vdots & \ddots & \vdots \\ 0 & 0 & \cdots & R_{M-1}(z) \end{bmatrix} \tag{2.51}$$

Fig. 2.9 shows the structure of a maximally-decimated M-channel DFT synthesis filterbank.

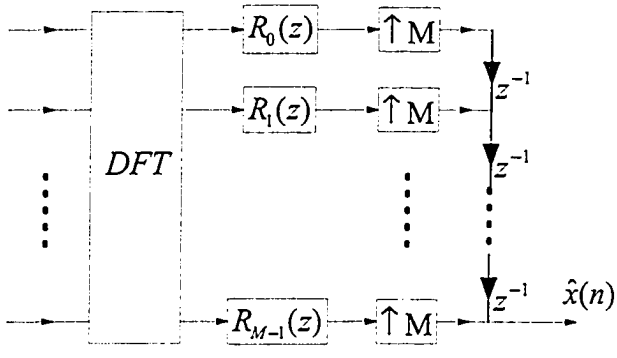

Figure 2.9: The structure of a maximally-decimated M-channel DFT synthesis filterbank

2.3.2 Aliasing cancelation in DFT filterbanks

In the DFT analysis and synthesis filterbanks in Fig. 2.8 and 2.9, there exists a general means for a PR reconstruction of the input signal $x(n)$ (to within constant delay). This means that $\hat{x}(n) = x(n-n_0)$ without any aliasing effects or reconstruction errors. Accordingly, the combination of the analysis and synthesis filterbanks of Fig. 2.8 and 2.9 becomes a LTI system [1], having a transfer function z^{-n_0}.

To place in evidence the process of aliasing cancelation in DFT filterbanks, let us consider a general M-channel multi-rate DSP system as shown in Fig. 2.10. Here, a

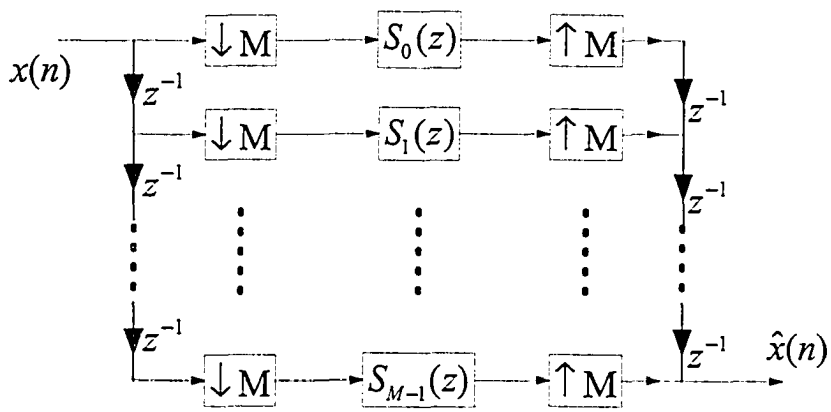

Figure 2.10: A general M-channel multirate DSP system

set of filters with transfer functions $S_k(z)$ are sandwiched between M-fold decimators and M-fold interpolators, where the decimators are preceded by a delay chain, and where the interpolators are followed by a delay chain.

Generally speaking, there is severe aliasing effect in the multi-rate DSP system in Fig. 2.10. However, it may be possible to choose the transfer functions $S_k(z)$ such that the aliasing effects are somehow eliminated by image cancelation caused by the constituent interpolators.

Let us first choose the transfer functions $S_k(z)$ in accordance with

$$S_k(z) = 1 \quad \text{for all } k, \tag{2.52}$$

Then, the decimators and interpolaters do not distort the input signal $x(n)$[2]. Next

[1] This is despite the fact that the constituent decimator and interpolater building blocks are time-varying

[2] In this case, on can formally prove that $\hat{x}(n)a = x(n - M + 1)$

let us choose the transfer functions $S_k(z)$ in accordance with

$$S_k(z) = S(z), \quad \text{for all } k, \tag{2.53}$$

implying that the functions $S_k(z)$ are independent of k, but are otherwise arbitrary. By making use of the noble identities in Section 1.2.2, one can move the transfer functions $S(z)$ successively past the interpolators and past the delay chain. In this way, the reconstructed signal $\hat{X}(z)$ can be expressed as

$$\hat{X}(z) = z^{-(M-1)}S(z^M)X(z). \tag{2.54}$$

Then, the system can be characterized by a transfer function of the form $T(z) = z^{-(M-1)}S(z^M)$, rendering the multirate DSP system as LTI. In particular, aliasing effects have been completely eliminated.

Formally speaking, it is possible to show that in the multirate DSP system in Fig. 2.10, the reconstructed signal $\hat{x}(n)$ is free from aliasing if, and only if, Eqn. 2.53 is satisfied.

Next, by combining the DFT analysis and synthesis filterbanks in Fig. 2.8 and 2.9, the DFT and IDFT building blocks can be combined together and replaced by $M\mathbf{I}$, where the constant M can be moved successively past the transfer function $R_k(z)$, the interpolators, and the delay chain as shown in Fig. 2.11. Consequently, one can

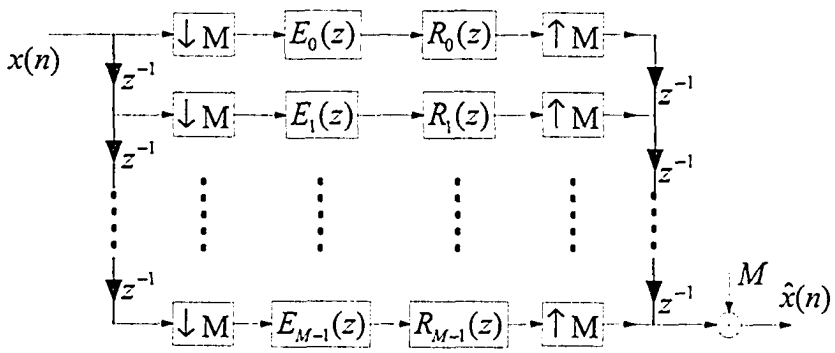

Figure 2.11: The equivalent representation of a maximally-decimated M-channel DFT analysis and synthesis filterbanks

show that the DFT filterbank will be free from aliasing effects provided that

$$E_k(z)R_k(z) = S(z), \quad \text{for all } k \text{ and arbitrary } S(z). \tag{2.55}$$

The technique in [32] provides for an aliasing-free DFT filterbank by satisfying the relationships

$$E_k(z)R_k(z) = \prod_{k=0}^{M-1} E_k(z) \tag{2.56}$$

2.3.3 Reconstruction of the input signal in DFT filterbanks

Having eliminated the aliasing effects in accordance with Eqn. 2.55, the overall transfer function of the DFT filterbank is obtained as

$$T(z) = z^{-(M-1)}S(z^M). \tag{2.57}$$

Then, one can achieve PR reconstruction by satisfying the relationships

$$E_k(z)R_k(z) = z^{-n_0}, \quad \text{for all } k. \tag{2.58}$$

If FIR filters are employed in the DFT analysis and synthesis filterbanks, it is possible to satisfy the PR reconstruction property through simple choices for the functions $E_k(z)$ and $R_k(z)$. However, the resulting prototype filter $H(z)$ may not be capable of producing a high-quality low-pass magnitude-frequency response characteristic. In practical situations, in order to produce such characteristic, it may become necessary to allow either amplitude distortion or phase distortion.

2.4 Modified-DFT Filterbanks

Although the realization of DFT filterbanks shown in Fig. 2.8 and 2.9 are of high computational efficiency, and, therefore, are particularly useful for practical implementations, the lengths of the synthesis filters $F_k(z)$ have to be much longer than those of the analysis filters $H_k(z)$ so as to produce high-quality low-pass magnitude-frequency response characteristic in each subchannel [32]. This problem can be overcome by resorting to Modified-DFT (MDFT) filterbanks [14], [12], [19], [18].

2.4.1 Structure of MDFT filterbanks

A MDFT filterbank is a complex modulated M-channel filterbank with a two-step decimation of the subband signals as shown in Fig. 2.12. The MDFT filterbank in

Fig. 2.12 consists of a decimation by a factor $M/2$ (M must be even), followed by another decimation by a factor 2, and followed by separate processing of the real and imaginary parts of the decimated signals.

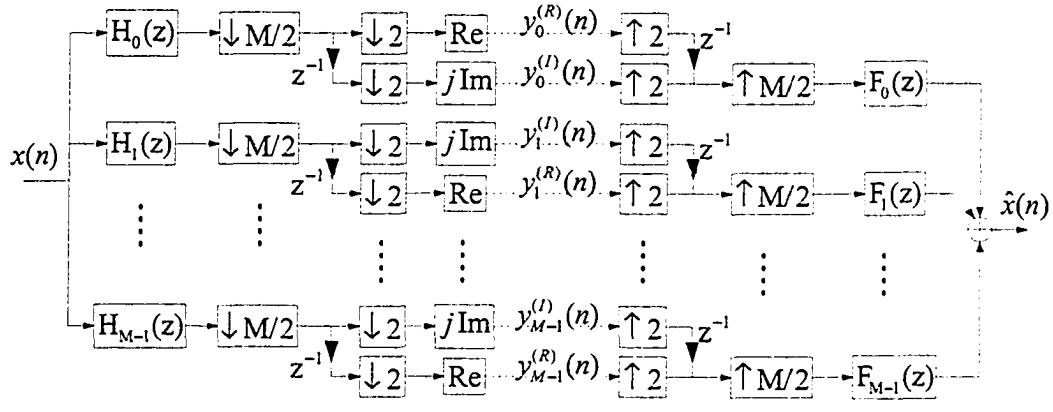

Figure 2.12: The Structure of a M-channel MDFT filterbank

The linear-phase analysis and synthesis filters $H_k(z)$ and $F_k(z)$ are all derived from one common zero-phase low-pass prototype filter $P(z)$ of length N. To achieve this, by using complex modulation, a set of zero-phase filters are derived in accordance with

$$\begin{aligned} P_k(z) &= P(zW_M^k) \\ p_k(n) &= W_M^{-kn} p(n) \end{aligned} \tag{2.59}$$

In order to obtain causal analysis and synthesis filters, the impulse responses $p_k(n)$ are delayed by $(N-1)/2$ samples, giving rise to the time-domain representation

$$\begin{aligned} h_k(n) = p_k(n - \frac{N-1}{2}) = p(n - \frac{N-1}{2}) W_M^{-k(n-(N-1)/2)} \\ \text{for } n = 0, \cdots, N-1, \quad k = 0, \cdots, M-1. \end{aligned} \tag{2.60}$$

of the analysis filters $h_k(n)$. The synthesis filters $f_k(n)$ are identical to the analysis filters $h_k(n)$, leading to

$$H_k(z) = F_k(z) = z^{-(N-1)/2} P(zW_M^k) \tag{2.61}$$

2.4.2 Partial image cancelation property of MDFT filter-banks

The complex input signal $x(n)$ can be expressed as

$$\begin{aligned} x(n) &= x_R(n) + jx_I(n), \quad \text{or} \\ X(z) &= X^{(R)}(z) + X^{(I)}(z) \end{aligned} \tag{2.62}$$

where

$$X^{(R)}(z) = Z\{x_R(n)\}, \quad \text{and } X^{(I)}(z) = Z\{jx_I(n)\} \tag{2.63}$$

Also,

$$\overline{X}(z) = Z\{\overline{x}(n)\} = X^{(R)}(z) - X^{(I)}(z) \tag{2.64}$$

Let us disregard the decimation effects in the subband signals, and concentrate on the consequence of taking the real and imaginary parts of the subband signals in each subchannel [3]:

$$\begin{aligned} &Re\{h_k(n) * x(n)\} \\ &= \frac{1}{2}[h_k(n) + h_k^*(n)] * x_R(n) + \frac{1}{2}[h_k(n) - h_k^*(n)] * jx_I(n) \\ &= \frac{1}{2}[h_k(n) \pm h_{M-k}(n)] * x_R(n) + \frac{1}{2}[h_k(n) \mp h_{M-k}(n)] * jx_I(n) \end{aligned} \tag{2.65}$$

$$\begin{aligned} &jIm\{h_k(n) * x(n)\} \\ &= \frac{1}{2}[h_k(n) - h_k^*(n)] * x_R(n) + \frac{1}{2}[h_k(n) + h_k^*(n)] * jx_I(n) \\ &= \frac{1}{2}[h_k(n) \mp h_{M-k}(n)] * x_R(n) + \frac{1}{2}[h_k(n) \pm h_{M-k}(n)] * jx_I(n) \end{aligned} \tag{2.66}$$

By taking Eqn. 2.62 and 2.64 into account, Eqn. 2.65 and Eqn. 2.66 can be expressed in the z-domain as

$$\begin{aligned} &Z\{Re\{h_k(n) * x(n)\}\} \\ &= \frac{1}{2}[H_k(z) \pm H_{M-k}(z)]X^{(R)}(z) + \frac{1}{2}[H_k(z) \mp H_{M-k}(z)]X^{(I)}(z) \\ &= \frac{1}{2}[H_k(z)X(z) \pm H_{M-k}(z)\overline{X}(z)] \end{aligned} \tag{2.67}$$

$$\begin{aligned} &Z\{jIm\{h_k(n) * x(n)\}\} \\ &= \frac{1}{2}[H_k(z) \mp H_{M-k}(z)]X^{(R)}(z) + \frac{1}{2}[H_k(z) \pm H_{M-k}(z)]X^{(I)}(z) \\ &= \frac{1}{2}[H_k(z)X(z) \mp H_{M-k}(z)\overline{X}(z)] \end{aligned} \tag{2.68}$$

[3] Here, "$\pm$" and "$\mp$" are because of the relationship $h_k^*(n) = \begin{cases} h_{M-k}(n), & \text{for odd } N \\ -h_{M-k}(n), & \text{for even } N \end{cases}$

Next, let us take into account the decimation effects in the subband signals. From Section 1.2.1, the relationship between a signal $a(n)$ and its decimated counterpart $b(n) = a(nM + \lambda)$ can be expressed as

$$z^{-\lambda}B(z^M) = \frac{1}{M}\sum_{l=0}^{M-1} A(zW_M^l)W_M^{\lambda l} \tag{2.69}$$

where λ denotes the phase shift associated with decimation.

In the MDFT filterbank shown in Fig. 2.12, the upper branch of each subband is decimated by the factor M without a phase shift (i.e., without a delay, corresponding to $\lambda = 0$ in Eqn. 2.69), whereas the lower branch is with a delay of $M/2$ samples, corresponding to $\lambda = -M/2$. Hence, by invoking Eqn. 2.69 in Eqn. 2.67 and Eqn. 2.68, one can obtain

$$\begin{aligned} Y_k^{(R)}(z^M) = \frac{1}{2M}\sum_{l=0}^{M-1} &[H_k(zW_M^l)X(zW_M^l) \\ &\pm H_{M-k}(zW_M^l)\overline{X}(zW_M^l)], \quad \text{for even } k \end{aligned} \tag{2.70}$$

$$\begin{aligned} Y_k^{(I)}(z^M) = \frac{1}{2M}\sum_{l=0}^{M-1} &[H_k(zW_M^l)X(zW_M^l) \\ &\mp H_{M-k}(zW_M^l)\overline{X}(zW_M^l)], \quad \text{for odd } k \end{aligned} \tag{2.71}$$

for the M upper branches. Similarly, for the M lower branches, one can obtain

$$\begin{aligned} Y_k^{(R)}(z^M) = \frac{z^{-M/2}}{2M}\sum_{l=0}^{M-1} &[H_k(zW_M^l)X(zW_M^l) \\ &\pm H_{M-k}(zW_M^l)\overline{X}(zW_M^l)]W_M^{-lM/2}, \quad \text{for odd } k \end{aligned} \tag{2.72}$$

$$\begin{aligned} Y_k^{(I)}(z^M) = \frac{z^{-M/2}}{2M}\sum_{l=0}^{M-1} &[H_k(zW_M^l)X(zW_M^l) \\ &\mp H_{M-k}(zW_M^l)\overline{X}(zW_M^l)]W_M^{-lM/2}, \quad \text{for even } k \end{aligned} \tag{2.73}$$

In the synthesis filterbank, the subchannel signals are combined together to produce the reconstructed signal

$$\hat{X}(z) = \sum_{k=0}^{M-1} \hat{X}_k(z), \tag{2.74}$$

where $\hat{X}_k(z)$ represents the output signal of the kth synthesis filter, and where

$$\hat{X}_k(z) = F_k(z)[z^{-M/2}Y_k^{(R)}(z^M) + Y_k^{(I)}(z^M)], \quad \text{for even } k \tag{2.75}$$

$$\hat{X}_k(z) = F_k(z)[Y_k^{(R)}(z^M) + z^{-M/2}Y_k^{(I)}(z^M)], \quad \text{for odd } k \tag{2.76}$$

By substituting Eqns. 2.70, 2.73 into Eqn. 2.75, and by substituting Eqns. 2.72, 2.71 into Eqn. 2.76, and by taking into account the identity $W_M^{-lM/2} = (-1)^l$, one obtains

$$\begin{aligned}\hat{X}_k(z) = \frac{z^{-M/2}}{M} F_k(z) \sum_{l=0}^{M/2-1} [H_k(zW_M^{2l})X(zW_M^{2l}) \\ \pm H_{M-k}(zW_M^{2l+1})\overline{X}(zW_M^{2l+1})], \quad \text{for even } k\end{aligned} \tag{2.77}$$

$$\begin{aligned}\hat{X}_k(z) = \frac{z^{-M/2}}{M} F_k(z) \sum_{l=0}^{M/2-1} [H_k(zW_M^{2l})X(zW_M^{2l}) \\ \mp H_{M-k}(zW_M^{2l+1})\overline{X}(zW_M^{2l+1})], \quad \text{for even } k\end{aligned} \tag{2.78}$$

Therefore, the reconstructed signal $\hat{X}(z)$ is given by

$$\begin{aligned}\hat{X}(z) = \frac{z^{-M/2}}{M} \sum_{k=0}^{M/2-1} F_k(z) \sum_{l=0}^{M/2-1} [H_k(zW_M^{2l})X(zW_M^{2l}) \\ \pm(-1)^k H_{M-k}(zW_M^{2l+1})\overline{X}(zW_M^{2l+1})]\end{aligned} \tag{2.79}$$

Since $F_k(z) = H_k(z)$, one has

$$\sum_{k=0}^{M/2-1} F_k(z) \sum_{l=0}^{M/2-1} \pm(-1)^k H_{M-k}(zW_M^{2l+1})\overline{X}(zW_M^{2l+1})] = 0 \tag{2.80}$$

As a result, Eqn. 2.79 can be rewritten in the form

$$\hat{X}(z) = \frac{z^{-M/2}}{M} \sum_{k=0}^{M/2-1} F_k(z) \sum_{l=0}^{M/2-1} [H_k(zW_M^{2l})X(zW_M^{2l})]. \tag{2.81}$$

Let us consider a non-maximally-decimated DFT filterbank with M subchannels and $M/2$-fold decimation as shown in Fig. 2.13. The reconstructed output signal $\hat{X}_{DFT}(z)$ in this DFT filterbank is given by

$$\hat{X}_{DFT}(z) = \frac{2}{M} \sum_{k=0}^{M-1} F_k(z) \sum_{l=0}^{M/2-1} [H_k(zW_M^{2l})X(zW_M^{2l})]. \tag{2.82}$$

Clearly, the reconstructed output signal $\hat{X}(z)$ of the maximally-decimated M-channel MDFT filterbank in Fig. 2.12 is the same as the reconstructed output signal $\hat{X}_{DFT}(z)$ of the DFT filterbank in Fig. 2.13 except for a scaling factor and an additional time delay.

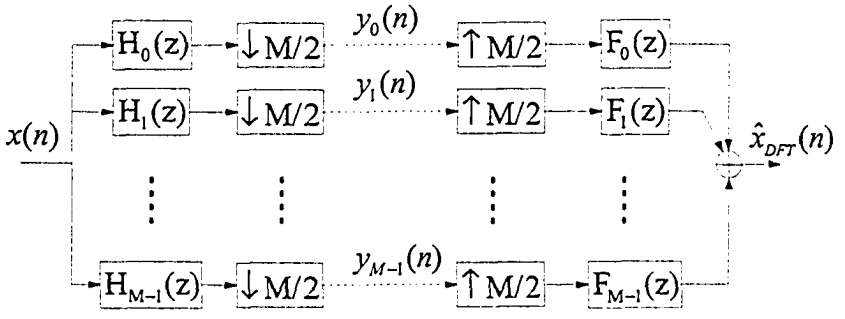

Figure 2.13: The M-channel Discrete Fourier Transform filterbank with $M/2$-fold decimation

2.5 Design of the Pseudo-QMF Filterbanks

Pseudo-QMF filterbanks are a class of QMF filterbanks which achieve PR reconstruction property approximately [28]. Several efficient methods have been put forward that facilitate the design of the prototype filters $P(z)$ for pseudo-QMF filterbanks. The technique proposed in [27] establishes a relationship between an Mth band filter and a set of quadratic constraints on the unit-impulse response coefficients of $P(z)$. These constraints and the stopband attenuation of the prototype filter $P(z)$ are subsequently minimized.

The above technique makes the filterbank extremely close to satisfying the PR reconstruction property. However, due to the underlying quadratic programming and quadratic constraints, the design of the prototype filter $P(z)$ requires a great deal of computational effort. By a slight compromise on the achievable PR reconstruction property, several approaches with simpler optimization cost functions have been developed. Among those approaches, windowing approach provides an efficient design for the prototype filter $P(z)$ of the pseudo-QMF filterbanks.

In the following, an overview is given of the optimizations based on the windowing approach together with nonlinear optimization.

2.5.1 Windowing approach to the design of the prototype filter

Because the analysis and synthesis filters $H_k(z)$ and $F_k(z)$ are modulated versions of a lowpass prototype filter $P(z)$ in pseudo-QMF filterbanks, the design of the overall

filterbank reduces to that of the prototype filter $P(z)$. Let us assume that the prototype filter $P(z)$ has a linear-phase characteristic. Then, the conditions for almost-PR can be stated in terms of the frequency response $P(e^{j\omega})$ as [31]:

$$|P(e^{j\omega})| \approx 0, \quad for|\omega| > 2\pi/M \tag{2.83}$$

$$T(e^{j\omega}) \approx 1, \tag{2.84}$$

where

$$T(e^{j\omega}) = \sum_{k=0}^{M-1} |P(e^{j(\omega-2k\pi/M)})|^2 \tag{2.85}$$

Therefore, provided that the prototype filter $P(z)$ satisfies the condition that $P^2(z)$ is a Mth band filter, the aliasing effects are eliminated approximately (c.f. Eqn. 2.83), resulting in a transfer function approximating a delay(c.f. Eqn. 2.84).

Let $P(z) = \sum_{n=0}^{N-1} p(n)z^{-n}$ be a real-coefficient, linear-phase digital filter of length N. Then, the corresponding Mth band filter $G(z)$ is given by

$$G(z) = P^2(z) = \sum_{n=0}^{2N-2} g(n)z^{-n} \tag{2.86}$$

satisfying

$$g(n) = \begin{cases} 0; & n = N-1-kM \\ \frac{1}{M}; & n = N-1. \end{cases} \tag{2.87}$$

The prototype filter $P(z)$ can be designed by a windowing technique, for example, by using the Kaiser window [25] or the Blackman window [9] techniques. As a result, the subchannel frequency characteristics of $P(z)$, e.g. its stopband attenuation and transition bandwidth, can be determined by the parameters of the windowing techniques at the outset. In this way, from Eqn. 2.87, a simple objective function can be chosen for optimization as given by

$$\phi = \max_k |g(N-1-kM)|, \quad \text{for } 1 \leq k \leq \frac{N-1}{M} \tag{2.88}$$

By adjusting the cutoff frequency ω_c, the best $p(n)$ is to be found to yield the smallest ϕ.

2.5.2 Nonlinear constrained optimization for prototype filter design

This design method [27] is best considered separately for the cases of an even-length and an odd-length prototype filter.

The case of an even-length prototype filter

By having the length of the prototype filter $N = 2(mM+m_1)$, where $0 \leq m_1 \leq M-1$, the vector $\mathbf{p}$ is defined to consist of the coefficients of the linear-phase prototype filter $p(n)$ as

$$\mathbf{p} = \begin{bmatrix} p(0) & p(1) & \cdots & p(mM+m_1-1) \end{bmatrix}^T \tag{2.89}$$

where $\mathbf{e}(z)$ is defined to be

$$\mathbf{e}(z) = \begin{bmatrix} 1 & z^{-1} & \cdots & z^{-(mM+m_1-1)} \end{bmatrix}^T \tag{2.90}$$

Then, the prototype filter $P(z)$ can be represented as

$$P(z) = \mathbf{p}^T \begin{bmatrix} \mathbf{I} & \mathbf{J} \end{bmatrix} \begin{bmatrix} \mathbf{e}(z) \\ z^{-(mM+m_1)}\mathbf{e}(z) \end{bmatrix} \tag{2.91}$$

where $\mathbf{I}$ is $m \times m$ identity matrix and $\mathbf{J}$ is $m \times m$ reverse identity matrix defined as

$$\mathbf{J} = \begin{bmatrix} 0 & \cdots & 0 & 1 \\ 0 & \cdots & 1 & 0 \\ \vdots & \ddots & \vdots & \vdots \\ 1 & \cdots & 0 & 0 \end{bmatrix} \tag{2.92}$$

In this way, the Mth band filter $G(z)$ is given by

$$\begin{aligned} G(z) &= \sum_{n=0}^{4mM+4m_1-2} g(n)z^{-n} = P^2(z) \\ &= \mathbf{p}^T \begin{bmatrix} \mathbf{I} & \mathbf{J} \end{bmatrix} \begin{bmatrix} \mathbf{e}(z) \\ z^{-(mM+m_1)}\mathbf{e}(z) \end{bmatrix} \begin{bmatrix} \mathbf{e}^T(z) & z^{-(mM+m_1)}\mathbf{e}^T(z) \end{bmatrix} \begin{bmatrix} \mathbf{I} \\ \mathbf{J} \end{bmatrix} \mathbf{p} \\ &= \mathbf{p}^T[\mathbf{U}(z) + z^{-(mM+m_1)}(\mathbf{JU}(z) + \mathbf{U}(z)\mathbf{J}) + z^{-2(mM+m_1)}\mathbf{JU}(z)\mathbf{J}]\mathbf{p} \end{aligned} \tag{2.93}$$

where

$$\begin{aligned} \mathbf{U}(z) = \mathbf{e}(z)\mathbf{e}^T(z) &= \begin{bmatrix} 1 \\ z^{-1} \\ \vdots \\ z^{-(mM+m_1-1)} \end{bmatrix} \begin{bmatrix} 1 & z^{-1} & \cdots & z^{-(mM+m_1-1)} \end{bmatrix} \\ &= \sum_{n=0}^{4mM+4m_1-2} z^{-n}\mathbf{S}_n \end{aligned} \tag{2.94}$$

It can be shown that the matrices $\mathbf{S}_n$ are constant matrices with elements 0 and 1 as given by

$$[\mathbf{S}_n]_{k,l} = \begin{cases} 1, & k+l=n \\ 0, & \text{otherwise} \end{cases} \tag{2.95}$$

Then, $G(z)$ can be expressed in terms of $\mathbf{S}_n$ as given by

$$\begin{aligned} G(z) &= \sum_{n=0}^{4mM+4m_1-2} z^{-n} g(n) \\ &= \mathbf{p}^T [\sum_{n=0}^{2mM+2m_1-2} z^{-n}\mathbf{S}_n + z^{-(mM+m_1)} (\mathbf{J} \sum_{n=0}^{2mM+2m_1-2} z^{-n}\mathbf{S}_n \\ &\quad + \sum_{n=0}^{2mM+2m_1-2} z^{-n}\mathbf{S}_n\mathbf{J}) + z^{-2(mM+m_1)}\mathbf{J} \sum_{n=0}^{2mM+2m_1-2} z^{-n}\mathbf{S}_n\mathbf{J}]\mathbf{p} \\ &= \sum_{n=0}^{4mM+4m_1-2} z^{-n}\mathbf{p}^T\mathbf{D}_n\mathbf{p} \end{aligned} \tag{2.96}$$

where $\mathbf{D}_n$ depends on $\mathbf{S}_n$ and $\mathbf{J}$ as follows:

$$\mathbf{D}_n = \begin{cases} \mathbf{S}_n; \quad 0 \le n \le mM+m_1-1 \\ \mathbf{S}_n + \mathbf{J}\mathbf{S}_{n-mM-m_1} + \mathbf{S}_{n-mM-m_1}\mathbf{J}; \\ \quad mM+m_1 \le n \le 2(mM+m_1-1) \\ \mathbf{J}\mathbf{S}_{mM+m_1-1} + \mathbf{S}_{mM+m_1-1}\mathbf{J}; \quad n = 2(mM+m_1)-1 \\ \mathbf{J}\mathbf{S}_{n-mM-m_1} + \mathbf{S}_{n-mM-m_1}\mathbf{J} + \mathbf{J}\mathbf{S}_{n-2mM-2m_1}\mathbf{J}; \\ \quad 2(mM+m_1) \le n \le 3(mM+m_1)-2 \\ \mathbf{J}\mathbf{S}_{n-2mM-2m_1}\mathbf{J}; \quad 3(mM+m_1)-1 \le n \le 4(mM+m_1)-2 \end{cases} \tag{2.97}$$

Therefore, the coefficients of $G(z)$ are obtained as

$$g(n) = \mathbf{p}^T\mathbf{D}_n\mathbf{p} \tag{2.98}$$

In order to find $\mathbf{p}$ such that $G(z)$ is a Mth band filter satisfying Eqn. 2.87, the following m constraints on $\mathbf{p}$ must be satisfied.

$$\begin{cases} \mathbf{p}^T\mathbf{S}_n\mathbf{p} = 0; \quad 0 \le n \le mM+m_1-1 \\ \mathbf{p}^T(\mathbf{S}_n + \mathbf{J}\mathbf{S}_{n-mM-m_1} + \mathbf{S}_{n-mM-m_1}\mathbf{J})\mathbf{p} = 0; \\ \quad mM+m_1 \le n \le 2(mM+m_1-1) \\ \mathbf{p}^T(\mathbf{J}\mathbf{S}_{mM+m_1-1} + \mathbf{S}_{mM+m_1-1}\mathbf{J})\mathbf{p} = \frac{1}{M} \end{cases} \tag{2.99}$$

In addition to the above constraints, $\mathbf{p}$ should also yield the prototype filter $P(z)$ with an acceptable stopband attenuation, i.e. $\mathbf{p}$ should minimize

$$\int_{\omega_s}^{\pi} |P(e^{j\omega})|^2 dw \tag{2.100}$$

where ω_s is the stopband-edge frequency of the prototype filter $H(z)$. The eigenfilter method [34], [26] represents the above integral as a quadratic form in accordance with

$$\int_{\omega_s}^{\pi} |P(e^{j\omega})|^2 dw = \mathbf{p}^T \mathbf{P} \mathbf{p} \tag{2.101}$$

where

$$[\mathbf{P}]_{k,l} = \int_{\omega_s}^{\pi} [\cos(k-l) + \cos(N-1-k-l)] dw, \quad 0 \leq k, l \leq mM + m_1 - 1 \tag{2.102}$$

The case of an odd length prototype filter

In this case, the length of the prototype filter is $N = 2(mM + m_1) + 1$, and the coefficient vector $\mathbf{p}$ for the prototype filter $P(z)$ is given by

$$\mathbf{p} = \begin{bmatrix} 2p(0) & 2p(1) & \cdots & 2p(mM + m_1 - 1) & p(mM + m_1) \end{bmatrix}^T \tag{2.103}$$

Through similar constraints on $\mathbf{p}$ can be obtained as

$$\begin{cases} \mathbf{p}^T \mathbf{S}_n \mathbf{p} = 0; \quad 0 \leq n \leq mM + m_1 - 1 \\ \mathbf{p}^T (\mathbf{S}_n + \mathbf{J}\mathbf{S}_{n-mM-m_1} + \mathbf{S}_{n-mM-m_1}\mathbf{J})\mathbf{p} = 0; \\ \quad mM + m_1 \leq n \leq 2(mM + m_1 - 1) \\ \mathbf{p}^T (\mathbf{J}\mathbf{S}_{mM+m_1-1} + \mathbf{S}_{mM+m_1-1}\mathbf{J})\mathbf{p} = \frac{1}{M} \quad = 0; \\ \quad \begin{cases} mM + m_1 \leq n \leq 2(mM + m_1 - 1) \\ \mathbf{p}^T (\mathbf{J}\mathbf{S}_{mM+m_1-1} + \mathbf{S}_{mM+m_1-1}\mathbf{J})\mathbf{p} = \frac{1}{M} \end{cases} \end{cases} \tag{2.104}$$

In order to have an acceptable stopband attenuation, $\mathbf{p}$ should have the same objective function as given by Eqn. 2.101.

2.6 Conclusions

In Section 2.1, an overview was given of the conventional 2-channel QMF filterbanks followed by an overview of their M-channel extensions in Section 2.2. A mathematical investigation was also undertaken to highlight various types of distortion in the reconstructed output signal in QMF filterbanks. In Section 2.3, DFT filterbanks were introduced as a special class of QMF filterbanks which are capable of maintaining a high computational efficiency in their hardware implementations. It was pointed out that in conventional DFT filterbanks, in order to produce high-quality low-pass magnitude-frequency response characteristics in the constituent subchannels, the lengths of the synthesis filters have to be much longer than those of the

analysis filters. In Section 2.4, MDFT filterbanks were introduced to overcome the aforementioned problem. Finally, the design of the QMF filterbanks capable of achieving the almost-PR reconstruction property was investigated in Section 2.5 by using windowing as well as nonlinear optimization techniques.

Chapter 3

The Multistage Interleaved Tree-Structured Filterbanks

In the conventional DFT filterbanks, the required transition bandwidth of the constituent prototype digital filter becomes narrower with increasing the number of subchannels. This happens at the expense of making the order of the prototype digital filter larger (relative to the number of subchannels), rendering the corresponding hardware implementation of the filterbank impractical beyond a certain number of subchannels.

This chapter presents a novel maximally-decimated multistage interleaved tree-structured filterbank. The resulting tree-structured filterbanks circumvent the above mentioned problem associated with a large number of subchannels, while satisfying the perfect reconstruction (PR) property to within acceptable approximations (0.1dB). The proposed filterbank incorporates identical subfilters at each stage of the tree-structured filterbank, permitting the application of interleaving techniques to implement the identical subfilters as but one subfilter. This gives rise to a reduction in the number of subfilters from $2^L - 1$ to $L - 1$ in the hardware implementation, where L represents the total number of stages (with $M = 2^L$ representing the total number of subchannels).

The remainder of the chapter is organized as follows. The proposed multistage tree-structured filterbank is introduced in Section 3.1. In Section 3.2, it is shown that half of the image components as generated due to a maximal decimation are automatically cancelled in the reconstructed output signal. Section 3.3 is concerned with the design of the tree-structured filterbank for suppressing the the remaining image com-

ponents, so as to render the filterbank as almost perfect reconstruction. Section 3.4 concerned with a practical hardware implementation of the proposed tree-structured filterbank based on the polyphase decomposition of the analysis and synthesis digital filters on one hand, and based on the application of interleaving techniques to the tree-structured filterbank, on the other. Section 3.5 is concerned with a computational investigation of deviations from PR property for 2-stage, 3-stage, and 6-stage tree-structured filterbanks, and with a comparison of the computational complexity of 4-stage, 5-stage, and 6-stage tree-structured filterbanks with the corresponding DFT and MDFT filterbanks.

3.1 The Proposed Tree-Structured Filterbank

The signal-flow diagram in Fig. 3.1 shows the proposed tree-structured filterbank, consisting of a L-stage analysis filterbank. The corresponding mirror image L-stage synthesis filterbank is shown in Fig. 3.2.

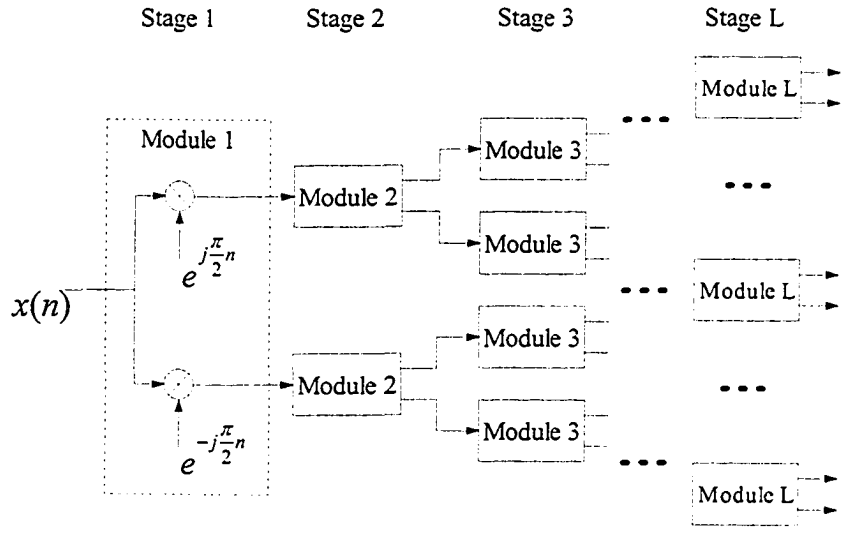

Figure 3.1: Multistage tree-structured analysis filterbank

The internal structures for analysis *Stage* 1 and synthesis *Stage* 1′ are as shown in Figs. 3.1 and 3.2, respectively. The structures for the 2^{l-1} intermediate analysis *Stage* l modules and the 2^{l-1} synthesis *Stage* l' modules are as shown in Figs. 3.3 and Fig. 3.4, respectively, where $H_l(z)$ represents an analysis digital filter in the *Stage*

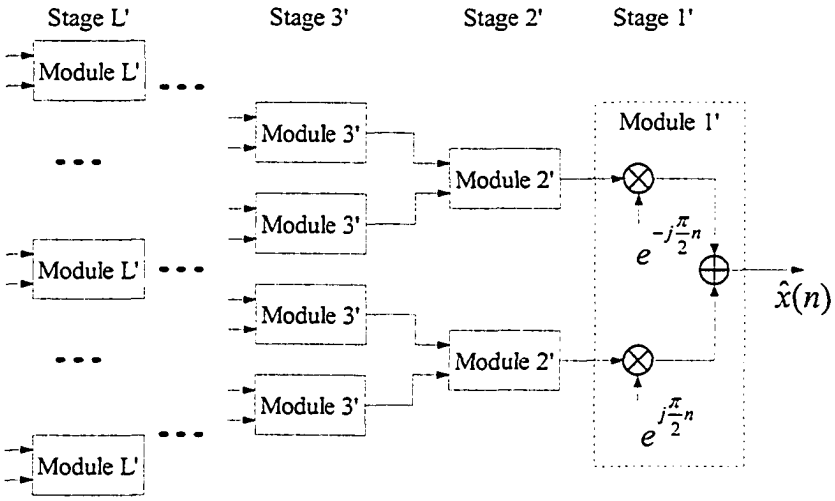

Figure 3.2: Multistage tree-structured synthesis filterbank

l modules, and where $F_l(z)$ represents the corresponding synthesis digital filter in *Stage* l' modules (for $l = 2, 3, \ldots, L-1$). Moreover, all the analysis digital filters $H_l(z)$ in *Stage* l modules and all the synthesis digital filters $F_l(z)$ *Stage* l' modules are assumed to be symmetric FIR digital filters to ensure the linear-phase property in each subchannel.

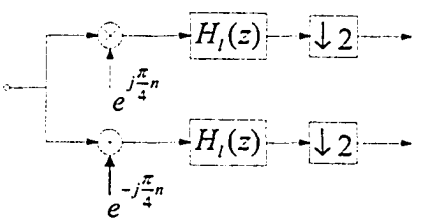

Figure 3.3: Intermediate *Stage* l modules for analysis filterbanks

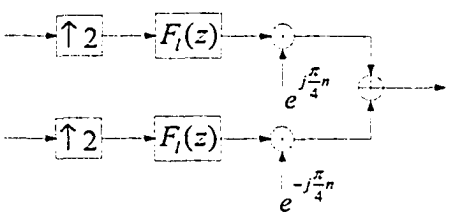

Figure 3.4: Intermediate *Stage* l' modules for synthesis filterbanks

The analysis filterbank: The purpose of analysis *Stage* 1 is to shift the frequency

band into two bands through modulation by complex exponentials $e^{\pm j\frac{\pi}{2}n}$, with the resulting positive and negative frequency-shifted bands to be processed in *Stage* 2 modules. In the intermediate decomposition *Stage* l modules, the input signal to each module which occupies a frequency band of $[-\frac{\pi}{2}, \frac{\pi}{2}]$ is first modulated by complex exponentials $e^{\pm j\frac{\pi}{4}n}$ respectively, and then the resulting two modulated signals are made to occupy the frequency band $[-\frac{\pi}{4}, \frac{\pi}{4}]$ through image suppressing by digital filters $H_l(z)$. Finally, after a two-fold decimation, the module output signals will occupy the frequency band $[-\frac{\pi}{2}, \frac{\pi}{2}]$. Due to the absence of decimation in *Stage* 1, the whole system operates at a rate twice that of the input signal sampling rate. An additional 2-fold decimation operation is included in *Stage* L modules as shown in Fig. 3.5 to expand the frequency band of each subchannel signal to $[-\pi, \pi]$ to achieve maximal decimation [19].

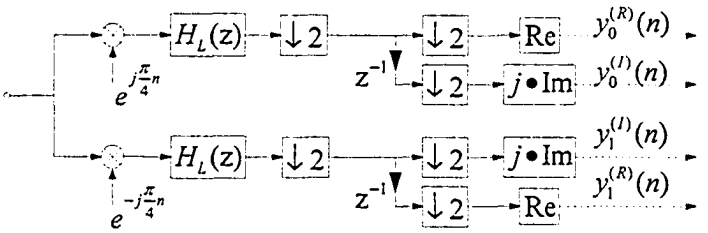

Figure 3.5: Internal structure of *Stage* L modules

The synthesis filterbank: In the intermediate reconstruction *Stage* l' modules, the two input signals to each module are first interpolated by a factor of 2 to occupy the frequency band $[-\frac{\pi}{4}, \frac{\pi}{4}]$, and then the resulting image components are eliminated by the digital filters $F_l(z)$. Finally, the resulting two signals are modulated by $e^{\pm j\frac{\pi}{4}n}$, and combined to form the module output signal which occupies the frequency band $[-\frac{\pi}{2}, \frac{\pi}{2}]$. The purpose of *Stage* 1′ is to demodulate the two input signals by $e^{\pm j\frac{\pi}{2}n}$, and to combine the resulting two signals to obtain the reconstructed output signal. An additional 2-fold interpolation operation is included in *Stage* L' modules as shown in Fig. 3.6, to shrink the frequency band of the combination of the two subchannel input signals into an output signal occupying the frequency band $[-\frac{\pi}{2}, \frac{\pi}{2}]$.

In order to simplify the following discussions, let us refer to the combination of modules from the analysis *Stage* l to the corresponding synthesis *Stage* l' as the l-th

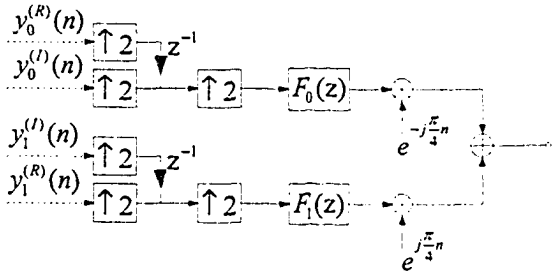

Figure 3.6: Internal structure of *Stage L'* modules

subsystem in the filterbank. In this way, in a tree-structured filterbank consisting of L analysis stages and L synthesis stages, there are 2^{L-1} L-th subsystems, each having a structure as shown in Fig. 3.7. Then, a $(L-1)$-th subsystem can be represented by

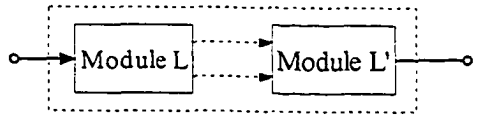

Figure 3.7: L-th subsystem structure

a *Stage* $(L-1)$ module, a *Stage* $(L-1)'$ module and two L-th subsystems as shown in Fig. 3.8. In this way, there are 2^{l-1} l-th subsystems, where each l-th subsystem

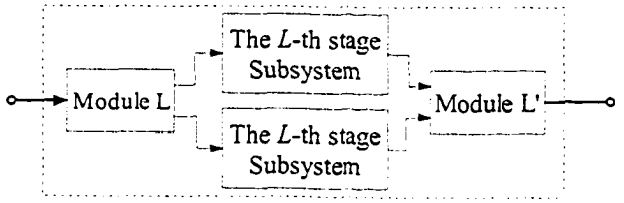

Figure 3.8: $(L-1)$-th subsystem structure

consists of a *Stage* l module, a *Stage* l' module and two $(l+1)$-th subsystems. [1]

3.2 Partial Image Cancelation Due to Anti-Phasing

In general, in a maximally-decimated tree-structured filterbank consisting of L stages, a total of 2^L image components are generated at each of the analysis filterbank outputs. Of these 2^L image components, one image constitutes a wanted component. In

[1] When $l = 1$, the subsystem becomes the entire filterbank including both the analysis and synthesis sides.

this section it is shown that out of the remaining $2^L - 1$ unwanted image components, a total of 2^{L-1} components are automatically canceled by anti-phasing provided that $H_l(z) = F_l(z)$ (for $l = 2, \cdots, L$).

3.2.1 Image cancelation in the L-th subsystem

Let us represent the details of the L-th subsystem in Fig. 3.7 as shown in Fig. 3.9. In the following, it is shown that the L-th subsystem generates 2 conjugated image

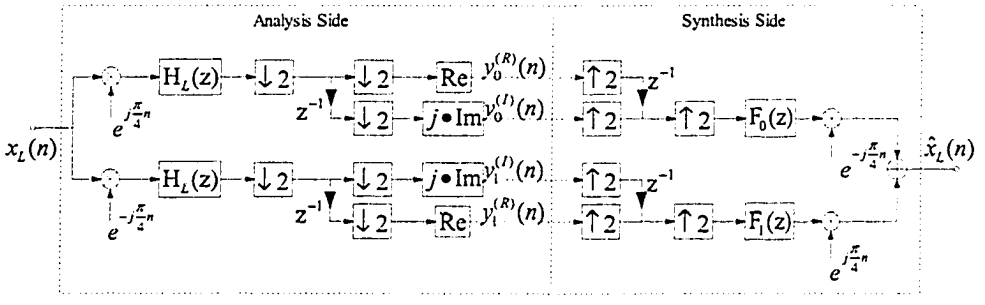

Figure 3.9: Detailed structure of the L-th subsystem

components of the subsystem input signal $X_L(z)$, and that one of these conjugated image components is canceled automatically (by anti-phasing).

Let us decompose the L-th subsystem input signal $x_L(n)$ into its real part $x_{L,R}(n)$ and its imaginary part $x_{L,I}(n)$ in accordance with

$$x_L(n) = x_{L,R}(n) + jx_{L,I}(n) \tag{3.1}$$

Then, by applying z-transform to both sides of Eqn. 3.1, one obtains

$$X_L(z) = X_{L,R}(z) + X_{L,I}(z) \tag{3.2}$$

where $X_{L,R}(z)$ represents the z-transform of $x_{L,R}(n)$, and $X_{L,I}(z)$ represents the z-transform of $jx_{L,I}(n)$. In this way, one can write

$$\begin{aligned} X_{L,R}(z) &= \frac{1}{2}\left[X_L(z) + \overline{X}_L(z)\right] \\ X_{L,I}(z) &= \frac{1}{2}\left[X_L(z) - \overline{X}_L(z)\right] \end{aligned} \tag{3.3}$$

where

$$\overline{X}_L(z) = X_{L,R}(z) - X_{L,I}(z) \tag{3.4}$$

represents the complex conjugate of $X_L(z)$ (treating z as if it were a real quantity).

In the analysis side of the L-th subsystem in Fig. 3.9, the input signal $x_L(n)$ is modulated by the complex exponentials $e^{\pm j\frac{\pi}{4}n}$ to generate the signals

$$\begin{aligned} X_{L0}(z) &= X_L\left(zW_4^{0.5}\right) \\ X_{L1}(z) &= X_L\left(zW_4^{-0.5}\right) \end{aligned} \tag{3.5}$$

Let us represent the complex conjugates of the signals $X_{L0}(z)$ and $X_{L1}(z)$ by

$$\overline{X}_{L0}(z) = \overline{X}_L\left(zW_4^{-0.5}\right) \tag{3.6}$$

and

$$\overline{X}_{L1}(z) = \overline{X}_L\left(zW_4^{0.5}\right) \tag{3.7}$$

respectively. Then, in the upper branch in Fig. 3.9, after the modulated signal passes through the digital filter $H_L(z)$, the real part of the filtered signal $y_{L0}(n)$ is decimated by a factor of 4, yielding

$$\begin{aligned} Y_{L0,R}\left(z^4\right) =& \frac{1}{4}\sum_{m=0}^{3} H_L\left(zW_4^m\right) X_{L0,R}\left(zW_4^m\right) \\ =& \frac{1}{8}\sum_{m=0}^{3} H_L\left(zW_4^m\right)\left[X_L\left(zW_4^m W_4^{0.5}\right) + \overline{X}_L\left(zW_4^m W_4^{-0.5}\right)\right] \end{aligned} \tag{3.8}$$

while its imaginary part is decimated by a factor of 4, followed by 2 equivalent unit-delays, yielding

$$\begin{aligned} Y_{L0,I}\left(z^4\right) =& \frac{z^{-2}}{4}\sum_{m=0}^{3} H_L\left(zW_4^m\right) X_{L0,I}\left(zW_4^m\right) \\ =& \frac{z^{-2}}{8}\sum_{m=0}^{3} H_L\left(zW_4^m\right)\left[X_L\left(zW_4^m W_4^{0.5}\right) - \overline{X}_L\left(zW_4^m W_4^{-0.5}\right)\right] W_4^{-2m} \end{aligned} \tag{3.9}$$

Similarly, in the lower branch, the imaginary part of the filtered signal $y_{L1}(n)$ is decimated by a factor of 4, while its real part is decimated by the factor of 4, followed by 2 equivalent unit-delays, as given by

$$Y_{L1,I}\left(z^4\right) = \frac{1}{8}\sum_{m=0}^{3} H_L\left(zW_4^m\right)\left[X_L\left(zW_4^m W_4^{-0.5}\right) - \overline{X}_L\left(zW_4^m W_4^{0.5}\right)\right] \tag{3.10}$$

$$Y_{L1,R}\left(z^4\right) = \frac{z^{-2}}{8}\sum_{m=0}^{3} H_L\left(zW_4^m\right)\left[X_L\left(zW_4^m W_4^{-0.5}\right) + \overline{X}_L\left(zW_4^m W_4^{0.5}\right)\right] W_4^{-2m} \tag{3.11}$$

In the synthesis side of the L-th subsystem, the interpolated signals in the upper and lower branches pass through the digital filter $F_L(z)$, yielding

$$\widehat{X}_{L0}(z) = F_L(z)\left[z^{-2}Y_{L0,R}\left(z^4\right) + Y_{L0,I}\left(z^4\right)\right] \tag{3.12}$$

and

$$\widehat{X}_{L1}(z) = F_L(z)\left[Y_{L1,R}\left(z^4\right) + z^{-2}Y_{L1,I}\left(z^4\right)\right] \tag{3.13}$$

Then, the L-th subsystem output signal $\widehat{X}_L(z)$ is obtained as the sum of these two signals after demodulation by complex exponentials $e^{\mp j\frac{\pi}{4}n}$ in accordance with

$$\widehat{X}_L(z) = \widehat{X}_{L,0}\left(zW_4^{-0.5}\right) + \widehat{X}_{L,1}\left(zW_4^{0.5}\right) \tag{3.14}$$

By invoking Eqns. 3.12 and 3.13 in Eqn. 3.14, and by invoking Eqns. 3.8, 3.9, and 3.11, 3.10 in the result, one obtains

$$\begin{aligned}
\widehat{X}_L(z) = {} & \frac{z^{-2}}{4}\left[F_L\left(zW_4^{-0.5}\right)H_L\left(zW_4^{-0.5}\right) + F_L^2\left(zW_4^{0.5}\right)H_L^2\left(zW_4^{0.5}\right)\right]X_L(z) \\
& + \frac{z^{-2}}{4}\left[F_L\left(zW_4^{-0.5}\right)H_L\left(zW_4^{-0.5+2}\right) + F_L\left(zW_4^{0.5}\right)H_L\left(zW_4^{0.5+2}\right)\right]X_L\left(zW_4^2\right) \\
& + \frac{z^{-2}}{4}\left[F_L\left(zW_4^{-0.5}\right)H_L\left(zW_4^{0.5}\right) - F_L\left(zW_4^{0.5}\right)H_L\left(zW_4^{-0.5}\right)\right]\overline{X}_L(z) \\
& + \frac{z^{-2}}{4}\left[F_L\left(zW_4^{-0.5}\right)H_L\left(zW_4^{2.5}\right) - F_L\left(zW_4^{0.5}\right)H_L\left(zW_4^{1.5}\right)\right]\overline{X}_L(zW_4^2)
\end{aligned} \tag{3.15}$$

Through inspection of Eqn. 3.15, if $H_L(z) = F_L(z)$, then the conjugate image component $\overline{X}_L(z)$ will be canceled automatically. Moreover, the remaining frequency-shifted conjugate image component $\overline{X}_L(zW_4^2)$ will have a weight factor of

$$A_L(z) = \frac{z^{-2}}{4}\left[H_L\left(zW_4^{3.5}\right)H_L\left(zW_4^{2.5}\right) - H_L\left(zW_4^{1.5}\right)H_L\left(zW_4^{0.5}\right)\right] \tag{3.16}$$

which satisfies a relationship of the form

$$A_L\left(z^2W_4^{-1}\right) = -A_L\left(z^2W_4^{1}\right). \tag{3.17}$$

3.2.2 Image cancelation in the $(L-1)$-th subsystem

Next, let us consider the details of a $(L-1)$-th subsystem as shown in Fig. 3.10. In this case, the remaining frequency-shifted conjugate image component $\overline{X}_L(zW_4^2)$ from the L-th subsystem gives rise to 2 conjugate image components in the $(L-1)$-th

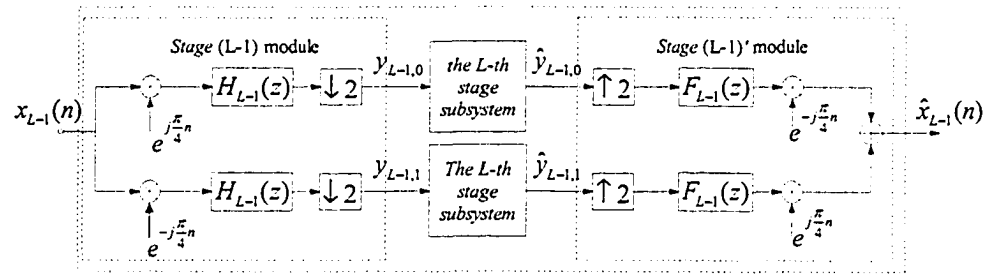

Figure 3.10: Detailed structure of $(L-1)$-th subsystem

subsystem. In the following, it is shown that one of these conjugate image components will again be canceled automatically.

In the upper branch of the $(L-1)$-th subsystem in Fig. 3.10, the input signal $Y_{L-1,0}(z)$ to the constituent L-th subsystem is given by

$$Y_{L-1,0}(z) = \frac{1}{2}\left[X_{L-1}\left(z^{\frac{1}{2}}W_4^{0.5}\right)H_{L-1}\left(z^{\frac{1}{2}}\right) + X_{l-1}\left(z^{\frac{1}{2}}W_4^{2.5}\right)H_{L-1}\left(z^{\frac{1}{2}}W_4^{2}\right)\right] \quad (3.18)$$

This signal will give rise to a signal $\widehat{Y}_{L-1,0}(z)$ at the output of the L-th subsystem consisting of a conjugate image component

$$C_{L-1,0}(z) = A_L(z)\overline{Y}_{L-1,0}\left(zW_4^2\right) \quad (3.19)$$

where

$$\begin{aligned}\overline{Y}_{L-1,0}\left(zW_4^2\right) =& \frac{1}{2}\left[\overline{X}_{L-1}\left(z^{\frac{1}{2}}W_4^1W_4^{-0.5}\right)H_{L-1}\left(z^{\frac{1}{2}}W_4^1\right)\right.\\ &\left.+\,\overline{X}_{L-1}\left(z^{\frac{1}{2}}W_4^1W_4^2W_4^{-0.5}\right)H_{L-1}\left(z^{\frac{1}{2}}W_4^1W_4^2\right)\right]\end{aligned} \quad (3.20)$$

(c.f. Eqn. 3.18). Similarly, in the lower branch, the signal $Y_{L-1,1}(z)$ will give rise to a signal $\widehat{Y}_{L-1,1}(z)$ at the output of the L-th subsystem consisting of a conjugate image component

$$C_{L-1,1}(z) = A_L(z)\overline{Y}_{L-1,1}(zW_4^2) \quad (3.21)$$

where

$$\begin{aligned}\overline{Y}_{L-1,1}\left(zW_4^2\right) =& \frac{1}{2}\left[\overline{X}_{L-1}\left(z^{\frac{1}{2}}W_4^1W_4^{0.5}\right)H_{L-1}\left(z^{\frac{1}{2}}W_4^1\right)\right.\\ &\left.+\,\overline{X}_{L-1}\left(z^{\frac{1}{2}}W_4^1W_4^2W_4^{0.5}\right)H_{L-1}\left(z^{\frac{1}{2}}W_4^1W_4^2\right)\right]\end{aligned} \quad (3.22)$$

In the *Stage* $(L-1)'$ module, the two input signals $\widehat{y}_{L-1,0}(n)$ and $\widehat{y}_{L-1,1}(n)$ are first interpolated by a factor of 2 before passing through the digital filters $F_{L-1}(z)$,

and then demodulated by the complex exponential $e^{\pm j\frac{\pi}{4}n}$. As a result, the output signal $\widehat{X}_{L-1}(z)$ is given by

$$\widehat{X}_{L-1}(z) = \widehat{Y}_{L-1,0}\left(z^2W_4^{-1}\right)F_{L-1}\left(zW_4^{-0.5}\right) + \widehat{Y}_{L-1,1}\left(z^2W_4^{1}\right)F_{L-1}\left(zW_4^{0.5}\right) \quad (3.23)$$

Let $\widehat{X}_{L-1,C}(z)$ represents the contribution of the conjugate image components $C_{L-1,0}(z)$ and $C_{L-1,1}(z)$ to the $(L-1)$-th subsystem output signal $\widehat{X}_{L-1}(z)$. Then, $\widehat{X}_{L-1,C}(z)$ can be obtained by replacing $\widehat{Y}_{L-1,0}\left(z^2W_4^{-1}\right)$ and $\widehat{Y}_{L-1,1}\left(z^2W_4^{1}\right)$ in Eqn. 3.23 by $C_{L-1,0}\left(z^2W_4^{-1}\right)$ and $C_{L-1,1}\left(z^2W_4^{1}\right)$, respectively, in accordance with

$$\widehat{X}_{L-1,C}(z) = C_{L-1,0}\left(z^2W_4^{-1}\right)F_{L-1}\left(zW_4^{-0.5}\right) + C_{L-1,1}\left(z^2W_4^{1}\right)F_{L-1}\left(zW_4^{0.5}\right) \quad (3.24)$$

By invoking Eqns. 3.19 and 3.21 in Eqn. 3.24, one can obtain

$$\begin{aligned}\widehat{X}_{L-1,C}(z) = &\left[F_{L-1}\left(zW_4^{0.5}\right)H_{L-1}\left(zW_4^{3.5}\right)A_L\left(z^2W_4^{-1}\right)\right.\\ &\left.+\,F_{L-1}\left(zW_4^{-0.5}\right)H_{L-1}\left(zW_4^{0.5}\right)A_L\left(z^2W_4^{1}\right)\right]\overline{X}_{L-1}(z)\\ &+\left[F_{L-1}\left(zW_4^{-0.5}\right)H_{L-1}\left(zW_4^{2.5}\right)A_L\left(z^2W_4^{-1}\right)\right.\\ &\left.+\,F_{L-1}\left(zW_4^{0.5}\right)H_{L-1}\left(zW_4^{1.5}\right)A_L\left(z^2W_4^{1}\right)\right]\overline{X}_{L-1}(zW_4^2)\end{aligned} \quad (3.25)$$

By substituting $H_{L-1}(z) = F_{L-1}(z)$ in Eqn. 3.25, and by making use of Eqn. 3.17, it becomes evident that the conjugate image component $\overline{X}_{L-1}(z)$ is canceled automatically. Consequently, at the output of the $(L-1)$-th subsystem, there remains only one conjugate image component $\overline{X}_{L-1}\left(zW_4^2\right)$, having a weight factor of

$$\begin{aligned}A_{L-1}(z) = &\left[H_{L-1}(zW_4^{3.5})H_{L-1}(zW_4^{2.5})\right.\\ &\left.-\,H_{L-1}(zW_4^{1.5})H_{L-1}(zW_4^{0.5})\right]A_L(z^2W_4^{-1})\end{aligned} \quad (3.26)$$

where $A_{L-1}(z)$ satisfies a relationship of the form

$$A_{L-1}\left(z^2W_4^{-1}\right) = -A_{L-1}\left(z^2W_4^{1}\right) \quad (3.27)$$

which is similar to Eqn. 3.17.

3.2.3 Image cancelation in the overall filterbank

In general, it can be shown that if $H_l(z) = F_l(z)$ (for $l = 2, 3, \cdots, L$), then there remains only one complex conjugate image component $\overline{X}_l\left(zW_4^2\right)$ at the output of the

l-th subsystem. This conjugate image component has a weight factor $A_l(z)$ satisfying the relationship of the form

$$A_l\left(z^2 W_4^{-1}\right) = -A_l\left(z^2 W_4^1\right). \tag{3.28}$$

Therefore, the entire filterbank (consisting of the analysis and synthesis sides) can be represented compactly by the system shown in Fig. 3.11, where the conjugate image

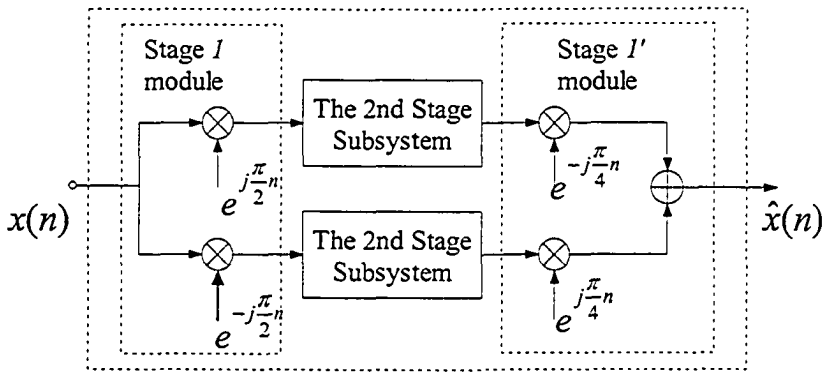

Figure 3.11: Entire system with the subsystems

component $\widehat{X}_C(z)$ in the reconstructed output signal $\widehat{X}(z)$ is given by

$$\widehat{X}_C(z) = \overline{X}(z)\left[A_2\left(zW_4^{-1}\right) + A_2\left(zW_4^1\right)\right] \tag{3.29}$$

However, in accordance with Eqn. 3.28, this conjugate image component is canceled automatically by anti-phasing ($\widehat{X}_C(z) = 0$), implying that the reconstructed output signal $\hat{X}(z)$ is devoid of a conjugate image component.

3.3 Filterbank Design and Signal Reconstruction

The design of the *Stage l* analysis digital filters $H_l(z)$ (or the *Stage l'* synthesis digital filters $F_l(z) = H_l(z)$) is achieved recursively, beginning with the design of the analysis digital filter $H_L(z)$, and ending with the design of $H_2(z)$. Then, the passband-edge frequencies $\omega_{p,l}$ and the stopband-edge frequencies $\omega_{s,l}$ of the digital filters $H_l(z)$ in the intermediate stages can be determined easily in terms of the stopband-edge frequency $\omega_{s,L}$ of the last-stage digital filter $H_L(z)$. In this way, with an appropriate choice of design for the digital filter $H_L(z)$, the proposed tree-structured filterbank can be designed to achieve the desired almost-PR property.

3.3.1 Design of $H_L(z)$ (or $F_L(z)$):

In accordance with the discussions in the previous section, the overall output signal as reconstructed by the filterbank is devoid of any complex conjugate image components (originally generated by the additional 2-fold decimation and 2-fold interpolation operations in *Stage L* and *Stage L'* modules). Consequently, in order to design the constituent digital filters in the filterbank, let us consider a modified subsystem as shown in Fig. 3.12. This subsystem is the same as the L-th subsystem in Fig.

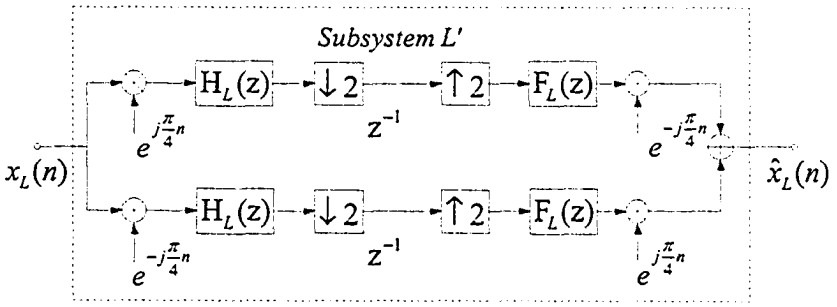

Figure 3.12: Alternative L-th subsystem

3.9, but without the second 2-fold decimation and corresponding 2-fold interpolation operation. The modified subsystem in Fig. 3.12 can easily be characterized by means of its input/output relationship

$$\begin{aligned}\widehat{X}_{L'}(z) = &\frac{1}{2}[H_L(zW_4^{-0.5})F_L(zW_4^{-0.5}) + H_L(zW_4^{0.5})F_L(zW_4^{0.5})]X_L(z) \\ &+ \frac{1}{2}[H_L(-zW_4^{-0.5})F_L(zW_4^{-0.5}) + H_L(-zW_4^{0.5})F_L(zW_4^{0.5})]X_L(zW_4^2)\end{aligned} \tag{3.30}$$

which has the same form as that in Eqn. 3.14 (except for the disappearance of the scaled delays $\frac{z^{-2}}{2}$) without the complex conjugate image components $\overline{X}_L(z)$ and $\overline{X}_L(zW_4^2)$. Therefore, in the the design of the filterbank, the L subsystem in Fig. 3.9 can be replaced by the modified subsystem in Fig. 3.12.

By inspection of Eqn. 3.30, the second term in the right-hand side constitutes an image component of the input signal $X_L(z)$. Since $F_L(z) = H_L(z)$, this image component can be suppressed when the stopband-edge frequency of the digital filter $H_L(z)$ is less than $\pi/2$ provided that the stopband attenuation of $H_L(z)$ is sufficiently high. By disregarding the latter image component, the modified subsystem can be

characterized by the transfer function

$$T_L(z) = \frac{1}{2}[H_L^2(zW_4^{-0.5}) + H_L^2(zW_4^{0.5})] \tag{3.31}$$

having a stopband-edge frequency of

$$\omega_{T,L} = \omega_{s,L} + \pi/4 \tag{3.32}$$

The design process for a general L-stage filterbank begins with that for a 2-stage filterbank as shown in Fig. 3.13, and extended to the case of the final desired filterbank in a recursive manner. The output signal of the 2-stage filterbank in Fig. 3.13 is given

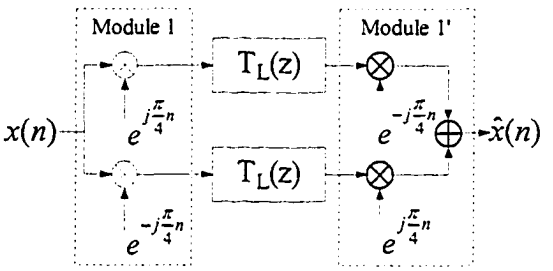

Figure 3.13: Alternative 2-stage filterbank (including analysis and synthesis sides)

by

$$\widehat{X}(z) = X(z)[T_L(zW_4^1) + T_L(zW_4^{-1})] \tag{3.33}$$

Then, $X(z)$ can be reconstructed perfectly provided that $T_L(z)$ is made a half-band digital filter [21]. To make $T_L(z)$ a half-band digital filter, $H_L^2(z)$ must in turn be made a 4th-band digital filter.

3.3.2 Design of H_{L-1} (F_{L-1}):

Having completed the design of the digital filter $H_L(z)$, let us consider the equivalent $(L-1)$-th subsystem as show in Fig. 3.14, producing an output signal as given by

$$\begin{aligned}\hat{X}_{L-1}(z) =& \frac{1}{4}\left[H_{L-1}\left(zW_4^{-0.5}\right) T_L\left(\left(zW_4^{-0.5}\right)^2\right) F_{L-1}\left(zW_4^{-0.5}\right)\right. \\ &\left. + H_{L-1}\left(zW_4^{0.5}\right) T_L\left(\left(zW_4^{0.5}\right)^2\right) F_{L-1}\left(zW_4^{0.5}\right)\right] X_{L-1}(z) \\ &+\frac{1}{2}\left[H_{L-1}\left(zW_4^{-0.5}W_4^2\right) T_L\left(\left(zW_4^{-0.5}\right)^2\right) F_{L-1}\left(zW_4^{-0.5}\right)\right. \\ &\left. + H_{L-1}\left(zW_4^{0.5}W_4^2\right) T_L\left(\left(zW_4^{0.5}\right)^2\right) F_{L-1}\left(zW_4^{0.5}\right)\right] X_{L-1}(-z)\end{aligned} \tag{3.34}$$

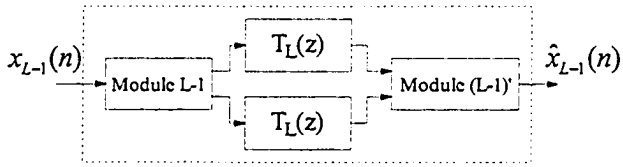

Figure 3.14: Alternative $(L-1)$-th subsystem

The second term in the right-hand side of Eqn. 3.34 is the image component generated by *Stage* $L-1$ and should be suppressed. This can be achieved by making sure that there is no overlap between the passbands and transition bands of $H_{L-1}\left(zW_4^2\right)H_{L-1}(z)$ and $T_L\left(z^2\right)$ (c.f. Fig. 3.15), yielding

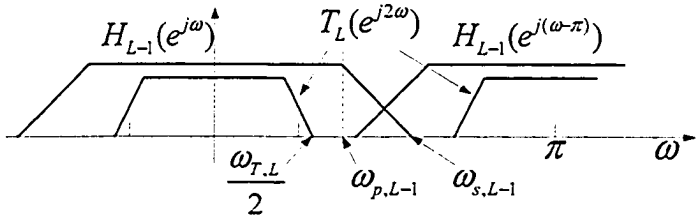

Figure 3.15: Relationships between the frequency characteristics of H_{L-1} and H_L

$$\omega_{s,L-1} \leq \pi - \omega_{T,L} = \pi - (\omega_{s,L} + \pi/4)/2 \tag{3.35}$$

In practice, the passband ripples of $H_{L-1}(z)$ gives rise to deviations from PR property, and the stopband attenuation of $H_{L-1}(z)$ determines the aliasing effect from the image component $X_{L-1}(-z)$. Therefore, the passband ripple $H_{L-1}(z)$ should be kept sufficiently small, and its stopband attenuation should be kept sufficiently large.

At the absence of the image term $X_{L-1}(-z)$, the equivalent $(L-1)$-th subsystem is characterized by a transfer function

$$\begin{aligned} T_{L-1}(z) = \frac{1}{2}\Big[&H_{L-1}\left(zW_4^{-0.5}\right)T_L\left(\left(zW_4^{-0.5}\right)^2\right)F_{L-1}\left(zW_4^{-0.5}\right) \\ &+ H_{L-1}\left(zW_4^{0.5}\right)T_L\left(\left(zW_4^{0.5}\right)^2\right)F_{L-1}\left(zW_4^{0.5}\right)\Big] \end{aligned} \tag{3.36}$$

If $T_L(z)$ is a half-band digital filter, then $T_{L-1}(z)$ will similarly be a half-band digital filter provided that the passband frequency region of the digital filter $H_{L-1}(z)$ extends over the passband and transition band frequency regions of $T_L(z)$ (c.f. Fig. 3.15), yielding

$$\omega_{p,L-1} \geq \omega_{T,L} = (\omega_{s,L} + \pi/4)/2 \tag{3.37}$$

In order to make the length of the digital filter $H_{L-1}(z)$ short, one can make its transition band somewhat wider in accordance with

$$\begin{aligned} \omega_{p,L-1} &= (\omega_{s,L} + \pi/4)/2 \\ \omega_{s,L-1} &= \pi - (\omega_{s,L} + \pi/4)/2 \end{aligned} \tag{3.38}$$

3.3.3 Design of intermediate H_l and F_l:

A general modified l-th subsystem, as shown in Fig. 3.16, has the output signal

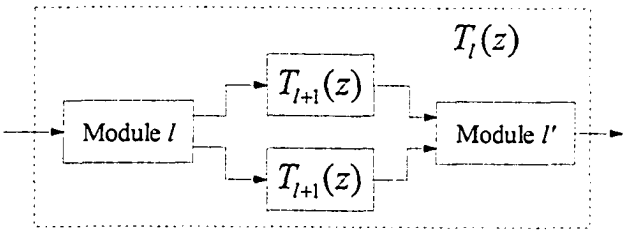

Figure 3.16: Alternative l-th subsystem

$$\begin{aligned} \hat{X}_l(z) = &\left[H_l\left(zW_4^{-0.5}\right) T_{l+1}\left(\left(zW_4^{-0.5}\right)^2\right) F_l\left(zW_4^{-0.5}\right)\right. \\ &\left. + H_l\left(zW_4^{0.5}\right) T_{l+1}\left(\left(zW_4^{0.5}\right)^2\right) F_l\left(zW_4^{0.5}\right)\right] X_l(z) \\ &+ \left[H_l\left(zW_4^{-0.5}W_4^2\right) T_{l+1}\left(\left(zW_4^{-0.5}\right)^2\right) F_l\left(zW_4^{-0.5}\right)\right. \\ &\left. + H_l\left(zW_4^{0.5}W_4^2\right) T_{l+1}\left(\left(zW_4^{0.5}\right)^2\right) F_l\left(zW_4^{0.5}\right)\right] X_l(-z) \end{aligned} \tag{3.39}$$

In a fashion similar to that for the design of the digital filter $H_L - 1(z)$ (or $F_L - 1(z)$), one can eliminate the image component $X_l(-z)$ provided that the stopband-edge frequencies of the digital filters $H_l(z)$ (or $F_l(z)$) are constrained by

$$\omega_{s,l} \leq \pi - \omega_{T,l+1} = \pi - (\omega_{p,l+1} + \pi/4)/2 \tag{3.40}$$

where $\omega_{T,l+1}$ represents the stopband edge-frequency of the transfer function $T_{l+1}(z)$. Moreover, in order to ensure that the alternative l-th subsystem has a half-band digital filter transfer function, one must ensure that the pass-band edge-frequencies of the digital filters $H_l(z)$ (or $F_l(z)$) satisfy the relationships

$$\omega_{p,l} \geq \omega_{T,l+1} = (\omega_{p,l+1} + \pi/4)/2 \tag{3.41}$$

Finally, the passband-edge and stopband-edge frequencies of the digital filter $H_l(z)$ can be selected as

$$\begin{aligned} \omega_{p,l} &= (\omega_{p,l+1} + \pi/4)/2 \\ \omega_{s,l} &= \pi - (\omega_{p,l+1} + \pi/4)/2 \end{aligned} \tag{3.42}$$

3.3.4 Reconstruction of the input signal

In accordance with the above discussions, the modified l-th subsystem can be characterized as a half-band digital filter satisfying the relationship

$$T_l\left(zW_4^1\right) + T_l\left(zW_4^{-1}\right) \approx \frac{z^{-(4+s_l)}}{8}. \tag{3.43}$$

where s_l depends on analysis and synthesis filter orders.

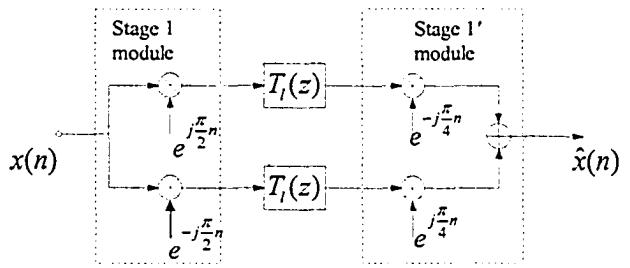

Figure 3.17: Alternative L-stage filterbank (including analysis and synthesis sides)

By adding the first decomposition stage and the corresponding reconstruction stage as shown in Fig. 3.17, one obtains the reconstructed output signal

$$\hat{X}(z) = [T_l\left(zW_4^{-1}\right) + T_l\left(z^2W_4^1\right)]X(z) \approx \frac{z^{-(4+s_l)}}{8}X(z) \tag{3.44}$$

rendering the filterbank as almost-PR.

3.4 Practical Implementation of the Tree-Structured Filterbank

For a practical hardware implementation of the proposed tree-structured PR filterbank, one has to resolve two different problems. The first problem relates to modulations by the complex exponentials $e^{\pm j\frac{\pi}{4}n}$ in all the intermediate-stage modules, involving multiplications by the irrational numbers $\pm\frac{\sqrt{2}}{2}$. The second problem relates

to the fact that the number of intermediate-stage modules increases exponentially with the numbers of stages, with the sampling rate being halved from one stage to the next (potentially reducing hardware utilization).

The above problems can be resolved, a) by exploiting a polyphase decomposition of the analysis and synthesis digital filters $H_l(z)$ and $F_l(z)$, and b) by the application of interleaving techniques to the tree-structured filterbank, as discussed in the following.

3.4.1 Polyphase decomposition for analysis and synthesis digital filters

By using the signal-flow diagram equivalencies shown in Fig. 3.18, the modulations by the complex exponentials $e^{\pm j\frac{\pi}{2}n}$ at *Stage l* decomposition modules reduce to multiplication by 0, 1 and -1, where

$$H_l(z) = H_{l0}\left(z^2\right) + z^{-1}H_{l1}\left(z^2\right) \tag{3.45}$$

and where $H_{l0}(z)$ and $H_{l1}(z)$ are the polyphase components of $H_l(z)$. Since $H_l(z)$ represents a half-band digital filter, only one multiplier coefficient of $H_{l1}(z)$ will be non-zero (having a value of 0.5), implying that $H_{l1}(z)$ consists of a single multiplication. Therefore, the new required multiplication by $e^{-j\frac{\pi}{4}}$ can be efficiently absorbed into the realization of $H_{l1}(z)$. Similarly, one can use the Fig. 3.19 for *Stage l'* reconstruction modules.

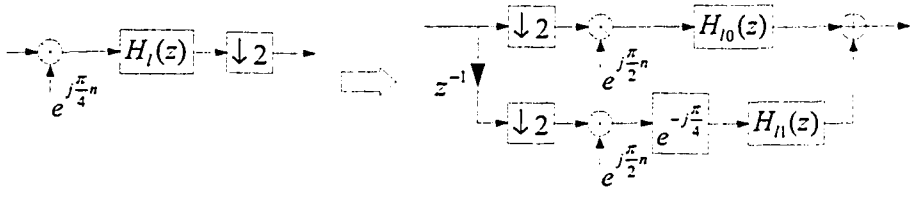

Figure 3.18: Equivalence for *Stage l* decomposition modules

3.4.2 Interleaving the tree-structured filterbank

In the proposed tree-structured filterbank, there are 2^{l-1} identical modules at *Stage l* (*Stage l'*), which can be efficiently implemented by interleaving all the $2 \times 2^{l-1}$ constituent identical digital filters $H_l(z)$ ($F_l(z)$) by one digital filter $\tilde{H}_l(z)$ ($\tilde{F}_l(z)$)

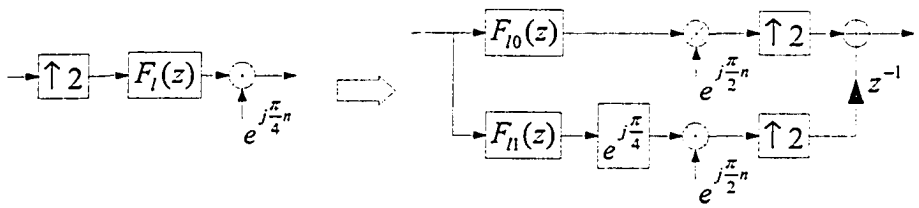

Figure 3.19: Equivalence for *Stage l'* reconstruction modules

only. The interleaving digital filter $\tilde{H}_l(z)$ $(\tilde{F}_l(z))$ is the same as the digital filters $H_l(z)$ $(F_l(z))$ except that each unit-delay component is replaced by $2 \times 2^{l-1}$ unit-delay components. For example, when two signal sequences are interleaved together, the digital filter $H(z)$ for processing these two signals should be modified by using two unit-delays instead of one unit-delay in the original digital filter. Figure 3.20a shows the realization of a FIR digital filter, and Fig. 3.20b shows its modification for 2-fold interleaving. In this way, one can obtain a corresponding interleaved [29] realization

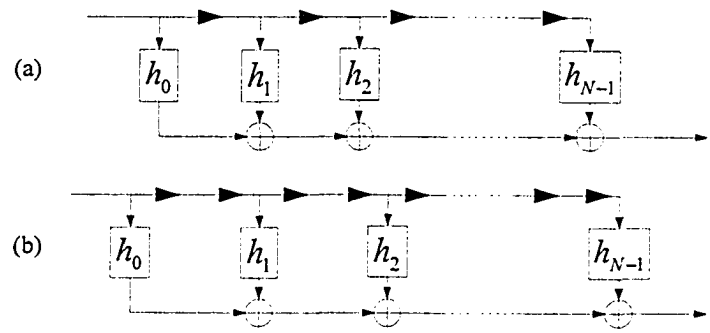

Figure 3.20: The realization of (a) a FIR digital filter, and (b) its modification for 2-fold interleaving

of the tree-structured PR filterbank as shown in Fig. 3.21, where each stage consists of only one digital filter operating at a rate twice that of the input sampling rate.

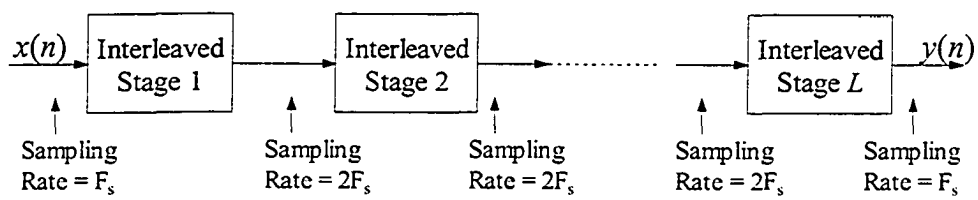

Figure 3.21: Realization of the interleaved tree-structured filterbank

3.4.3 Processing of complex signals

The proposed filterbank involves processing of complex signal sequences. In order to bypass an explicit recourse to complex signal processing, a complex signal sequence is split into two signals, one representing the real part (called the in-phase component), and the other representing the imaginary part (called the quadrature component) of the signal.

As mentioned in Section 3.4, all complex exponential modulations can be replaced by modulations with $e^{\pm j\frac{\pi}{2}n}$ by using polyphase representation. By separating the complex signal into in-phase and quadrature components, the combined complex exponential modulation and filtering shown in Fig. 3.22a can be replaced by a real signal processing signal-flow diagram as shown in Fig. 3.22b. Note that modulations

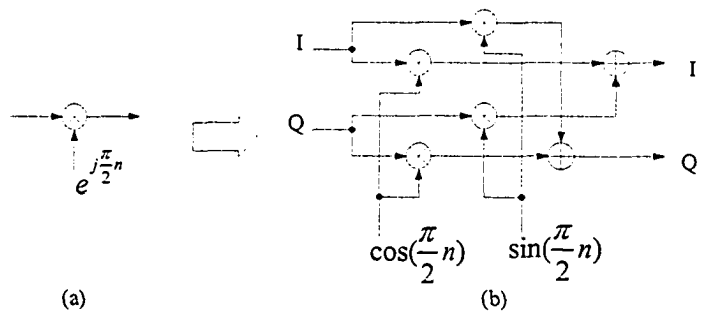

Figure 3.22: Real processing of complex signal sequences

by $\cos\frac{\pi}{2}n$ and $\sin\frac{\pi}{2}n$ involve multiplications by 0, 1 and -1. The multiplication by 0 can be skipped in the practice, leading to the implementation shown in Fig. 3.23. The remaining multiplications by 1 and -1 can be realized easily as straight through or sign inversion, respectively.

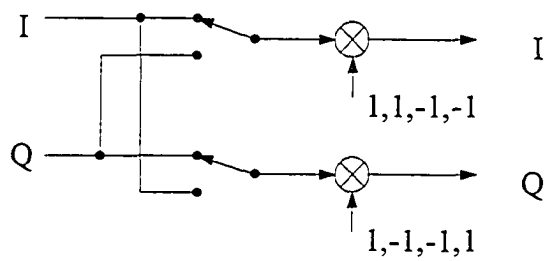

Figure 3.23: Simplified realization for real processing of complex signal sequences

3.5 Investigation of Deviations from PR Property and Computational Complexity

In accordance with the discussions in Section 3.3, the last-stage filters $H_L(z)$ are required to be such that to render $H_L^2(z)$ as a 4th-band filter. This requirement is best met by using the windowing technique [9] [25] or the nonlinear optimization technique [27] for the design of the filters $H_L(z)$. The windowing technique provides a simple method for the design of the last-stage filters $H_L(z)$, leading to tolerable deviations from the PR property. In order to obtain more acceptable deviations, one can resort to nonlinear optimization.

Having designed the last-stage filters $H_L(z)$, the design of the intermediate-stage filters $H_l(z)$ can be performed in the straightforward fashion, e.g. by using the Remez exchange algorithm.

This section is concerned with separate applications of the windowing technique and the nonlinear optimization technique to the design of the last-stage filters $H_L(z)$ for the incorporation in 2-stage, 3-stage and 6-stage tree-structured filterbanks, and with a comparison of the computational complexity of 4-stage, 5-stage, and 6-stage tree-structured filterbanks with the corresponding DFT and MDFT filterbanks.

3.5.1 Applications employing windowing technique

To begin with, let us use the windowing technique in [25] to optimize the last-stage filters $H_L(z)$ to achieve a stopband-edge frequency of 0.45π, and a minimum stopband attenuation of 60 dB. The multiplier coefficient values of the required filters $H_L(z)$ are obtained as given in Table 3.1, leading to a magnitude-frequency response characteristic as shown in Fig. 3.24.

Table 3.1: Coefficients of the last-stage filters $H_L(z)$ employing the windowing approach

$h_L(0) = h_L(20)$	-5.2345e-004	$h_L(1) = h_L(19)$	-6.6618e-004
$h_L(2) = h_L(18)$	1.5909e-003	$h_L(3) = h_L(17)$	6.3758e-003
$h_L(4) = h_L(16)$	8.4970e-003	$h_L(5) = h_L(15)$	-2.7582e-004
$h_L(6) = h_L(14)$	-2.1200e-002	$h_L(7) = h_L(13)$	-3.8911e-002
$h_L(8) = h_L(12)$	-2.5281e-002	$h_L(9) = h_L(11)$	3.9652e-002
$h_L(10)$	2.4361e-001		

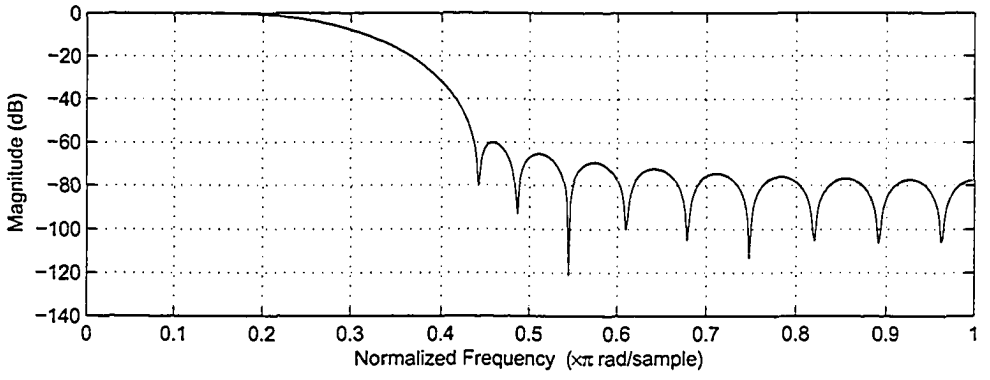

Figure 3.24: Magnitude-frequency response of the last-stage filters $H_L(z)$ employing the windowing approach

A) The case of a 2-stage filterbank: In this case, there are no intermediate-stages. Therefore, any deviation from the PR property is entirely caused by the last-stage digital filter $H_L(z)$. In this way, the overall distortion (including both the transfer function and aliasing function distortions) of the reconstructed output signal as referred to the original input signal is obtained as shown in Fig. 3.25.

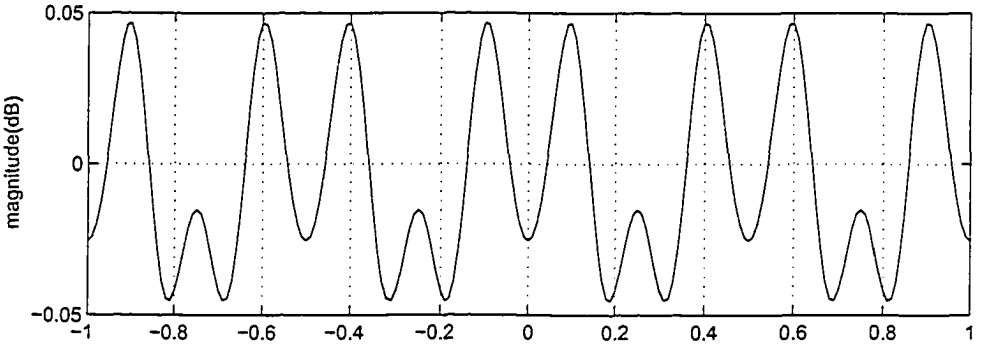

Figure 3.25: (a)The overall distortion of 2-Stage filterbank employing the windowing approach

B) The case of a 3-stage filterbank: In this case, by keeping the last-stage filters $H_L(z)$ as above, it is only required to design the intermediate-stage filters $H_L - 1(z)$. In accordance with Eqn. 3.38, the passband-edge and stopband-edge frequencies of the intermediate stage filters $H_{L-1}(z)$ are chosen as given in Table 3.2. Let us consider the case when the intermediate stage filters $H_{L-1}(z)$

Table 3.2: Stopband-edge and passband-edge frequencies of the intermediate stage filter $H_l(z)$ for 3-Stage filterbank

Stage	$\omega_{p,l}$	$\omega_{s,l}$
$l = 2$	0.345π	0.655π

have a low stopband attenuation of 40 dB[2]. Then, the overall distortion of the reconstructed output signal as referred to the original input signal is obtained as shown in Fig. 3.26. By comparing Figs. 3.26 and 3.25, it is observed that the 3-stage filterbank exhibits higher distortion in the transfer function magnitude-frequency response than the 2-stage filterbank. This is mainly due to a relatively high passpand ripple of about 0.0864 dB in the intermediate stage filters $H_{L-1}(z)$.

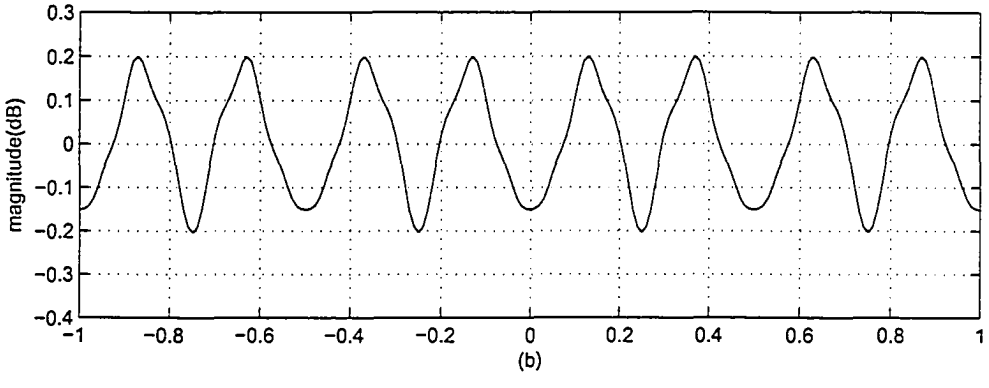

Figure 3.26: (a) The overall distortion of the 3-stage filterbank using windowing technique with high passpand ripple intermediate stage filters $H_l(z)$

To put the above observations into perspective, let us consider the case when the intermediate stage filters $H_{L-1}(z)$ have a higher stopband attenuation of 60 dB. Then, the overall distortion is obtained as shown in Fig. 3.27. In this way, the overall distortion does not increase appreciably in comparison with that in Fig. 3.25.

C) *The case of the 6-stage filterbank:* In this case, the last-stage digital filter $H_L(z)$ and the intermediate-stage digital filters $H_{L-1}(z)$ are kept as in *B)*, and the

[2]Since the filters $H_{L-1}(z)$ are half-band digital filters, their passband ripple relative to unity is as same as their stopband ripple relative to zero magnitude-frequency response.

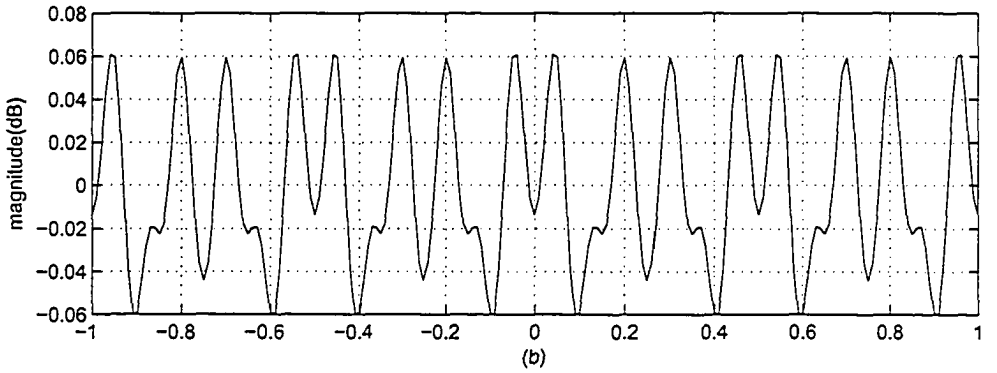

Figure 3.27: (a) The overall distortion of the 3-Stage filterbank using windowing technique with low passpand ripple intermediate stage filters $H_l(z)$

passband-edge and stopband-edge frequencies of the remaining intermediate-stage digital filters $H_l(z)$ are chosen as given in Table 3.3 together with a minimum stopband attenuation of 60 dB. Then, the overall deviation from the PR property is obtained as shown in Fig. 3.28.

Table 3.3: Passband-edge and stopband-edge frequencies of the intermediate stage filters $H_l(z)$ for a 6-stage filterbank

Stage	$\omega_{p,l}$	$\omega_{s,l}$
$l = 4$	0.35π	0.65π
$l = 3$	0.3π	0.7π
$l = 2$	0.275π	0.725π
$l = 2$	0.26255π	0.7375π

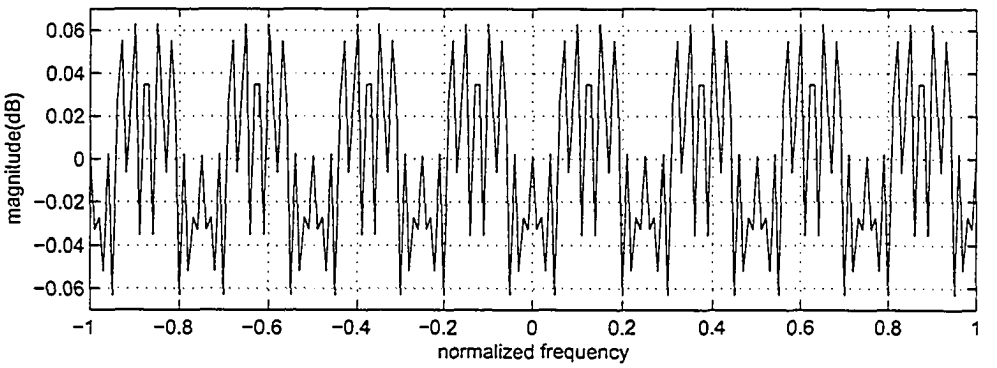

Figure 3.28: The overall distortion of 6-stage filterbank (window approach)

Through inspection of the frequency distortions in Figs. 3.25, 3.27 and 3.28, it is observed that the distortion increases only slightly if the number of the stage is increased from 3 to 6 while the stop band attenuations of the intermediate-stage filters are kept sufficiently high.

3.5.2 Applications employing the nonlinear optimization

Let us optimize the last-stage digital filter $H_L(z)$ by using the technique in [27] to achieve a stopband-edge frequency of 0.45π, and a stopband attenuation of 60 dB. Then, the multiplier coefficient values for the resulting $H_L(z)$ can be obtained as given in Table 3.4, leading to a magnitude-frequency response characteristic as shown in Fig. 3.29.

Table 3.4: Coefficients of the optimized last-stage digital filters $H_L(z)$

$h_L(0) = h_L(32)$	-1.6667e-010	$h_L(1) = h_L(31)$	1.6222e-005
$h_L(2) = h_L(30)$	-1.7927e-004	$h_L(3) = h_L(29)$	-2.0789e-004
$h_L(4) = h_L(28)$	-2.0060e-004	$h_L(5) = h_L(27)$	-2.9863e-004
$h_L(6) = h_L(26)$	8.3665e-004	$h_L(7) = h_L(25)$	4.2300e-003
$h_L(8) = h_L(24)$	6.8286e-003	$h_L(9) = h_L(23)$	9.8198e-004
$h_L(10) = h_L(22)$	-1.7130e-002	$h_L(11) = h_L(21)$	-3.5416e-002
$h_L(12) = h_L(20)$	-2.5720e-002	$h_L(13) = h_L(19)$	3.5889e-002
$h_L(14) = h_L(18)$	1.4158e-001	$h_L(15) = h_L(17)$	2.4483e-001
$h_L(16)$	2.8793e-001		

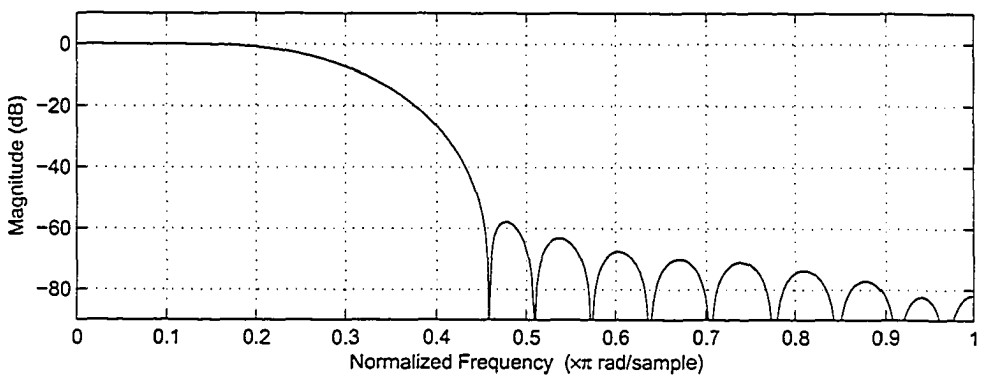

Figure 3.29: magnitude-frequency response of the optimized last-stage filter $H_L(z)$

A) The case of a 2-stage filterbank: In this case, there are no intermediate-stages. Therefore, any deviation from the PR property is entirely caused by the last-

stage digital filter $H_L(z)$. In this way, the overall distortion of the reconstructed output signal as referred to the original input signal is obtained as shown in Fig. 3.30.

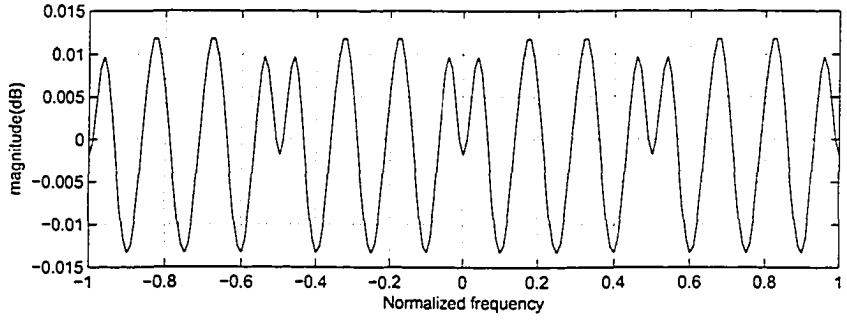

Figure 3.30: Overall distortions of the 2-stage filterbanks

B) *The case of a 3-stage filterbank:* In this case, by keeping the last-stage digital filter $H_L(z)$ as in *A)*, it is only required to design the intermediate-stage digital filters $H_L - 1(z)$. In accordance with Eqn. 3.38, the passband-edge and stopband-edge frequencies of the digital filters $H_{L-1}(z)$ are chosen as given in Table 3.2. Then, the overall deviations from the PR property of 3-stage filterbanks are shown in Fig. 3.31.

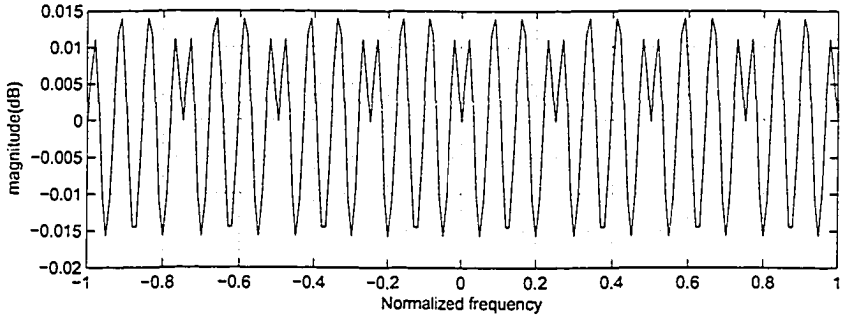

Figure 3.31: The overall distortions for the 3-stage filterbank

C) *The case of the 6-stage filterbank:* In this case, the last-stage digital filter $H_L(z)$ and the intermediate-stage digital filters $H_{L-1}(z)$ are kept as in *B)*, and the passband-edge and stopband-edge frequencies of the remaining intermediate-stage digital filters $H_l(z)$ are chosen as given in Table 3.3 together with a mini-

mum stopband attenuation of 60 dB. Then, the overall deviation from the PR property is obtained as shown in Fig. 3.32.

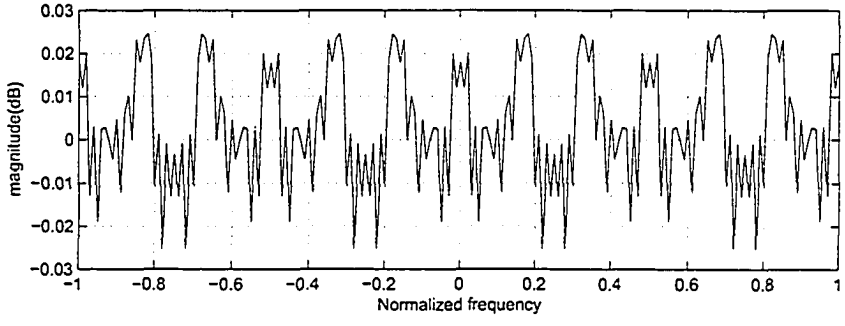

Figure 3.32: The overall distortion for the 6-stage filterbank

Compared to the windowing technique, it is observed that the nonlinear optimization gives the much smaller distortion, while the distortion increases slightly when the number of the stages is increased from 3 to 6.

3.5.3 Comparison of computational complexity

Let us set consider the design M-channel DFT, Modified DFT and tree-structured filterbanks possessing subchannel minimum stopband attenuations of 60 dB.

A) *The case of the conventional DFT filterbanks:* In this case, by using the design technique in [32], the lengths of the prototype digital filters associated with the constituent analysis filterbanks are $N_a = 88, 176$ and 352 for $M = 16, 32$ and 64, respectively. In order to avoid aliasing effects, the lengths of the corresponding prototype digital filters associated with the constituent synthesis filterbanks are $N_s = (M-1)N_a$. In this way, the total number of digital filter coefficients reach MN_a.

B) *The case of Modified-DFT filterbanks:* By using the design techniques in [27] and [34], the lengths of the prototype digital filters in each of the analysis and synthesis filterbanks are obtained as $N = 96, 192$ and 384 for $M = 8, 16$ and 32, respectively.

C) *The case of the tree-structured filterbank:* In this case, the number of stages are given by $L = 4, 5$ and 6 for $M = 16, 32$ and 64, respectively. Then, the lengths of the digital filters in each stage are obtained as given in Table 3.5.

Table 3.5: The length of digital filters for the tree-structured filterbanks

	$H_2(z)$	$H_3(z)$	$H_4(z)$	$H_4(z)$	$H_5(z)$
$L = 4$	21	25	33		
$L = 5$	17	21	25	33	
$L = 6$	15	17	21	25	33

The total number of digital filter coefficients required for the proposed tree-structured filterbanks are given in Table 3.6 for $M = 8, 16$ and 32, together with the total number of digital filter coefficients required for the corresponding conventional DFT filterbanks and modified DFT filterbanks. It is observed that the tree-structured filterbank requires substantially less digital filter coefficients than the conventional DFT and modified DFT filterbanks for the same subchannel minimum stopband attenuations. In addition, the proposed tree-structured filterbank does not make any recourse to DFT operations.

Table 3.6: The Number of non-zero digital filter coefficients in DFT, modified DFT, and tree-structured filterbanks

	$M = 16$	$M = 32$	$M = 64$
Traditional DFT filterbanks	1408	5632	22528
Modified-DFT filterbanks	192	384	768
Proposed tree-structured filterbanks	114	132	162

3.6 Conclusions

This chapter has presented the design details and investigation of a novel maximally-decimated interleaved tree-structured filterbank. The salient feature of the resulting tree-structured filterbank is that it permits the realization of a large number of subchannels, and that it leads to high computational efficiency in the corresponding hardware implementations (c.f. Table 3.6). Due to the tree-structured configuration of the proposed tree-structured filterbank, a $(L + 1)$-stage filterbank can be designed

in terms of an already designed L-stage filterbank, merely through the addition of one extra stage. It has been shown that by using a two-step decimation in the last stage of the constituent analysis and synthesis filterbanks, half of the image components (arising from the maximal decimation) are automatically cancelled in the reconstructed output signal. Computational investigations have been undertaken to show that deviation from the PR reconstruction property can be kept minimal by maintaining moderate stopband attenuations in the analysis and synthesis digital filters. The interleaving technique has been employed to reduce the number of the required subfilters from $2^L - 1$ to $L - 1$ for a L-stage filterbank. It has been shown that compared to DFT and MDFT filterbanks, when the number of subchannels increases, the proposed interleaved tree-structured filterbank leads to a substantial reduction in the computational complexity of the filterbank. This partly due to the fact that the tree-structured filterbank does not make any recourse to DFT operations, and partly due to the fact that it requires much less non-zero coefficients for the realization of the constituent analysis and synthesis digital filters.

Chapter 4

MDFT Filterbanks with Frequency-Response Masking Technique

In DFT filterbanks, when subchannels have very narrow transition bandwidths, the length of the constituent prototype filter also becomes prohibitively large, curtailing the computational efficiency of the filterbank. It is well known that the frequency response masking (FRM) technique is an attractive technique for the realization of digital filter with very narrow transition bandwidths and has be exploited for the realization of cosine modulated filterbanks for transmultiplexing [30] [10].

In this chapter, the concept of frequency-response masking is exploited for the development of a new technique for the design of MDFT filterbanks with highly frequency selective subchannels. The proposed design technique is based on the decomposition of the MDFT filterbank prototype filter into suitable base and masking subfilters. By using the polyphase components of the decomposed subfilters, it is shown that the constituent analysis and synthesis filters can be realized as a cascaded pair of DFT filterbanks in the case of a narrow-band prototype filter, and as a parallel combination of two cascaded pairs of DFT filterbanks in the case of arbitrary-bandwidth prototype filter. The resulting MDFT filterbanks are substantially more computationally efficient than the conventional MDFT filterbanks for highly frequency-selective subchannels, due to a substantial reduction in the number of filtering multiplications.

This chapter is organized as follows. Section 4.1 gives an introduction of the

FRM technique. In Section 4.2, the structure of the proposed MDFT filterbank is derived based on the polyphase decompositions of FRM sub-filters, leading to the realization of the constituent analysis and synthesis filters. Section 4.3 is concerned with the optimization of the FRM sub-filters to ensure the near perfect-reconstruction (PR) property in the resulting MDFT filterbank. In Section 4.4, two application examples as well as the complexity comparison to the conventional MDFT filterbank are given to illustrate the design and computational efficiency of the proposed MDFT filterbanks for the cases of a narrow-band and an arbitrary-bandwidth prototype filter. The conclusions are given in Section 4.5.

4.1 Frequency-Response Masking Technique

The FRM technique can be used to advantage for the design of very narrow transition-bandwidth digital filters. This technique can be used in a straightforward fashion for the design of the corresponding digital filters with narrow-widths, and, with some modifications, for the design of the corresponding digital filters with arbitrary passband-widths.

4.1.1 Narrow passband-width FRM digital filters

Consider a low-pass digital filter $H_b(z)$ having a passband-edge frequency of $\omega_{b,p}$, having a stopband-edge frequency of $\omega_{b,s}$, and having a magnitude-frequency response $|H_b(e^{j\omega})|$ as shown in Fig. 4.1(a). In this way, the digital filter $H_b(z)$ has a transition bandwidth of $\Delta_b = \omega_{b,s} - \omega_{b,p}$.

By replacing each unit-delay in the digital filter $H_b(z)$ by L unit-delays, one obtains a new digital filter $H_L(z) = H_b(z^L)$ having a magnitude-frequency response $|H_L(e^{j\omega})| = |H_b(e^{jL\omega})|$ as shown in Fig. 4.1(b). Moreover, by using a digital filter $H_{Mb}(z)$ having a magnitude-frequency response $|H_{Mb}(e^{j\omega})|$ shown in Fig. 4.1(c), one can mask out the unwanted images components of the digital filter $H_L(z)$ so as to arrive at a lowpass digital filter $H(z)$ given by

$$H(z) = H_L(z)H_{Mb}(z) = H_b(z^L)H_{Mb}(z) \tag{4.1}$$

The resulting digital filter $H(z)$ has a magnitude response $|H(e^{j\omega})|$ as shown in Fig. 4.1(d), which is characterized by a narrow transition bandwidth of Δ_b/L.

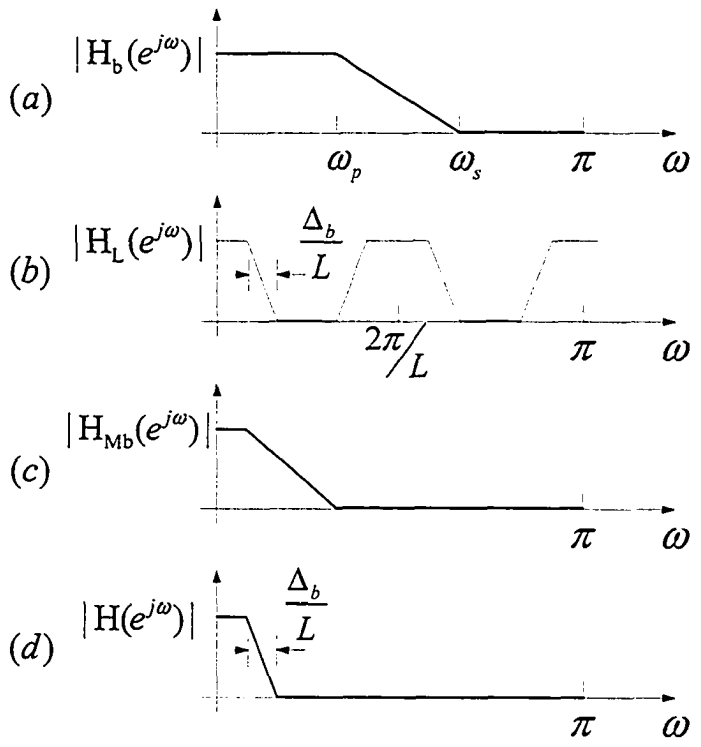

Figure 4.1: Magnitude-frequency responses for obtaining a narrow-band FRM digital filter $H(z)$

Figure 4.1 illustrates the FRM technique for deriving narrow transition-bandwidth digital filters from digital filters with substantially wider transition-bandwidths. However, this simple technique suffers from a fundamental problem: Although replacing each unit-delay in the digital filter $H_b(z)$ by L unit-delays reduces the transition-bandwidth by a factor of L, the passband-width is also reduced by the same factor. Therefore, this technique is not suitable for the design of arbitrary passband-width digital filters.

4.1.2 Arbitrary passband-width FRM digital filters

Let $H_b(z)$ represent a linear-phase lowpass digital filter of length N_b having a magnitude-frequency response as shown in 4.2(a), with a passband-edge frequency of $\omega_{b,p}$, with a stopband-edge frequency of $\omega_{b,s}$, and with a transition-bandwidth of $\Delta_b = \omega_{b,s} - \omega_{b,p}$. Moreover, let $H_c(z)$ represent a linear-phase digital filter complementary to the digital

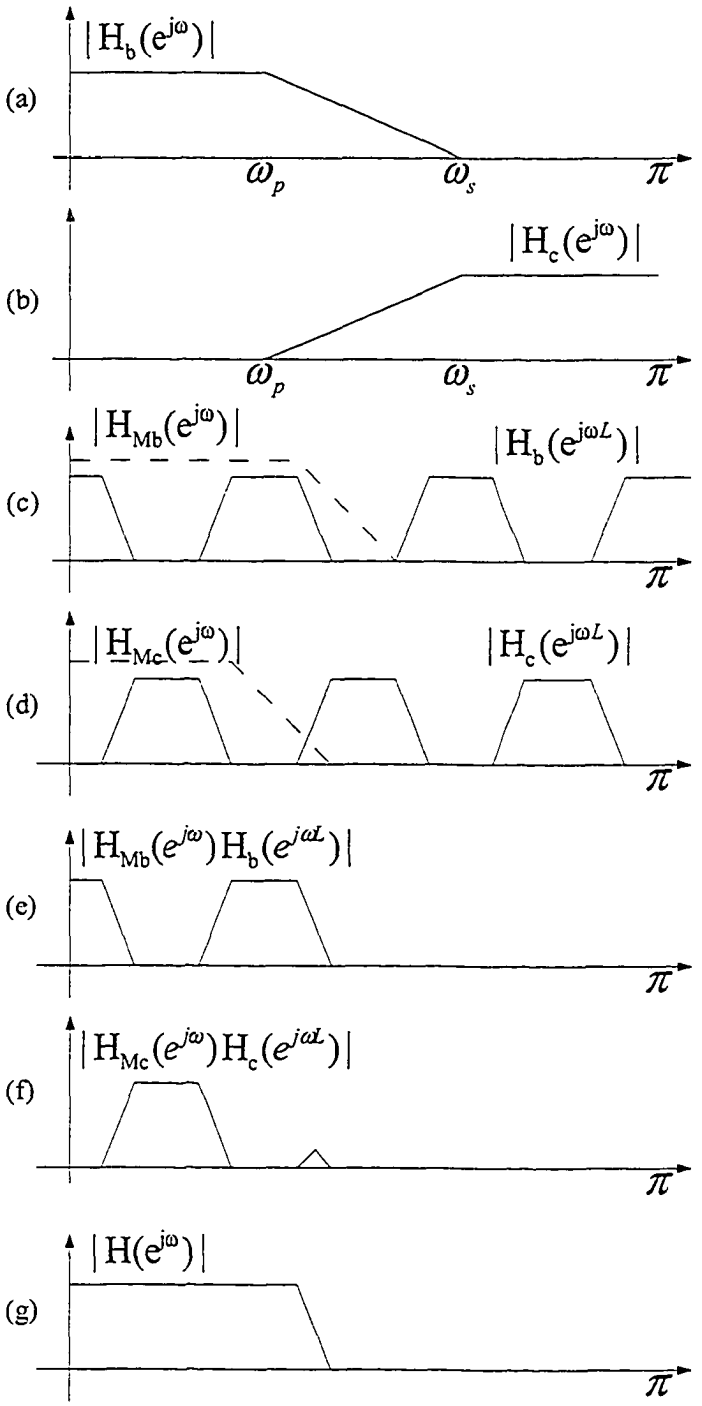

Figure 4.2: Magnitude-frequency responses for obtaining an arbitrary-bandwidth FRM digital filter $H(z)$

filter $H_b(z)$ in accordance with

$$H_c(z) = z^{-(N_b-1)/2} - H_b(z), \tag{4.2}$$

having a magnitude-frequency response as shown in 4.2(b). Then, one can obtain the desired arbitrary-bandwidth FRM digital filter $H(z)$ in accordance with [24]

$$H(z) = H_b(z^L)H_{Mb}(z) + H_c(z^L)H_{Mc}(z) \tag{4.3}$$

In Eqn. 4.3, $H_b(z^L)$ ($H_c(z^L)$) represents the interpolated version of $H_b(z)$ ($H_c(z)$) with the interpolation factor of L, having a magnitude-frequency response as shown in Fig. 4.2(c) (Fig. 4.2(d)). Moreover, $H_{Mb}(z)$ ($H_{Mc}(z)$) represents a masking digital filter acting to partially suppress unwanted image bands of the interpolated filter $H_b(z^L)$ ($H_c(z^L)$), having a magnitude-frequency response as shown in Fig. 4.2(c) (Fig. 4.2(d)). Consequently, the product $H_b(z^L)H_{Mb}(z)$ ($H_c(z^L)H_{Mc}(z)$) represents the remaining image bands of $H_b(z^L)$ ($H_c(z^L)$), having a magnitude-frequency response as shown in Fig. 4.2(e) (Fig. 4.2(f)). In this way, the totality of the remaining image bands of $H_b(z^L)$ and $H_c(z^L)$ determine the bandwidth of the arbitrary-bandwidth FRM digital filter $H(z)$, giving rise to an overall magnitude-frequency response as shown in Fig. 4.2(f), with a narrow transition bandwidth of $(\omega_{b,s} - \omega_{b,p})/L$. The bandwidth of the FRM digital filter $H(z)$ can be controlled arbitrarily by the bandwidths of digital filters $H_b(z)$ and $H_c(z)$, in addition to the number of remaining image bands of the interpolated filters $H_b(z^L)$ and $H_c(z^L)$ [24].

By substituting Eqn. 4.2 into Eqn. 4.3, one can obtain

$$H(z) = H_b(z^L)H_{Mb}(z) + [z^{-L(N-1)/2} - H_b(z^L)]H_{Mc}(z) \tag{4.4}$$

leading to a corresponding realization of the FRM digital filter $H(z)$ as shown in Fig. 4.3.

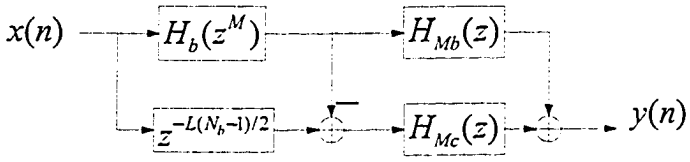

Figure 4.3: Realization of the arbitrary-bandwidth FRM digital filter $H(z)$

4.2 Realization of MDFT Filterbanks Employing Narrow-Band or Arbitrary-Bandwidth FRM Digital Filters

This section presents a novel technique for the realization of MDFT filterbanks (introduced in Section 2.4) based on the realization of the constituent prototype filter $P(z)$ as a FRM digital filter. For the sake of completeness, the treatments include both the cases of narrow-band as well as arbitrary-bandwidth FRM digital filters.

4.2.1 Realization employing a narrow-band FRM prototype digital filter

In this case, the prototype filter $P(z)$ for a M-channel MDFT filterbank can be decomposed in accordance with

$$P(z) = H_{b0}\left(z^L\right) H_{Mb0}(z) \tag{4.5}$$

where $H_{b0}(z)$ and $H_{Mb0}(z)$ represent zero-phase symmetrical FIR digital filters of lengths N_b and N_{Mb}, respectively. This decomposition gives rise to a prototype filter $P(z)$ of length $N_p = L(N_b - 1) + N_{Mb}$.

By invoking Eqn. 4.5 in Eqn. 2.61, the analysis filters $H_k(z)$ are obtained as

$$H_k(z) = z^{-(N_p-1)/2} H_{b0}\left(\left(zW_M^k\right)^L\right) H_{Mb0}\left(zW_M^k\right) \tag{4.6}$$

Let

$$H_{Lb}(z) = z^{-L(N_b-1)/2} H_{b0}\left(z^L\right) \tag{4.7}$$

and

$$H_{Mb}(z) = z^{-(N_{Mb}-1)/2} H_{Mb0}(z) \tag{4.8}$$

represent linear-phase causal digital filters associated with the FIR digital filters $H_{b0}(z^L)$ and $H_{Mb0}(z)$ in Eqn. 4.5, respectively. Then, by using Eqns. 4.7 and 4.8 in Eqn. 4.6, one obtains

$$H_k(z) = W_M^{ak} H(zW_M^k) \tag{4.9}$$

where

$$H(z) = H_{Lb}(z) H_{Mb}(z), \tag{4.10}$$

and where $a = \frac{N_p-1}{2}$.

By using polyphase decomposition, $H_{Mb}(z)$ can be expressed in the form

$$H_{Mb}(z) = \sum_{m=0}^{M-1} z^{-m} H_{Mb,m}\left(z^M\right) \tag{4.11}$$

By substituting Eqn. 4.11 into Eqn. 4.10, and by invoking the result in Eqn. 4.9, one can write

$$H_k(z) = W_M^{ak} H_{Lb}\left(zW_M^k\right) \sum_{m=0}^{M-1} \left(zW_M^k\right)^{-m} H_{Mb,m}\left(z^M\right) \tag{4.12}$$

Then, the analysis filter vector $\mathbf{h}(z) = \begin{bmatrix} H_0(z) & H_1(z) & \cdots & H_{M-1}(z) \end{bmatrix}^T$ can be expressed compactly in the form[1]

$$\mathbf{h}(z) = \mathbf{W}_0 \mathbf{W}^* \mathbf{e}_H(z) \tag{4.13}$$

where the vector $\mathbf{e}_H(z)$ is defined as $\mathbf{e}_H(z) = \begin{bmatrix} E_{H,0}(z) & E_{H,1}(z) & \cdots & E_{H,M-1}(z) \end{bmatrix}^T$, and where

$$E_{H,k}(z) = z^{-k} H_{Mb,k}\left(z^M\right) H_{Lb}\left(zW_M^k\right) \tag{4.14}$$

In Eqn. 4.13, $\mathbf{W}_0$ is a diagonal matrix defined as $[\mathbf{W}_0]_{k,k} = W_M^{ak}$, and $\mathbf{W}$ represents the M-point DFT matrix defined as $[\mathbf{W}]_{k,l} = W_M^{kl}$.

In accordance with Eqn. 4.13, the analysis filters can be realized by the structure shown in Fig. 4.4 [3].

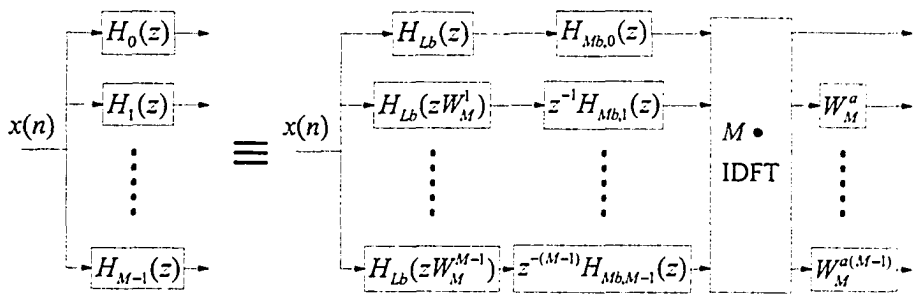

Figure 4.4: Realization of the analysis filters $H_k(z)$ in terms of the polyphase components of $H_{Mb}(z)$ for a narrow-band FRM prototype digital filter $P(z)$

By making use of the polyphase decomposition

$$H_{Lb}(z) = \sum_{l=0}^{M-1} z^{-l} H_{L,l}\left(z^M\right), \tag{4.15}$$

[1]A superscript T represents transposition, and a superscript $*$ represents complex conjugation.

the filters $H_{Lb}(zW_M^k)$ can be realized in terms of the polyphase components of $H_{Lb}(z)$ as shown in Fig. Consequently, the analysis filters in Fig. 4.4 can be replace by those in Fig. 4.6.

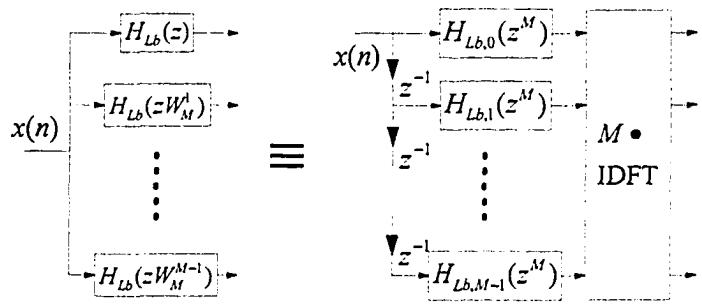

Figure 4.5: Realization of the filters $H_{Lb}(zW_M^k)$ in terms of the polyphase components of $H_{Lb}(z)$

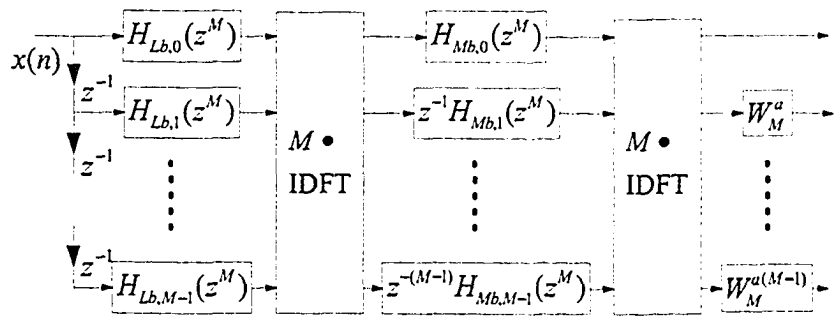

Figure 4.6: Realization of the analysis filters $H_k(z)$ in terms of the polyphase components of $H_{Lb}(z)$ and $H_{Mb}(z)$ for a narrow-band FRM prototype digital filter $P(z)$

In order to realize the corresponding synthesis filters $F_k(z)$, let us use Eqn. 4.12, and let us recall that $F_k(z) = H_k(z)$ to write

$$F_k(z) = W_M^{ak} H_{Lb}\left(zW_M^k\right) \sum_{m=0}^{M-1} \left(zW_M^{-(M-k)}\right)^{-m} H_{Mb,m}\left(z^M\right) \tag{4.16}$$

Then, the synthesis filter vector $\mathbf{f}(z) = \begin{bmatrix} F_0(z) & F_1(z) & \cdots & F_{M-1}(z) \end{bmatrix}$ can be expressed compactly in the form

$$\mathbf{f}(z) = \mathbf{e}_F(z)\mathbf{W}\mathbf{W}_0 \tag{4.17}$$

where the vector $\mathbf{e}_F(z)$ is defined as $\mathbf{e}_F(z) = \begin{bmatrix} E_{F,0}(z) & E_{F,1}(z) & \cdots & E_{F,M-1}(z) \end{bmatrix}$, and where

$$E_{F,k}(z) = \begin{cases} H_{Mb,0}\left(z^M\right) H_L(z) & \text{for } k = 0; \\ z^{-k} H_{Mb,k}\left(z^M\right) H_L\left(zW_M^k\right) & \text{others} \end{cases} \tag{4.18}$$

In accordance with Eqn. 4.16, the synthesis filters can be realized by the structure shown in Fig.4.7.

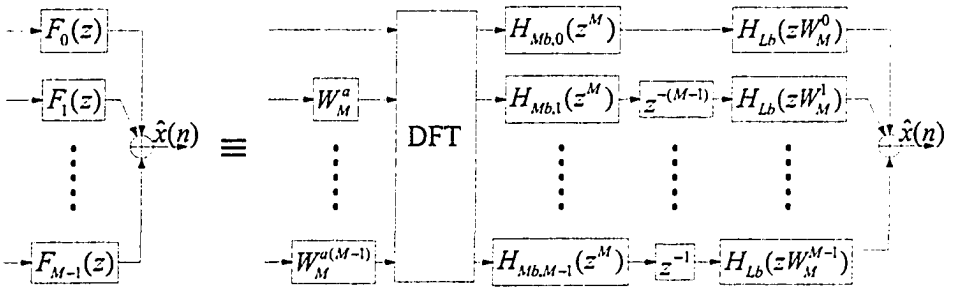

Figure 4.7: Realization of the synthesis filters $F_k(z)$ in terms of the polyphase components of $H_{Mb}(z)$ for a narrow-band FRM prototype digital filter $P(z)$

Finally, by invoking the polyphase decomposition of $H_{Lb}(z)$ in Eqn. 4.15, the synthesis filters in Fig. 4.7 can be replaced by those in Fig. 4.8.

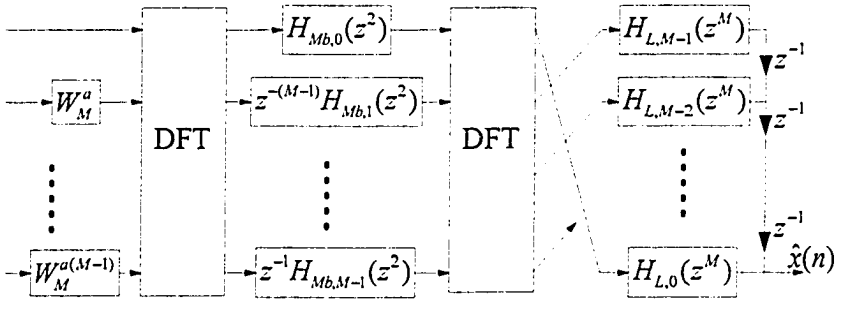

Figure 4.8: Realization of the synthesis filters in terms of the polyphase components of $H_{Lb}(z)$ and $H_{Mb}(z)$ for a narrow-band FRM prototype digital filter $P(z)$

The analysis filters in Fig. 4.6 and the synthesis filters in Fig. 4.8 can subsequently be substituted into the MDFT filterbank in Fig. 2.12 to arrive at the desired filterbank.

4.2.2 Realization employing an arbitrary-bandwidth FRM prototype digital filter

In this case, the prototype digital filter $P(z)$ for an M-channel MDFT filterbank can be expressed in the form

$$P(z) = H_{b0}(z^L)H_{Mb0}(z) + H_{c0}(z^L)H_{Mc0}(z) \tag{4.19}$$

where $H_{b0}(z)$, $H_{Mb0}(z)$ and $H_{Mc0}(z)$ represent zero-phase symmetrical FIR digital filters of lengths N_b, N_{Mb} and N_{Mc}, respectively, and where

$$H_{c0}(z) = 1 - H_{b0}(z) \tag{4.20}$$

Let

$$H_{Lb}(z) = z^{-L(N_b-1)/2} H_{b0}(z) \tag{4.21}$$

and

$$H_{Lc}(z) = z^{-L(N_b-1)/2} \left[1 - H_{b0}(z)\right] \tag{4.22}$$

represent the linear-phase causal digital filters associated with the FIR digital filters $H_{b0}(z)$ and $H_{c0}(z)$, respectively. Moreover, let

$$H_{Mb}(z) = z^{-L(N_{Mbc}-1)/2} H_{Mb0}(z) \tag{4.23}$$

and

$$H_{Mc}(z) = z^{-(N_{Mbc}-1)/2} H_{Mc0}(z) \tag{4.24}$$

represent linear-phase causal digital filters associated with the digital filters $H_{Mb0}(z)$ and $H_{Mc0}(z)$, respectively, where $N_{Mbc} = max\{N_{Mb}, N_{Mc}\}$. Then by invoking Eqns. 4.21-4.24 in Eqn. 4.19, and by invoking the result in Eqn. 2.61, the analysis filters $H_k(z)$ are obtained as

$$H_k(z) = W_M^{bk} H_{Lb}\left(zW_M^k\right) H_{Mb}\left(zW_M^k\right) + W_M^{bk} H_{Lc}\left(zW_M^k\right) H_{Mc}\left(zW_M^k\right) \tag{4.25}$$

where $b = \frac{N_p-1}{2}$, and where $N_p = L(N_b - 1) + N_{Mbc}$.

The first term $W_M^{bk} H_L\left(zW_M^k\right) H_{Mb}\left(zW_M^k\right)$ in the right-hand side of Eqn. 4.25 can be realized as shown in Fig. 4.6 in previous subsection. In order to realize the second term $W_M^{bk} H_{Lc}\left(zW_M^k\right) H_{Mc}\left(zW_M^k\right)$, let us use polyphase decompositions of $H_{Lc}(z)$ and $H_{Mc}(z)$ to obtain

$$\begin{aligned} & W_M^{bk} H_{Lc}\left(zW_M^k\right) H_{Mc}\left(zW_M^k\right) \\ =& W_M^{bk} \sum_{l=0}^{M-1} \left(zW_M^k\right)^{-l} H_{Lc,l}\left(z^M\right) \sum_{m=0}^{M-1} \left(zW_M^k\right)^{-m} H_{Mc,m}\left(z^M\right) \end{aligned} \tag{4.26}$$

where $H_{Lc,l}(z)$ and $H_{Mc,m}(z)$ represent the polyphase components of $H_{Lc}(z)$ and $H_{Mc}(z)$, respectively. But, since $H_{Lc}(z) = z^{-L(N_b-1)/2} - H_{Lb}(z)$, one has

$$H_{Lc,l}\left(z^M\right) = \begin{cases} z^{-[L(N_b-1)/2-q]} - H_{Lb,q}\left(z^M\right) & \text{for } l = q \\ -H_{Lb,l}\left(z^M\right) & \text{otherwise} \end{cases} \tag{4.27}$$

where q is the residue of $\frac{L(N_b-1)}{2M}$. Then, the second term in the right-hand side of Eqn. 4.25 can be realized as shown in Fig. 4.9. Finally, By combining the realization in Fig. 4.9 with that in Fig. 4.6, one arrives at the desired realization for the analysis filters $H_k(z)$ as shown in Fig. 4.10.

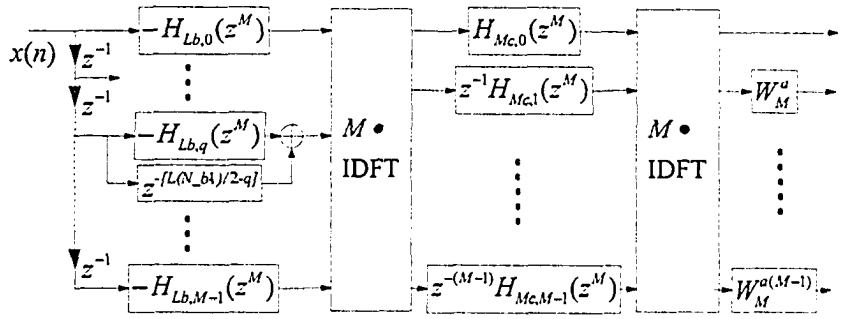

Figure 4.9: Realization of the second term in the right-hand side of Eqn. 4.25, based on an arbitrary-bandwidth FRM digital filter $P(z)$

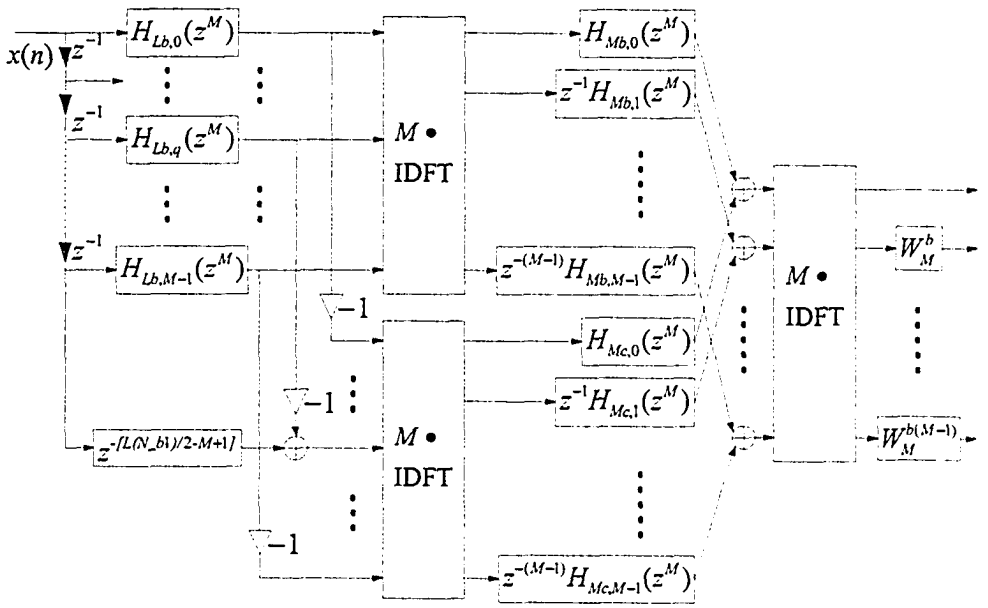

Figure 4.10: Realization of the analysis filters $H_k(z)$ in terms of the polyphase components of $H_{Lb}(z)$ and $H_{Mb}(z)$ for an arbitrary-bandwidth FRM prototype digital filter $P(z)$

Similarly, the corresponding synthesis filters $F_k(z)$ can be realized as shown in Fig. 4.11.

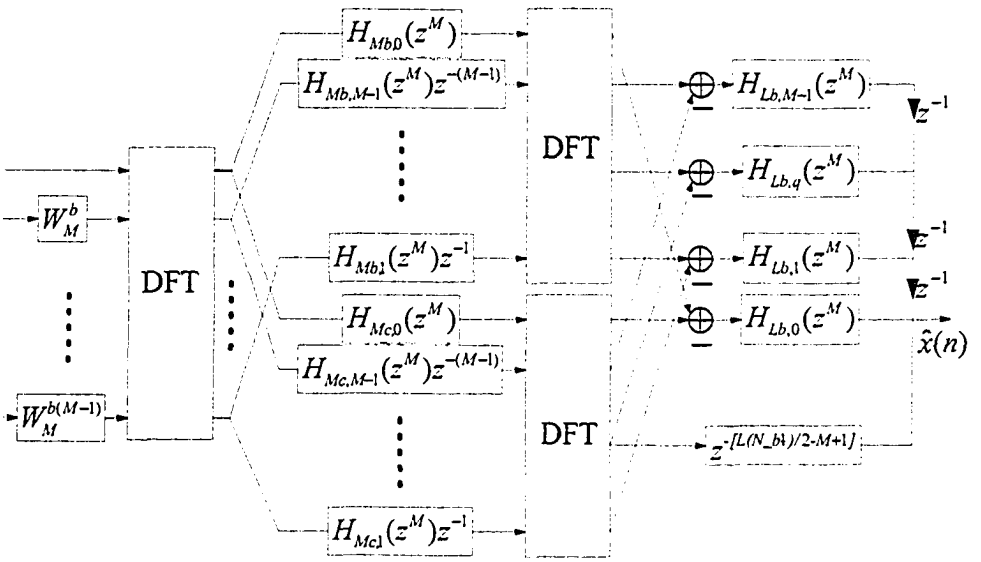

Figure 4.11: Realization of the synthesis filters $F_k(z)$ in terms of the polyphase components of $H_{Lb}(z)$ and $H_{Mb}(z)$ for an arbitrary-bandwidth FRM prototype digital filter $P(z)$

4.3 The Optimization of the Proposed MDFT Filterbanks

The optimization of the proposed MDFT filterbank gives rise to two different (although interrelated) problems. The first problem amounts to minimizing the detrimental effects of aliasing by suppressing the unwanted image components of the input signal. The second problem, on the other hand, amounts to ensuring the PR property (to within acceptable approximations) in the transfer function of the filterbank.

In accordance with Eqn. 2.81, the transfer function of the proposed MDFT filterbank is given by

$$T(z) = \frac{z^{-M/2}}{M} \sum_{k=0}^{M-1} F_k(z) H_k(z) \tag{4.28}$$

By substituting Eqn. 2.61 into Eqn. 4.28, one obtains

$$T(z) = \frac{z^{-(M/2+N_p-1)}}{M} \sum_{k=0}^{M-1} P^2(zW_M^k) \tag{4.29}$$

where $P(z)$ is given by Eqn. 4.5 for the case of a narrow-band, and by Eqn. 4.19 for the case of an arbitrary-bandwidth FRM prototype digital filter $P(z)$.

Due to the zero-phase property of the prototype filter $P(z)$, the transfer function $T(z)$ in Eqn. 4.29 exhibits a linear-phase characteristics. Therefore, in order to satisfy the PR property, one must have

$$M\left|T(e^{j\omega})\right| = 1, \quad 0 \leq \omega \leq \pi \tag{4.30}$$

Then, from Eqn. 4.29 and Eqn. 4.30, one can show that [27]

$$\sum_{k=0}^{M-1} P^2(zW_M^k) = 1 \tag{4.31}$$

In a similar fashion, from Eqn. 2.81, the aliasing function [13] for the proposed MDFT filterbank is given by

$$A(z) = \sqrt{\sum_{l=1}^{M/2-1} |\frac{1}{M}\sum_{k=0}^{M-1} F_k(z)H_k(zW_M^{2l})|^2} \tag{4.32}$$

By substituting Eqn. 2.61 into Eqn. 4.32, one obtains

$$A(z) = \sqrt{\sum_{l=1}^{M/2-1} \left|\frac{1}{M}\sum_{k=0}^{M-1} P(zW_M^k)P(zW_M^{k+2l})\right|^2} \tag{4.33}$$

Through inspection of Eqn. 4.33, it can be shown that the aliasing effects can be minimized by ensuring a sufficiently high stopband attenuation in the prototype FRM digital filter $P(z)$. This can be achieved by using the following objective function [26]

$$minimize \int_{\omega_{p,s}}^{\pi} |P(e^{j\omega})|^2 d\omega \tag{4.34}$$

where $\omega_{p,s}$ represents the stopband-edge frequency of the prototype filter $P(z)$. Alternatively, the objective function in Eqn. 4.34 can be simplified to

$$mimimize\ \phi_1 + \phi_2 \tag{4.35}$$

where

$$\phi_1 = \int_{\omega_{b,s}}^{\pi} |H_{b0}(e^{j\omega})|^2 d\omega \tag{4.36}$$

represents the stopband energy of the digital filter $H_{b0}(z)$.

In Eqn. 4.35,

$$\phi_2 = \sum_{i=1}^{L/2} \int_{\omega_{i,1}}^{\omega_{i,2}} |H_{Mb0}(e^{j\omega})|^2 d\omega \tag{4.37}$$

represents the stopband energy of the masking filter $H_{Mb0}(z)$ for the case of a narrow-band FRM prototype digital filter $P(z)$, where

$$\begin{aligned} \omega_{i,1} &= (2i\pi - \omega_{b,s})/L; \\ \omega_{i,2} &= (2i\pi + \omega_{b,s})/L; \quad i = 1, 2, \cdots, L/2 \end{aligned} \tag{4.38}$$

represent the edge frequencies of the unwanted image bands of interpolated filter $H_{Lb0}(z)$. Moreover,

$$\phi_2 = \int_{\omega_{Mb,s}}^{\pi} |H_{Mb0}(e^{j\omega})|^2 d\omega + \int_{\omega_{Mc,s}}^{\pi} |H_{Mc0}(e^{j\omega})|^2 d\omega \tag{4.39}$$

represents the stopband energies of the masking filters $H_{Mb0}(z)$ and $H_{Mc0}(z)$ for the case of an arbitrary-bandwidth FRM prototype digital filter $P(z)$, where $\omega_{b,s}$ and $\omega_{c,s}$ represent the stopband-edge frequencies of $H_{Mb0}(z)$ and $H_{Mc0}(z)$, respectively.

In this way, the problem of satisfying the almost-PR property in the proposed cascaded MDFT filterbank reduces to that of solving the following optimization problem

$$\begin{aligned} &mimimize\ \phi_1 + \phi_2 \\ &\qquad subject\ to\ \left| \sum_{k=0}^{M-1} P^2(e^{j(\omega - 2k\pi/M)}) - 1 \right| < \varepsilon \end{aligned} \tag{4.40}$$

where ε represents a sufficiently small positive number.

4.4 Application Examples and Complexity Comparison

This section illustrates the design of the proposed MDFT filterbanks in terms of two application examples. One of these examples is concerned with the case of a narrow-band whereas the other example is concerned with the case of an arbitrary-bandwidth FRM prototype digital filter $P(z)$.

Example 1: A 32-channel MDFT filterbank employing a narrow-band FRM prototype digital filter $P(z)$ is designed to satisfy the specifications given in Table 4.1, where Δ represents the normalized transition bandwidth and β represents the stopband attenuation of the prototype filter $P(z)$. Moreover, the length of the digital filter $H_{b0}(z)$ is selected as 51 ($N_b = 51$), and that of the masking filter $H_{Mb0}(z)$ is selected as 34 ($N_{Mb} = 34$). The approximation of the transfer function $T(z)$ to a unity

Table 4.1: MDFT filterbank design specifications in the case of a narrow-band FRM prototype digital filter $P(z)$

M	L	Δ	$\beta(dB)$	$\lvert T(e^{j\omega})\rvert(dB)$
32	8	0.02	-60	$< 5 \times 10^{-3}$

magnitude-frequency response as given in Table 4.1 is equivalent to $\varepsilon = 5.7581 \times 10^{-4}$ in the optimization problem in Eqn. 4.40. Then, by solving the optimization problem in Section 4.3, the digital filters $H_{b0}(z)$ and $H_{Mb0}(z)$ are obtained to have the unit-impulse responses $h_{b0}(n)$ and $h_{Mb0}(n)$, respectively, as shown in Fig. 4.12. The magnitude-frequency response associated with $H_{b0}(z)$ and $H_{Mb0}(z)$ are obtained as shown in Fig 4.13. Through an inspection of the magnitude-frequency responses in Fig 4.13, it is observed that the optimized digital filter $H_{b0}(z)$ possess a normalized passband-edge frequency of 0.187, a normalized stopband-edge frequency of 0.347, and, consequently, a normalized transition bandwidth of 0.16.

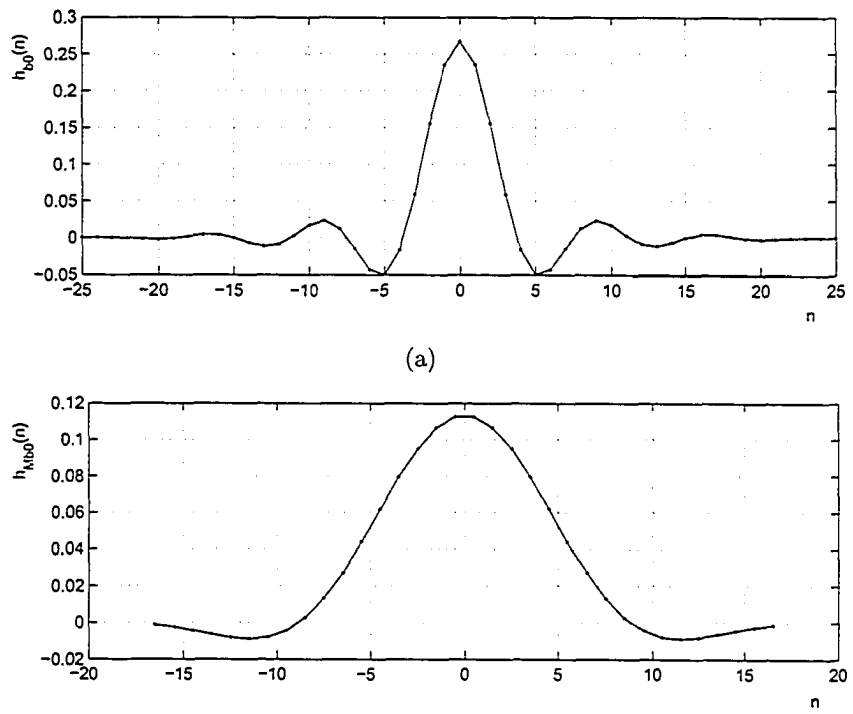

Figure 4.12: Multiplier coefficient values of (a) the filter $H_b(z)$, and (b) the masking filter $H_{Mb0}(z)$

Having designed the digital filters $H_{b0}(z)$ and $H_{Mb0}(z)$, one can proceed to deter-

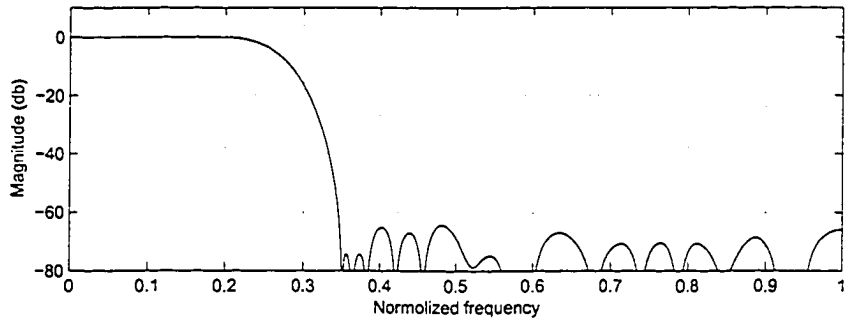

(a)

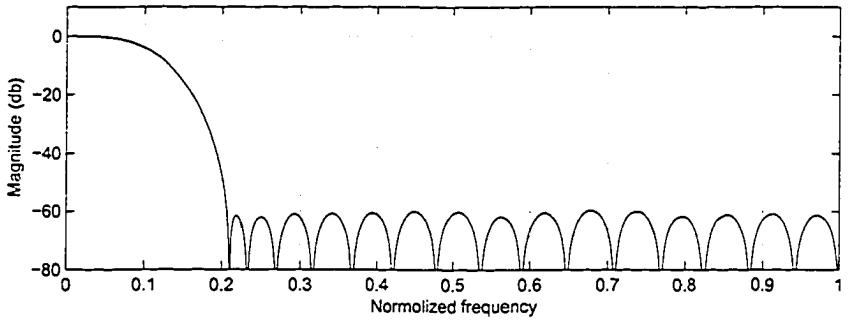

(b)

Figure 4.13: Magnitude-frequency response of (a) filter $H_{b0}(z)$ and (b) masking filter $H_{Mb0}(z)$

mine the FRM prototype digital filter $P(z)$ by using Eqn. 4.5. Fig. 4.14 shows the magnitude-frequency response of the resulting digital filter $P(z)$. Through an inspection of the magnitude-frequency response in Fig. 4.14, it is observed that the filter $P(z)$ exhibits a stopband attenuation of 60dB and a narrow normalized transition-bandwidth of 0.02. Consequently, the magnitude-frequency responses associated with the 32-channel cascaded MDFT filterbank are obtained as shown in Fig. 4.15.

Finally, Fig. 4.16 shows the deviation of the overall MDFT filterbank transfer function $T(z)$ in Eqn. 4.29 from a unity magnitude-frequency response, yielding peak deviations of $\pm 5 \times 10^{-3}$dB. Moreover, Fig. 4.17 shows the magnitude-frequency response associated with the aliasing function in Eqn. 4.32, exhibiting a maximum value of $-65dB$.

In order to achieve the same specifications in Table 4.1, the prototype filter in the corresponding conventional MDFT filterbank requires 327 multiplier coefficients.

Example 2: A 8-channel MDFT filterbank based on an arbitrary-bandwidth FRM

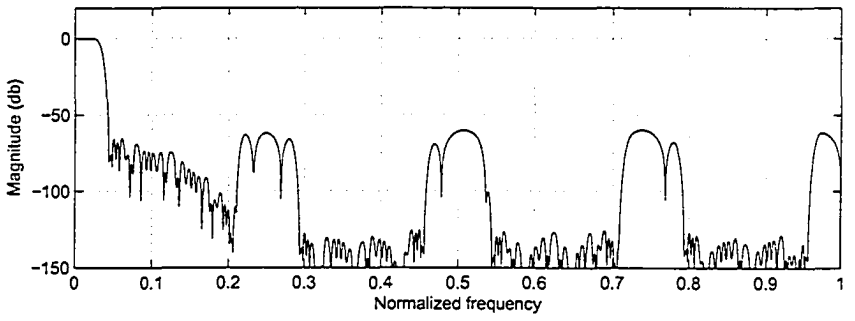

Figure 4.14: Magnitude-frequency response of the FRM prototype digital filter $P(z)$ in Example 1

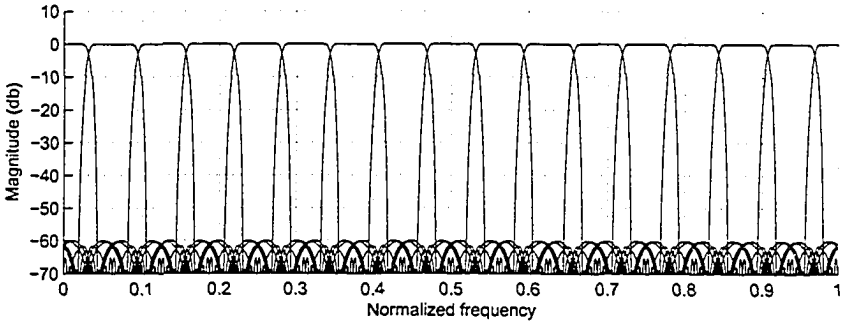

Figure 4.15: Magnitude-frequency responses associated with the proposed M-channel MDFT filterbank in Example 1

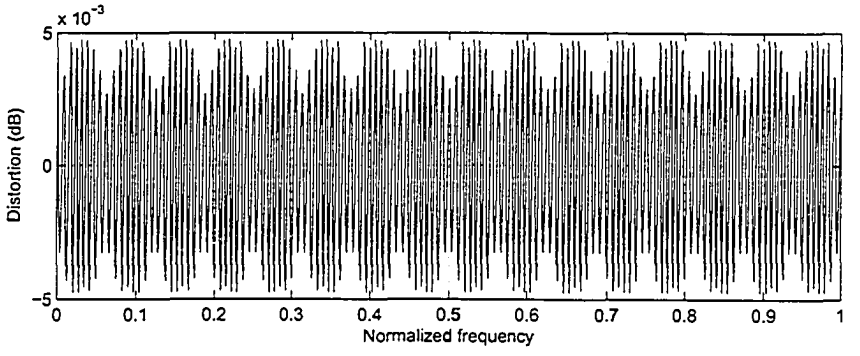

Figure 4.16: Distortion from a unity magnitude-frequency response for the MDFT filterbank in Example 1

prototype filter $P(z)$ is designed to satisfy the specifications given in Table 4.2. Moreover, the length of the digital filter $H_b(z)$ is selected as 125 $N_b = 125$), and those of the masking filters $H_{Mb}(z)$ and $H_{Mc}(z)$ are selected as 150 and 146 ($N_{Mb} = 150$ and $N_{Mc} = 146$), respectively. By solving the optimization problem in Eqn. 4.40 (with

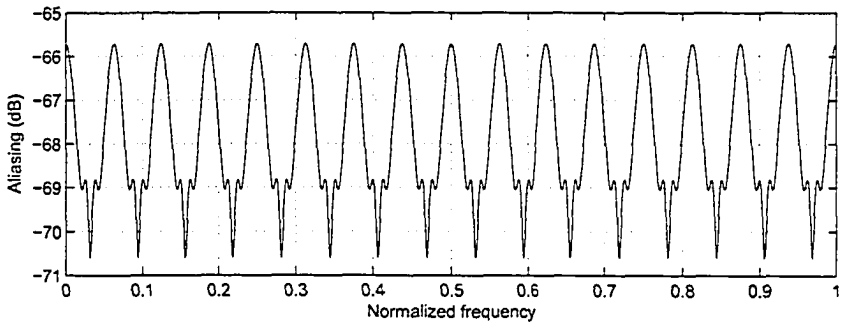

Figure 4.17: Aliasing function $A(z)$ for the MDFT filterbank in Example 1

Table 4.2: MDFT filterbank design specifications in the case of an arbitrary-bandwidth FRM prototype digital filter $P(z)$

M	L	Δ	$\beta(dB)$	$\lvert T(e^{j\omega})\rvert(dB)$
8	20	0.004	-60	$< 4 \times 10^{-3}$

$\varepsilon = 4.606 \times 10^{-4}$), the digital filters $H_{b0}(z)$, $H_{Mb0}(z)$ and $H_{Mc0}(z)$ are obtained to have the unit-impulse responses $h_{b0}(n)$, $h_{Mb0}(n)$ and $h_{Mc0}(n)$, respectively, as shown in Fig. 4.18. The magnitude-frequency response associated with $H_{b0}(z)$, $H_{Mb0}(z)$ and $H_{Mc0}(z)$ are obtained as shown in Fig 4.19. Through an inspection of the magnitude-frequency responses in Fig 4.19, it is observed that the optimized digital filter $H_{b0}(z)$ possess a normalized passband-edge frequency of 0.4740, a normalized stopband-edge frequency of 0.5385, and, consequently, a normalized transition bandwidth of 0.0645.

Having designed the digital filters $H_{b0}(z)$, $H_{Mb0}(z)$ and $H_{Mc0}(z)$, one can proceed to determine the FRM prototype digital filter $P(z)$ by using Eqn. 4.19. Fig. 4.20 shows the magnitude-frequency response of the resulting prototype digital filter $P(z)$. Through an inspection of the magnitude-frequency response in Fig. 4.20, it is observed that the digital filter $P(z)$ exhibits a stopband attenuation of 60dB and a narrow normalized transition bandwidth of 0.003225. Consequently, the magnitude-frequency responses associated with the 8-channel cascaded MDFT filterbank are obtained as shown in Fig. 4.21.

Finally, Fig. 4.22 shows the deviation of the overall MDFT filterbank transfer function $T(z)$ in Eqn. 4.29 from a unity magnitude-frequency response, yielding peak deviations of $\pm 4 \times 10^{-3}$dB. In addition, Fig. 4.23 shows the magnitude-frequency

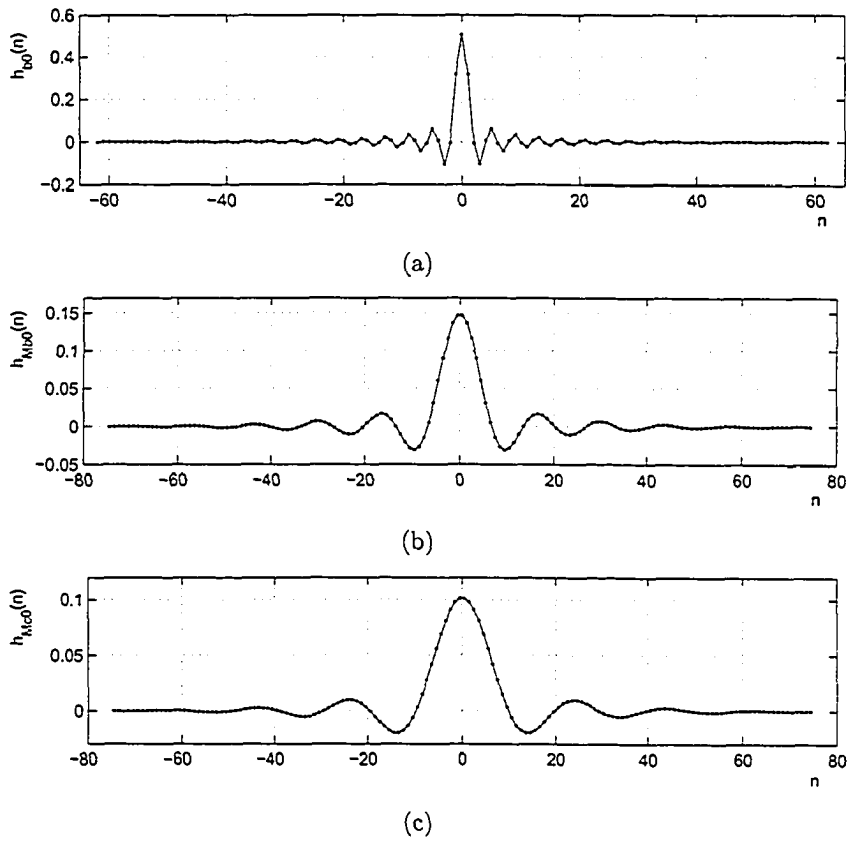

Figure 4.18: Multiplier coefficient values for (a) filter $H_{b0}(z)$, (b) masking filter $H_{Mb0}(z)$, and (c) masking filter $H_{Mc0}(z)$

response associated with the aliasing function in Eqn. 4.32, exhibiting a maximum value of $-62dB$.

In order to achieve the same specifications in Table 4.2, the prototype filter in the corresponding conventional MDFT filterbank requires 2270 multiplier coefficients.

In conventional M-channel MDFT filterbank, when the prototype filter has a length of N, the filtering operations require $N + M - 1$ multiplications and N additions, while the M-point DFT operation requires $(M/2)\log_2 M$ multiplications and $M \log_2 M$ additions [15]. In the proposed MDFT filterbank, there are $N_b+N_{Mb}+M-1$ multiplications, $N_b + N_{Mb}$ additions and 2 M-point DFT operations for the case of a narrow-band prototype filter, and $N_b + N_{Mb} + N_{Mc} + M - 1$ multiplications, $N_b+N_{Mb}+N_{Mb}$ additions and 3 M-point DFT operations for the case of an arbitrary-bandwidth prototype filter.

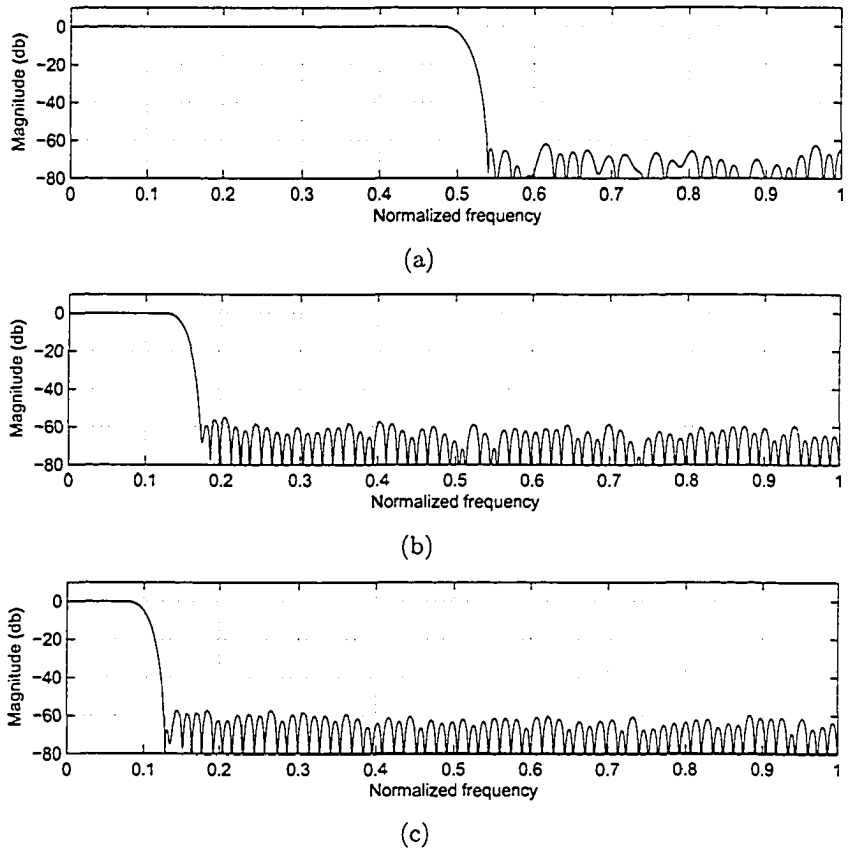

Figure 4.19: Magnitude-frequency response associated with (a) filter $H_{b0}(z)$, (b) masking filter $H_{Mb0}(z)$, and (c) masking filter $H_{Mc0}(z)$

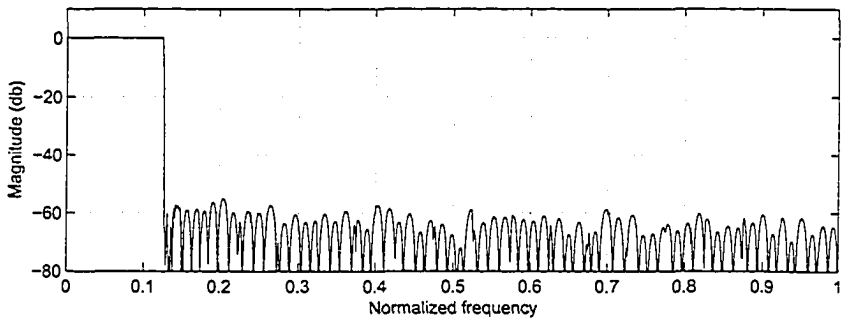

Figure 4.20: Magnitude-frequency response of the arbitrary bandwidth FRM prototype digital filter $P(z)$ in Example 2

Table 4.3 compares the computational complexity of the conventional MDFT filterbank and the proposed MDFT filterbank for the above examples, placing in evidence the overall savings in the number of multiplications and additions achieved by using the proposed MDFT filterbank. It is important to point out that Example

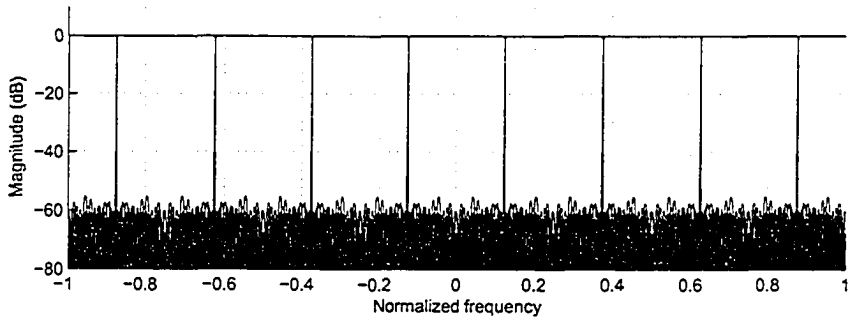

Figure 4.21: Magnitude-frequency response of the analysis filterbank in Example 2

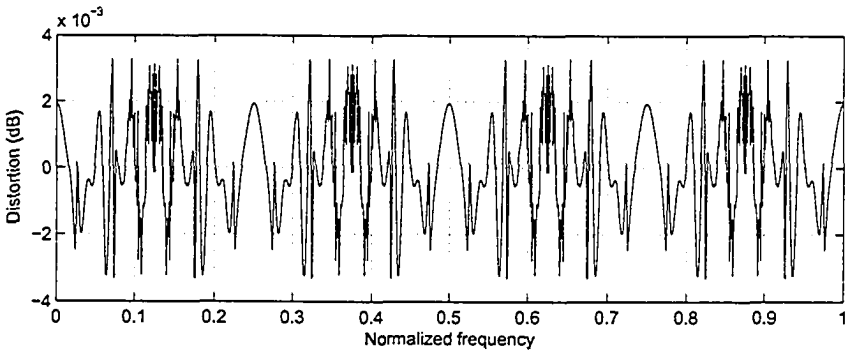

Figure 4.22: Deviation from a unity magnitude-frequency response for the MDFT filterbank in Example 2

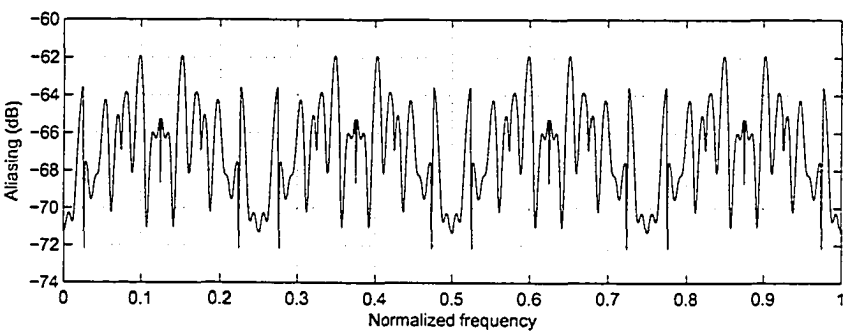

Figure 4.23: Aliasing function $A(z)$ for the MDFT filterbank in Example 2

2 gives rise to much higher savings than Example 1, mainly because the interpolation factor of 20 in Example 2 is relatively much larger the corresponding factor of 8 for Example 1. In this way, by using larger interpolation factors, one can obtain narrower transition bandwidth in each subchannel, meaning that more savings result when narrower transition bandwidths are realized.

Table 4.3: Comparisons of the computational complexity between the conventional MDFT filterbanks and the proposed MDFT filterbanks

	Example 1		Example 2	
	MULTS	ADDS	MULTS	ADDS
Conventional filterbanks	438	519	2289	2342
Proposed filterbanks	276	469	464	493
Savings	37.99%	9.63%	79.72%	78.94%

4.5 Conclusions

In this chapter, the frequency-response masking (FRM) digital filter design technique has been exploited and applied to the design of a novel pair of MDFT filterbanks. The resulting design technique includes not only the case of a narrow-band but also that of an arbitrary-bandwidth FRM prototype filter. The proposed MDFT filterbanks lend themselves to the realization of selective subchannels with very narrow transition bandwidths. Two application examples have been given to illustrate the design of the proposed filterbanks. It has been shown that as compared to the corresponding conventional MDFT filterbanks, the proposed MDFT filterbanks reduce the total number of multiplications (additions) by 37.99% (9.63%) in the case of a practical narrow-band, and by 79.72% (78.94%) in the case of a practical arbitrary-bandwidth FRM prototype filter.

Chapter 5

Conclusions and Future Work

5.1 Conclusions

This thesis has been concerned with the development of two different techniques for the design and realization of maximally-decimated filterbanks lending themselves to hardware implementations with high computational efficiency.

In Chapter 1, a qualitative background was given for multirate DSP together with a discussion of the advantages of multirate DSP compared to the conventional single-rate DSP. The multirate DSP operations and their respective theories were also studied as the fundamentals of multirate DSP. In addition, several practical applications of the multirate DSP were outlined.

In Chapter 2, an overview was given of the conventional 2-channel QMF filterbanks followed by an overview of their M-channel extensions. A mathematical investigation was also undertaken to highlight various types of distortion in the reconstructed output signal in QMF filterbanks. DFT filterbanks were introduced as a special class of QMF filterbanks which are capable of maintaining a high computational efficiency in their hardware implementations. It was pointed out that in the conventional DFT filterbanks, in order to produce high-quality low-pass magnitude-frequency response characteristics in the constituent subchannels, the lengths of the synthesis filters have to be much longer than those of the analysis filters . Consequently, MDFT filterbanks were introduced to overcome the aforementioned problem. Finally, the design of the QMF filterbanks capable of achieving the almost-PR reconstruction property was investigated by using the windowing as well as the nonlinear optimization technique.

In Chapter 3, a novel maximally-decimated filterbank was proposed, which per-

mits the realization of a large number of subchannels, and which leads to a high computational efficiency in the corresponding hardware implementation. Due to the tree-structured configuration of the resulting filterbank, a $(L+1)$-stage filterbank can be designed in terms of an already designed L-stage filterbank, merely through the addition of one extra stage. In addition, by using a two-step decimation in the last stage of the constituent analysis and synthesis filterbanks, half of the image components (arising from the critical decimation) are automatically cancelled in the reconstructed output signal. Computational investigations have been undertaken to show that deviation from perfect reconstruction can be kept minimal by maintaining moderate stopband attenuations in the analysis and synthesis digital filters. The interleaving technique were employed to produce a reduction in the number of subfilters from $2^L - 1$ to $L - 1$ for a L-stage filterbank. Compared to the traditional MDFT filterbanks, the tree-structured filterbank gives rise to savings of 40.6%, 65.6% and 78.9% in the number of filtering coefficients for the cases of 16, 32 and 64 subchannels, respectively. In addition, the tree-structured filterbank does not make any recourse to DFT operations.

In Chapter 4, the frequency-response masking (FRM) digital filter design technique was exploited and applied to the design of a novel pair of MDFT filterbanks. The resulting design technique includes not only the case of a narrow-band but also that of an arbitrary-bandwidth FRM prototype filter. The proposed MDFT filterbanks lend themselves to the realization of selective subchannels with very narrow transition bandwidths. Two application examples were given to illustrate the design of the proposed filterbanks. It was shown that as compared to the corresponding conventional MDFT filterbanks, the proposed MDFT filterbanks reduces the total number of multiplications (additions) by 37.99% (9.63%) in the case of a practical narrow-band, and by 79.72% (78.94%) in the case of a practical arbitrary-bandwidth FRM prototype filter.

5.2 Future Work

In the interleaved multistage tree-structured filterbank, the last-stage filter is designed by using optimization techniques, whereas the intermediate-stage filters are designed

by using the conventional digital filter design techniques (such as Parks-McMellen algorithm). However, the latter techniques cannot be used to design intermediate-stage filters exhibiting flat magnitude frequency responses in their passbands and stopbands. As discussed in Section 3.3, the resulting passband and stopband ripples associated with the intermediate-stage filters affect the overall distortion present in the reconstructed output signal. If the intermediate-stage filters are also optimized in connection with the PR reconstruction property, the overall distortion present in the reconstructed output signal can be reduced further.

In the MDFT filterbanks employing FRM technique, the proposed realizations for the resulting filterbanks are based on the implicit assumption of uniform subchannels. FRM technique can be also exploited for the case of filterbanks with non-uniform subchannels, for examples, for subchannels having different bandwidths or the different magnitude-frequency response gains.

Moreover, filterbank design techniques in this thesis are based on infinite-precision representation of the constituent digital filter coefficients. It is possible to design the digital filters for finite-precision operation employing binary, signed-binary, canonical signed-digit or mixed-radix computer arithmetic. This involves the development of discrete optimization techniques (e.g. by using genetic algorithms) for the finite-precision optimization of FIR digital filters. Consequently, the computationally intensive multiplication operations become combined shift-and-add operations, rendering the resulting filterbank to have higher computational efficiency in the corresponding hardware implementation. In practical DSP applications, the resulting hardware implementations are best targeted to field programmable gate array (FPGA) platforms.

Bibliography

[1] T. P. III Barnwell, "Sub-band coder design incorporating recursive quadrature filters and optimum ADPCM coders", *IEEE Transactions on Acoustics, Speech and Signal Processing*, vol. ASSP-30, pp. 751–765, Oct. 1982.

[2] M. G. Bellanger, G. Bonnerot, and M. Coudreuse, "Digital filtering by polyphase network: Aplication to sample-rate alteration and filter banks", *IEEE Trans. Acoustics, Speech, Signal Processing*, vol. ASSP-24, pp. 109–114, April 1976.

[3] M. G. Bellanger and J. L. Daguet, "TDM-FDM transmultiplexer: Digital polyphase and FFT", *IEEE Transactions on Communications*, vol. CON-22, pp. 1199–1204, Sept. 1974.

[4] P. J. Bloom, "High-quality digital audio in the entertainment industry: an overview of achievements and challenges", *IEEE Acoustics, Speech, and Signal Processing Magazine*, vol. 2, pp. 2–25, Oct. 1985.

[5] B. Brannon, "Wide-dynamic-range A/D converters pave the way for wideband digital-radio receivers", *Electron. Des. News*, pp. 187–205, Nov. 1996.

[6] P. L. Chu, "Quadrature mirror filter design for an arbitary number of equal band-with channels", *IEEE Transactions on Acoustics, Speech and Signal Processing*, vol. ASSP-33, no. 1, pp. 203–218, Feb. 1985.

[7] R. E. Crochiere and L. R. Rabiner, *Multirate digital signal processing*, Prentice Hall, Englewood Cliffs, NJ, 1983.

[8] A. Croisier, D. Esteban, and C. Galand, "Perfect channel splitting by use of interpolation/decimation/tree decomposition techniques", *Int. Symp. on Info., Circuits and Systems*, Patras, Greece, 1976.

[9] F. Cruz-Roldán, P. Amo-López, S. Maldonado-Bascón, and S. S. Lawson, "An efficient and simple method for designing prototype filters for cosine-modulated pseudo-QMF banks", *IEEE Signal Processing Letters*, vol. 9, pp. 29–31, Jan. 2002.

[10] P. S. R. Diniz, L. C. R. de Barcellos, and S. L. Netto, "Design of high-resolution cosine modulated transmultiplexers with sharp transition band", *IEEE Trans. on Signal Processing*, vol. 52, no. 5, pp. 1278–1288, May 2004.

[11] D. Esteban and C.Galand, "Application of quadature mirror filters to split band voice coding schemes", *Proc. IEEE Int. Conf. Acoustics, Speech, and Signal Processing*, pp. 191–195, May 1977.

[12] N. J. Fliege, "Computational efficiecy of modified DFT-polyphase filter banks", *Proc. 27th Asilomar Conf. Signals, Systems and Computers, Asilomar*, pp. 1296–1300, Nov. 1993.

[13] N. J. Fliege, *Multirate Digital Signal Processing*, Wiley, Chichester, U.K., 1994.

[14] N. J. Fliege and G. Rosel, "Optimized design of MDFT filter banks", *Proc. Int. Conf. Digital Signal Processing*, pp. 171–176, Limassol, Cryprus, June 1995.

[15] Emmamuel C. Ifeachor and Barrie W. Jervis, *Digital Signal Processing*, Prentice Hall, 1993.

[16] Special Issue, "Digital Audio", *IEEE Acoustics, Speech, and Signal Processing Magazine*, vol. 2, Oct. 1985.

[17] J. D. Johnston, "A filter family designed for use in Quadrature mirror filter banks", *Proc. IEEE International Conference on Acoustics, Speech and Signal Processing*, pp. 291–294, April 1980.

[18] T. Karp and N. J. Fliege, "MDFT filter banks with perfect reconstruction", *Proc. IEEE Int Symp. Circuits ans System*, pp. 744–747, Seattle, WA, May 1995.

[19] Tanja Karp and N.J. Fliege, "Modified DFT Filter Banks with Perfect Reconstruction", *IEEE Transactions on Circuits and Systems-II*, vol. 46, no. 11, pp. 1404–1414, Nov. 1999.

[20] N. Li and B. Nowrouzian, "An Efficient Interleaved Multistage Tree-Structured Filterbank Amenable to a Large Number of Subchannels", *submitted to IEEE Canadian Journal of Electrical and Computer Engineering.*

[21] N. Li and B. Nowrouzian, "A recursive approach to the design of linear-phase half-band digital filters having very sharp transition bands", *The 2002 45th Midwest Symposium on Circuits and Systems*, vol. 2, pp. 4–7, Aug. 2002.

[22] N. Li and B. Nowrouzian, "An efficient interleaved tree-structured almost-perfect reconstruction filterbank", *ISCAS '03. Proceedings of the 2003 International Symposium on Circuits and Systems*, vol. 4, pp. 25–28, May 2003.

[23] N. Li and B. Nowrouzian, "Application of Frequency-Response Masking Technique to the Design of a Novel Modified-DFT Filterbank", *submitted to Proc. IEEE International. Symposium on Circuits and Systems (ISCAS)*, June 2005.

[24] Yong Ching Lim, "Frequency-Response Masking Approach for the Synthesis of Sharp Linear Phase Digital Filters", *IEEE Transactions on Circuits and Systems*, vol. CAS-33, no. 4, pp. 357–364, April 1986.

[25] Yuan-Pei Lin and P. P. Vaidyanathan, "A Kaiser Window Approach for the Design of Prototype Filters of Cosine Modulated Filterbanks", *IEEE Signal Processing Letters*, vol. 5, no. 6, pp. 132–134, June 1998.

[26] T. Q. Nguyen, "Eigeinfilter for the design of linear-phase filters with arbitrary magnitude response", *Proc. IEEE International Conference on Acoustics, Speech and Signal Processing*, pp. 1981–1984, May 1991.

[27] T. Q. Nguyen, "Near-perfect-reconstruction pseudo-QMF filter banks", *IEEE Transactions on Signal Processing*, vol. 42, pp. 65–76, Jan. 1994.

[28] H. J. Nussbaumer, "Pseudo QMF filter bank", *IBM Tech. Disclosure Bulletin*, vol. 24, pp. 3081–3087, Nov. 1981.

[29] RF Engines Limited, "The Pipelined Frequency Transform", *RF Engines Limited White Paper*, Feb. 2002.

[30] P.; Johansson M.; Rosenbaum, L.; Lowenborg, "Cosine and sine modulated FIR filter banks utilizing the frequency-response masking approach", *ISCAS '03. Proceedings of the 2003 International Symposium on Circuits and Systems*, vol. 3, pp. 25–28, May 2003.

[31] J. H. Rothweiler, "Polyphase quadrature filters –A new subband coding technique", *Proc. IEEE International Conference on Acoustics, Speech and Signal Processing*, pp. 1280–1283, 1983.

[32] K. Swaminathan and P.P. Vaidyanathan, "Theory and design of uniform DFT, parallel, Quadrature Mirror Filter banks", *IEEE Transactions on Circuits and Systems*, vol. CAS-33, no. 12, pp. 1170–1190, Dec. 1986.

[33] P. P. Vaidyanathan, *Multirate Systems and Filter Banks*, Prentice Hall, 1993.

[34] P. P. Vaidyanathan and Truong Q. Nguyen, "Eigenfilters: A new aproach to least-squares FIR filter design and applications including Nyquist filters", *IEEE Transactions on Circuits and Systems*, vol. CAS-34, no. 1, pp. 11–23, January 1987.

[35] P. Vary, "On the design of digital filter banks based on a modified principle of polyphase", *AEU*, vol. 33, pp. 293–300, 1979.

[36] S. R. Velazquez, T. Q. Nguyen, and S. R. Broadstone, "Design of Hybrid Filter Banks for Analog/Digital Conversion wideband digital-radio receivers", *IEEE Trans on Sgnal Processing*, vol. 46, no. 4, pp. 956–967, April 1998.

[37] R. N. J. Veldhuis, M. Breeuwer, and R. G. Van der wall, "Subband coding of ditigal audio signals", *Philips Journal of Research*, vol. 44, pp. 329–343, 1989.

[38] J. W. Woods and S. D. O'Neil, "Subband coding of images", *IEEE Trans. Acoustics, Speech and Signal Processing*, vol. 34, pp. 1278–1288, Oct. 1986.